AWARD NUMBER: W81XWH-16-2-0030

TITLE: Role of Matrix Metalloproteinase-3 in Deployment-Related Pulmonary Fibrosis

PRINCIPAL INVESTIGATOR: Derek Radisky, Ph.D.

RECIPIENT: Mayo Clinic Jacksonville

REPORT DATE: December 2020

TYPE OF REPORT: Final Report

PREPARED FOR: U.S. Army Medical Research and Materiel Command
Fort Detrick, Maryland 21702-5012

REPORT DOCUMENTATION PAGE

Form Approved
OMB No. 0704-0188

1. REPORT DATE	**2. REPORT TYPE**	**3. DATES COVERED:**
December 2020	Final	15Aug2016 - 14Aug2020

4. TITLE AND SUBTITLE

Role of Matrix Metalloproteinase-3 in Deployment-Related Pulmonary Fibrosis

5a. CONTRACT NUMBER

5b. GRANT NUMBER
W81XWH-16-2-0030

5c. PROGRAM ELEMENT NUMBER

6. AUTHOR(S)

Derek Radisky, Ph.D.
Gregory P. Downey, M.D.

E-Mail: Radisky.Derek@mayo.edu

5d. PROJECT NUMBER

5e. TASK NUMBER

5f. WORK UNIT NUMBER

7. PERFORMING ORGANIZATION NAME(S) AND ADDRESS(ES)

Mayo Clinic Jacksonville
4500 San Pablo Road
Jacksonville, Fl.
32224-1865

8. PERFORMING ORGANIZATION REPORT NUMBER

9. SPONSORING / MONITORING AGENCY NAME(S) AND ADDRESS(ES)

U.S. Army Medical Research and Materiel Command
Fort Detrick, Maryland 21702-5012

10. SPONSOR/MONITOR'S ACRONYM(S)

11. SPONSOR/MONITOR'S REPORT NUMBER(S)

12. DISTRIBUTION / AVAILABILITY STATEMENT

Approved for Public Release; Distribution Unlimited

13. SUPPLEMENTARY NOTES

14. ABSTRACT

Since the onset of military operations in Afghanistan in 2001 and Iraq in 2003 through Operations Iraqi Freedom, Enduring Freedom, and New Dawn (OIF/OEF/OND), more than 2.8 million military personnel, DoD contractors, US government, and NGO employees have been deployed to these regions. These personnel have been exposed to high levels of airborne particulate matter (PM; 'desert dust') generated by wind erosion of desert sand, movement of vehicles and troops, combustion and construction activities, and combat, with both short and long-term health consequences. In deployed military personnel, high levels of PM have been causally implicated in the observed increase in respiratory symptoms, asthma, bronchiolitis, and eosinophilic and interstitial lung disease. The goal of this application is to determine the mechanisms by which inhalational exposure to silicate-containing respirable PM during military deployment to Southwest Asia leads to chronic pulmonary inflammation and fibrosis and to investigate strategies to diagnose and repair this damage. Aim 1 is to determine the role of MMP-3 in preclinical (murine) models of pulmonary fibrosis induced by instillation of bleomycin, silica, or silicate-containing particulate matter (PM) from Iraq and Afghanistan. Aim 2 is to develop an MMP-3-selective Tissue Inhibitor of Metalloproteinase (TIMP) as therapeutic target for progressive pulmonary fibrosis using both in silico and in vitro approaches. Aim 3 is to determine if MMP-3 levels are elevated in the lungs and blood of patients with pulmonary fibrosis and in military personnel previously deployed to Southwest Asia and can be used as a biomarker for disease progression.

15. SUBJECT TERMS

None Listed

16. SECURITY CLASSIFICATION OF:			**17. LIMITATION OF ABSTRACT**	**18. NUMBER OF PAGES**	**19a. NAME OF RESPONSIBLE PERSON**
					USAMRMC
a. REPORT	**b. ABSTRACT**	**c. THIS PAGE**			**19b. TELEPHONE NUMBER** *(include area code)*
Unclassified	Unclassified	Unclassified	Unclassified	70	

Standard Form 298 (Rev. 8-98)
Prescribed by ANSI Std. Z39.18

TABLE OF CONTENTS

1. INTRODUCTION:

Since the onset of military operations in Afghanistan in 2001 and Iraq in 2003 through Operations Iraqi Freedom, Enduring Freedom, and New Dawn (OIF/OEF/OND), more than 2.8 million military personnel, DoD contractors, US government, and NGO employees have been deployed to these regions. These personnel have been exposed to high levels of airborne particulate matter (PM; 'desert dust') generated by wind erosion of desert sand, movement of vehicles and troops, combustion and construction activities, and combat, with both short and long-term health consequences. In deployed military personnel, high levels of PM have been causally implicated in the observed increase in respiratory symptoms, asthma, bronchiolitis, and eosinophilic and interstitial lung disease. The goal of this application is to determine the mechanisms by which inhalational exposure to silicate-containing respirable PM during military deployment to Southwest Asia leads to chronic pulmonary inflammation and fibrosis and to investigate strategies to diagnose and repair this damage. Aim 1 is to determine the role of MMP-3 in preclinical (murine) models of pulmonary fibrosis induced by instillation of bleomycin, silica, or silicate-containing particulate matter (PM) from Iraq and Afghanistan. Aim 2 is to develop an MMP-3-selective Tissue Inhibitor of Metalloproteinase (TIMP) as therapeutic target for progressive pulmonary fibrosis using both *in silico* and *in vitro* approaches. Aim 3 is to determine if MMP-3 levels are elevated in the lungs and blood of patients with pulmonary fibrosis and in military personnel previously deployed to Southwest Asia and can be used as a biomarker for disease progression.

2. KEYWORDS:

Pulmonary fibrosis; lung injury; matrix metalloproteinases; tissue inhibitors of metalloproteinases; airborne particulate matter; bronchiolitis; field emission scanning electron microscopy; inductively coupled plasma mass spectrometry; immunohistochemistry.

3. ACCOMPLISHMENTS:

What were the major goals of the project?

Major Task 1: Define the role of MMP-3 in PM-induced pulmonary fibrosis.
Milestone: ACURO Approval 6 Months Achieved
Milestone: **Major Task 1** **Milestone:** Achieved by 36 months

Major Task 2: Develop an MMP-3-selective tissue inhibitor of metalloproteinase (TIMP) and evaluate its efficacy in animal models of PM-induced pulmonary fibrosis.
Milestone: **Major Task 2** **Milestone:** Achieved by 36 months

Major Task 3: Determine if levels of MMP-3 and MMP-3 proteolytic products are elevated in the lungs and blood of patients with pulmonary fibrosis and in military personnel previously deployed to Southwest Asia and can be used as a biomarker for disease progression.
Milestone: **Major Task 3** **Milestone:** Achieved by 36 months

What was accomplished under these goals?

Major Task 1: Define the role of MMP-3 in PM-induced pulmonary fibrosis

Subtask 1. Obtain Local (National Jewish Health) IACUC Approval

We obtained local (National Jewish Health) IACUC approval on 06/14/2016 (NJH protocol # AS2830-05-19).

Subtask 2. Obtain USAMRMC Animal Care and Use Review Office approval for mouse experiments

We obtained USAMRMC Animal Care and Use Review Office (ACURO) approval for experiments to be conducted at National Jewish Health on 08/3/2016. The protocol was renewed on Sept 10, 2019 for an additional 3 years that allowed us to complete additional experiments during the no cost extension that ended in September 2020.

We collaborated with Drs. Karen Mummy and Brian Wong at NAMRU-Dayton and the protocol was approved by the Wright Patterson Air Force Base IACUC and remained active throughout the study.

Subtask 3. Develop animal models of pulmonary fibrosis induced by intratracheal administration of silicate-containing PM and compare to the standard bleomycin model.

This section will summarize the studies conducted over the course of the grant. We developed several preclinical models of pulmonary fibrosis including (i) single and multiple dose intratracheal (i.t.) bleomycin; (ii) single dose purified silica; and (iii) single and multiple dose i.t. silicate-containing PM from Iraq and Afghanistan. We used these models to determine the importance of MMP-3 in the pathogenesis of pulmonary fibrosis by comparing fibrogenic responses between wild type (WT) and *Mmp3*$^{-/-}$mice.

Initially, we titrated the dose of bleomycin to achieve consistent pulmonary fibrosis as measured biochemically using the hydroxyproline assay or measuring collagen 1 mRNA without excess mortality (**Fig. 1**). In the single dose bleomycin model, *Mmp3*$^{-/-}$mice were largely protected from bleomycin-induced fibrosis compared to WT littermate controls (**Fig. 2**).

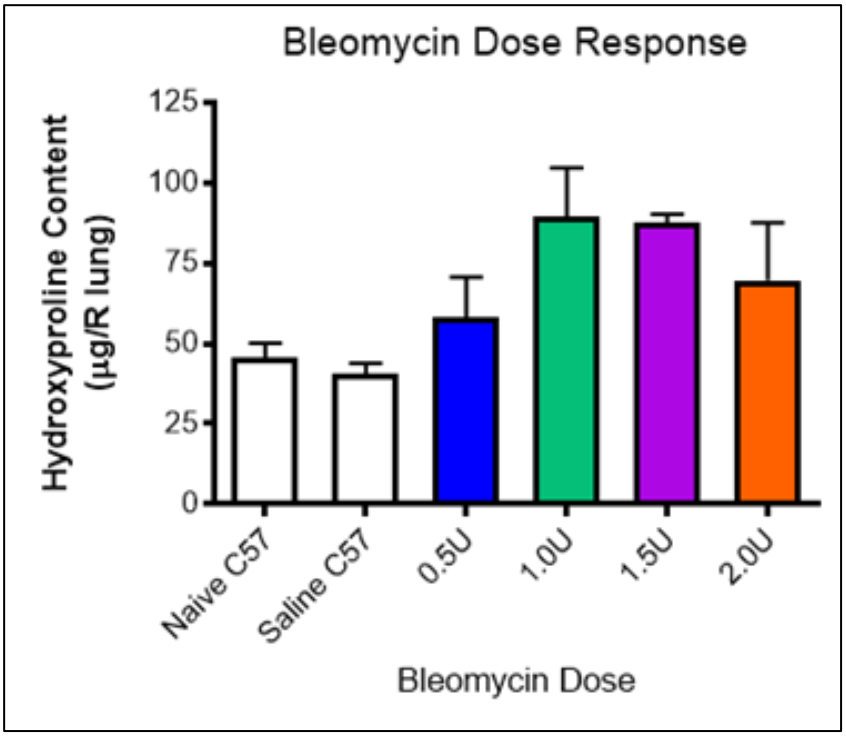

Fig. 1. Single dose intratracheal bleomycin induces dose-dependent lung fibrosis in WT BL/6 mice (n=6-8 per group).

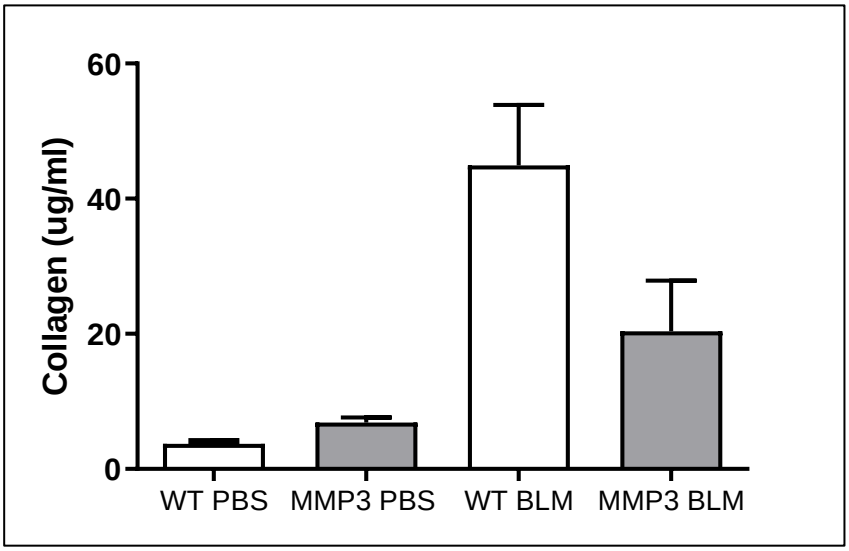

Fig. 2. *Mmp3*$^{-/-}$ mice are protected from bleomycin-induced pulmonary fibrosis compared to WT C57Bl/6 controls (single dose model). Lung collagen is measured using hydroxyproline (n=6 per group).

Similarly, in the multiple-dose bleomycin model, *Mmp3*$^{-/-}$mice were largely protected from bleomycin-induced fibrosis compared to WT littermate controls. Of note is that the multiple dose

bleomycin model is considered to be more reflective of human pulmonary fibrosis than is the single dose model.

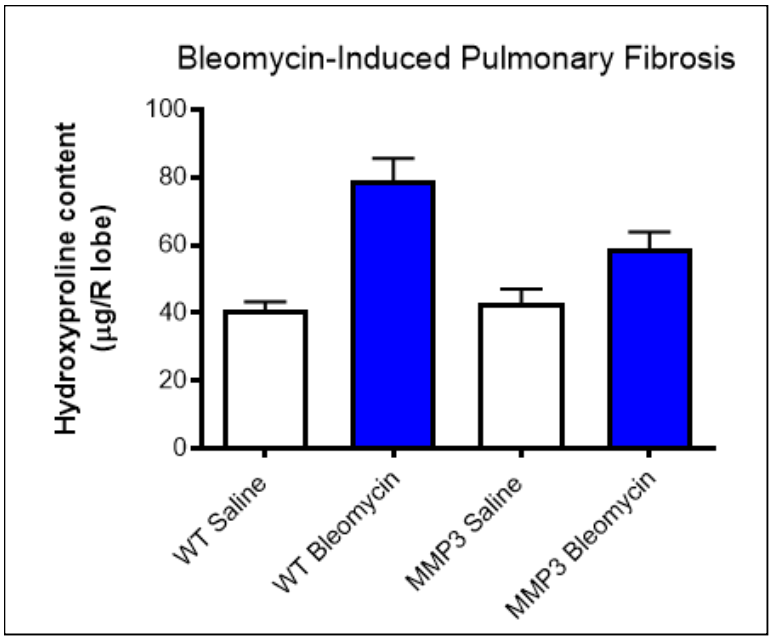

Fig. 3. *Mmp3* null mice (MMP3) are protected from lung fibrosis in the multiple-dose bleomycin model compared to WT C57Bl/6 controls (n=6-8 per group).

We next sought to determine whether *Mmp3*$^{-/-}$mice were protected from pulmonary fibrosis induced by instillation of particulate matter (PM). We began using purified silica that is known to induce pulmonary fibrosis. We tested 5 µm diameter silica from three different sources: NIST, NanoAmor (amorphous silica) and US Silica (Minusil: structured crystalline silica). **Fig 4** illustrates the size distribution of the purified silica confirming the stated mean diameter of 5 µm.

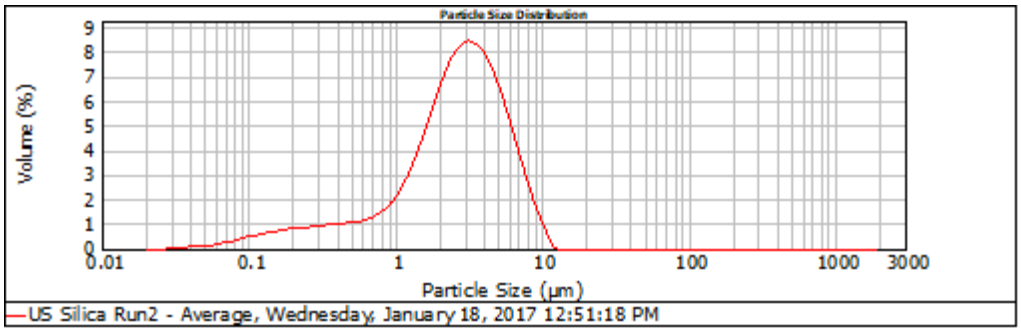

Fig. 4. Size distribution of purified silica

Initially we delivered the purified silica (200 mg/kg) directly into the lung using either intratracheal instillation or oropharyngeal aspiration (OPA) to ensure optimal intrapulmonary delivery of the silica. We found that OPA gave the most consistent results in terms of induction

of pulmonary fibrosis as determined by lung hydroxyproline content (**Fig. 5**). Histologically, the silica induced a granulomatous reaction in the lung **(Fig. 6)** and localized fibrosis (**Fig. 7**) as anticipated.

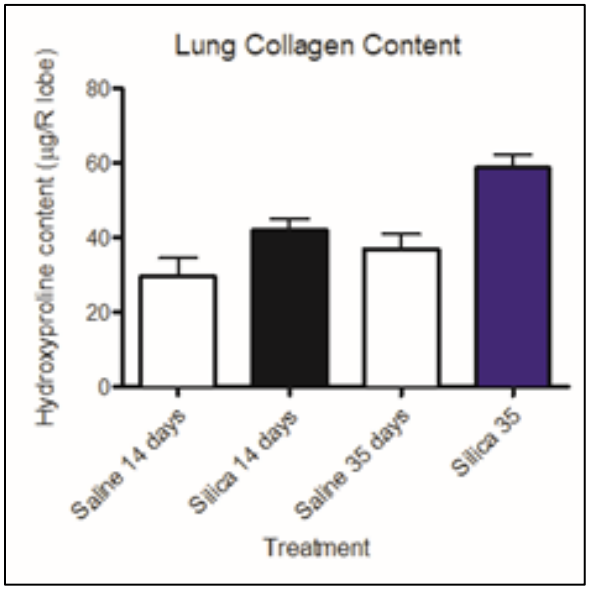

Fig. 5. Increase in lung collagen content in WT C57BL/6 mice induced by direct intrapulmonary silica instillation as measured by hydroxyproline content (n=6 per group).

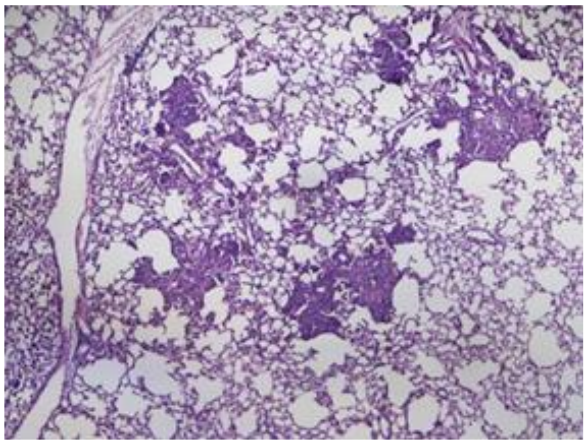

Fig. 6. Formation of granuloma in lungs of mice given silica by i.t. instillation (H&E stain: 4 X magnification).

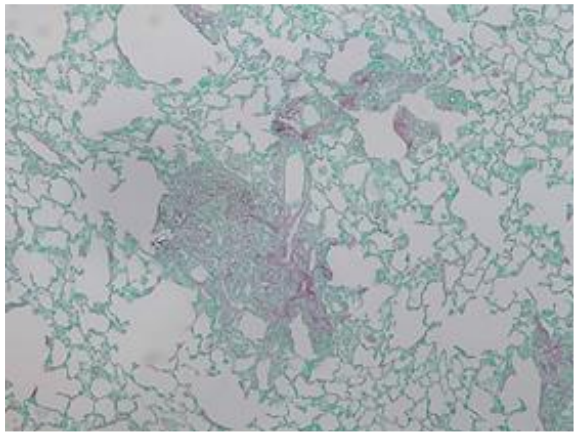

Fig. 7. Formation of granuloma containing increased collagen in lungs of mice given silica by i.t. instillation (picrosirius red stain; 10 X magnification).

In contrast to the bleomycin model, *Mmp3*$^{-/-}$ mice were not protected from pulmonary fibrosis induced by intrapulmonary instillation silica (**Fig. 8**). We also observed that the degree of pulmonary fibrosis induced in WT mice was similar whether we used crystalline (Minusil) or amorphous (NanoAmor) silica (not illustrated).

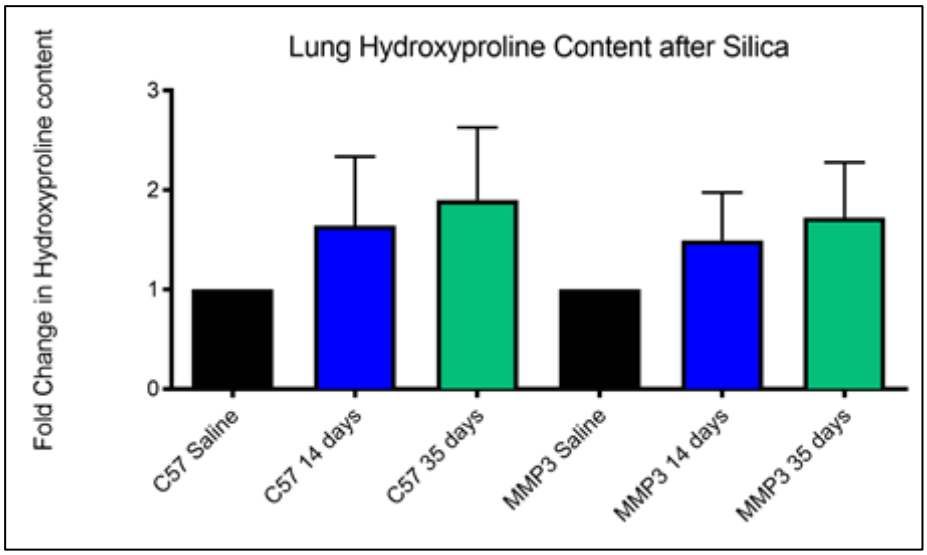

Fig. 8. Comparison of the degree of lung fibrosis at days 14 and 35 between WT (C57BL/6) and *Mmp3* null mice (MMP3) in response to intratracheal instillation of silica (n=6 per group).

We next sought to determine whether intrapulmonary administration of silicate-containing particulate matter (PM) from Iraq and Afghanistan induced pulmonary fibrosis. PM from the inland desert area of California (China Lake) was used as a 'control' to determine whether the pulmonary effects were related to the geographical source of the PM. The PM from Iraq were collected from high volume air sampling filters in theater near Baghdad airport (Camp Victory). The PM from Afghanistan was generated from topsoil collected from Bagram Air Force Base by the US Army Core of Engineers and then transported back to the United States, sterilized by autoclaving, and then aerosolized and collected on Teflon filters in the inhalation toxicology facility at NAMRU-Dayton on the Wright Peterson Air Force base. The mean diameter of these sources of PM was 5 µm, comparable to mean diameter of the PM from Iraq.

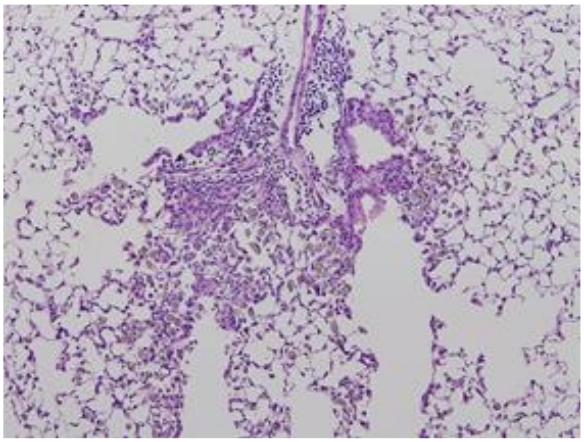

Fig. 9. Instillation of multiple doses of PM from Iraq or Afghanistan induces inflammation centered on the terminal bronchioles and alveolar ducts. PM can be identified in macrophages in these areas (H&E: 20 X magnification)

Initial experiments used a single dose 5 mg/kg of PM delivered by oropharyngeal aspiration with end points at 14 and 35 days. These studies demonstrated a variable increase in lung collagen content from PM from Iraq and Afghanistan that did not achieve statistical significance. We next studied the effects of multiple sequential instillations of PM (5 doses of 5 mg/kg given every other day for 10 days) with end points at 14 and 35 days after the last instillation. **Fig. 9**

illustrates that intrapulmonary instillation of multiple doses of PM from Iraq and Afghanistan induced inflammation centered on the terminal bronchioles and alveolar ducts. **Fig. 10** illustrates that multiple sequential instillations of PM from Iraq and Afghanistan induced significant pulmonary fibrosis in a dose-dependent manner. PM from Afghanistan induced the highest degree of pulmonary fibrosis whereas PM from California did not induce significant pulmonary fibrosis in these experiments **(Fig. 10)**.

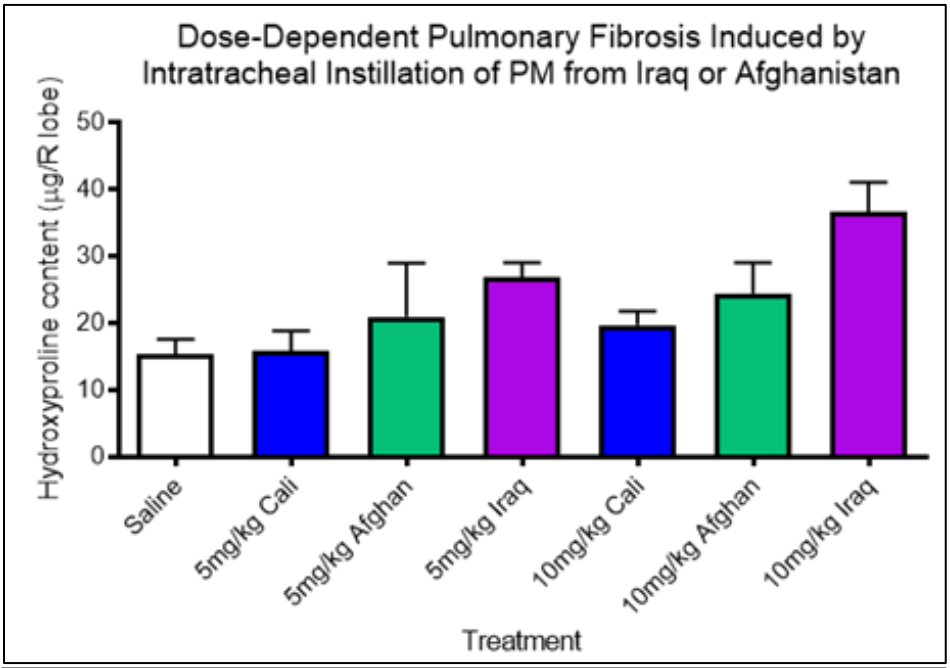

Fig. 10. Five doses of PM from Iraq or Afghanistan but not California (Cali) given every other day for 10 days induces dose-dependent lung fibrosis in WT type C57BL/6 mice (n=6-8 per group).

We next sought to determine whether *Mmp3*$^{-/-}$mice were protected from pulmonary fibrosis induced by instillation of particulate matter (PM). For these experiments, we compared the fibrogenic effects of PM from Afghanistan and California (China Lake) administered into the lung by oropharyngeal aspiration (OPA). PM from Iraq was not included in these experiments because supplies were very limited at the time these experiments were conducted. **Fig 11** illustrates that *Mmp3*$^{-/-}$mice were not protected from pulmonary fibrosis induced by instillation of silicate containing PM from Afghanistan. In fact, *Mmp3*$^{-/-}$ mice exhibited higher degrees of fibrosis in response to intrapulmonary administration of Afghanistan PM compared to WT mice and *Mmp3*$^{-/-}$mice developed pulmonary fibrosis in response to intrapulmonary administration of PM from China Lake.

To determine if there were sex-specific fibrogenic responses to PM exposure, we compared responses in male and female mice (**Figs. 12 and 13**). However, both male and female mice responded similarly to PM exposure.

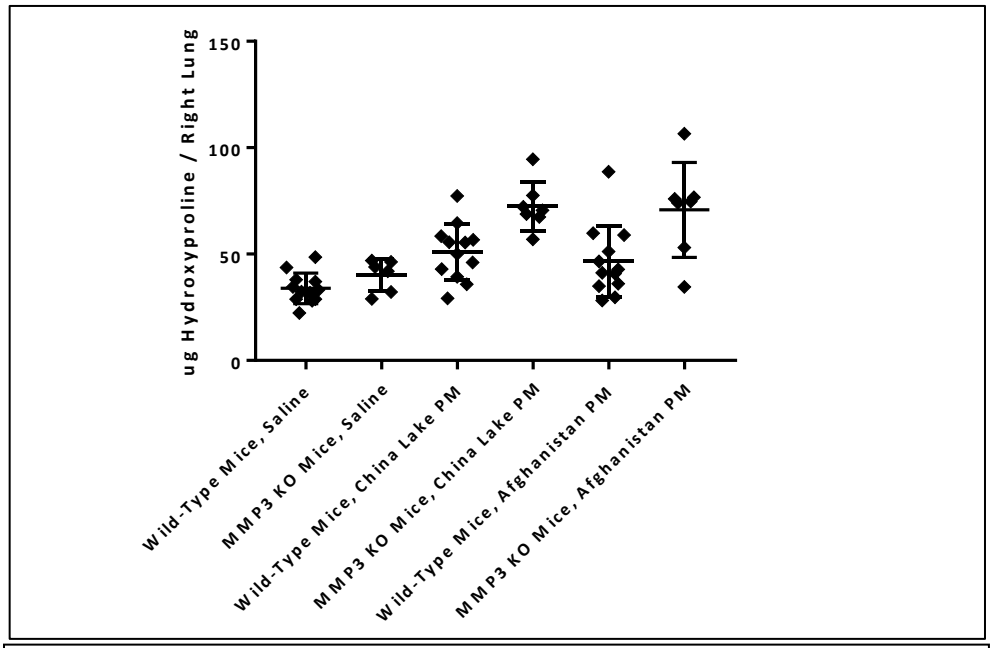

Fig. 11. Comparison of the degree of lung fibrosis at day 35 between WT (C57BL/6) and *Mmp3*$^{-/-}$ mice (MMP3 KO) in response to intrapulmonary delivery of PM from Afghanistan and California (China Lake) (n=12).

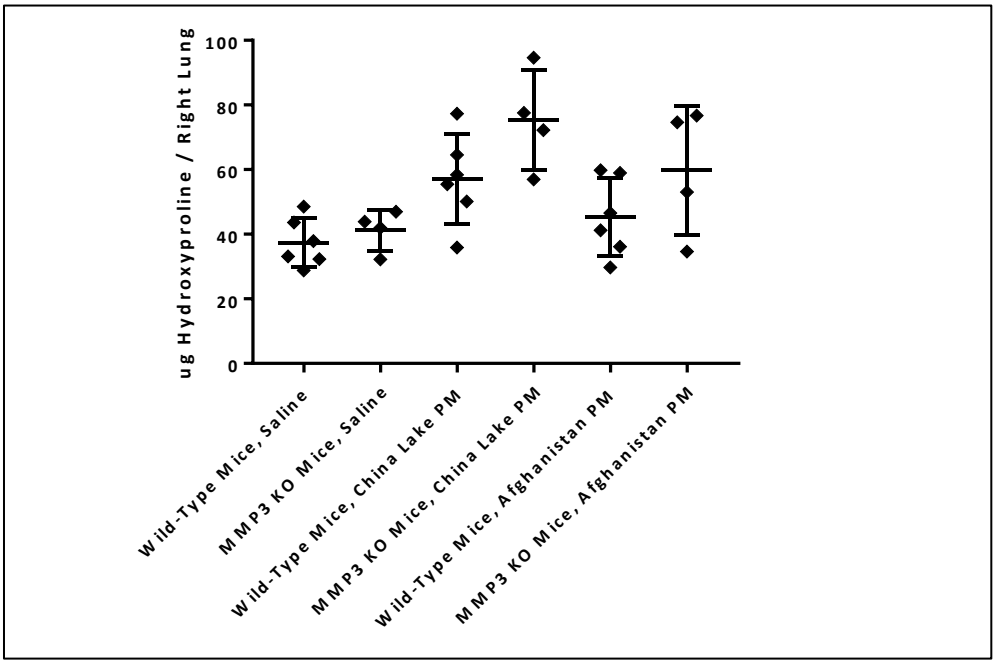

Fig. 12. Comparison of lung fibrosis at day 35 between male WT (C57BL/6) and *Mmp3*$^{-/-}$ mice (MMP3 KO) in response to intrapulmonary delivery of PM from Afghanistan and California (China Lake) (n=6).

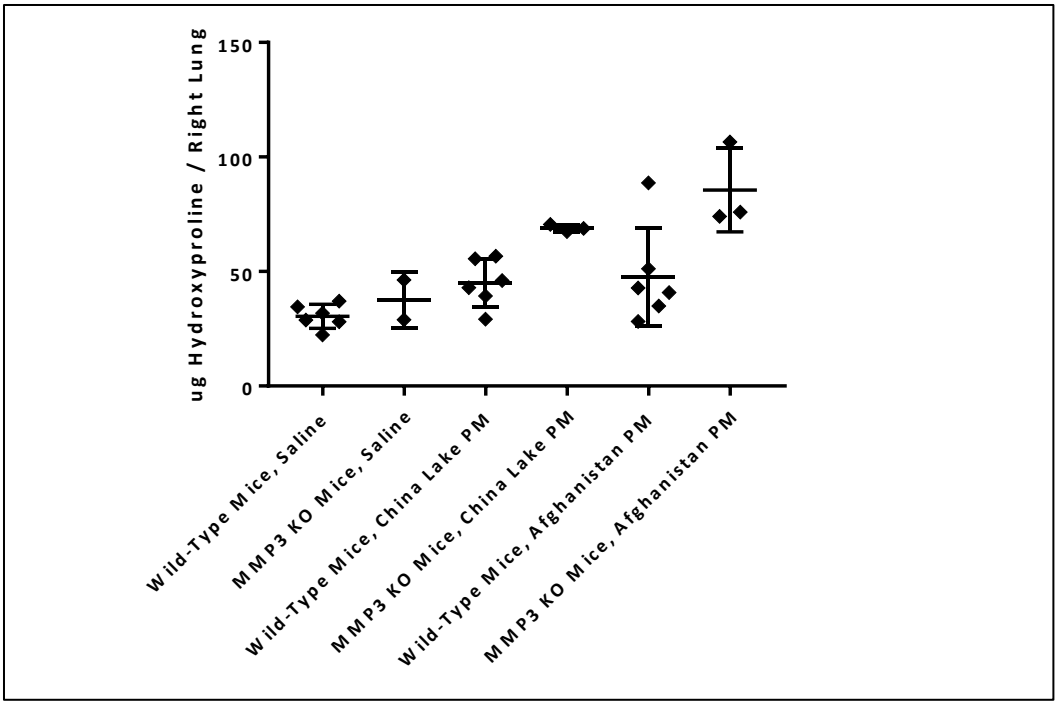

Fig. 13. Comparison of lung fibrosis at day 35 between female WT (C57BL/6) and *Mmp3*$^{-/-}$ mice (MMP3 KO) in response to intrapulmonary delivery of PM from Afghanistan and California (China Lake) (n=6).

To summarize the results of this section, we observed that *Mmp3*$^{-/-}$mice are protected from pulmonary fibrosis induced by single dose or multiple dose intrapulmonary bleomycin whereas they are not protected from pulmonary fibrosis induced by either purified silica or by silicate-containing PM from Afghanistan. These observations provide evidence that different mechanisms drive fibrosis in response to bleomycin (bleomycin-induced fibrosis is likely dependent on initial epithelial injury followed by production of fibrogenic mediators from the injured epithelial cells) compared to fibrosis driven by purified silica or silicate-containing PM. The latter is likely driven by fibrogenic mediators produced by macrophages that ingest the particulate matter and then produce fibrogenic mediators.

Subtask 4. Develop animal models of pulmonary fibrosis induced by aerosolized silicate-containing PM.

Over the course of this study, we undertook three large experiments designed to characterize the effects of aerosol exposure to purified silica and to PM from Afghanistan and purified silica at the NAMRU-Dayton/Wright Patterson Air Force Base inhalation toxicology facility in collaboration with our co-investigators Drs. Karen Mumy and Brian Wong. The first set of exposure experiments (n= 344 mice) were conducted in whole body aerosolization chambers using a protocol that had been developed for exposure of rats to aerosolized PM (5 mg/m3 for 20 hr/day, 5 d/week, over 4 weeks, for a total of 20 exposure days). Mice were then shipped to National Jewish Health in Denver for end point analysis 3 days later. As illustrated below in **Figs. 14 and 15**, aerosol exposure to PM from Afghanistan or California or to silica resulted in

lung inflammation as measured by an increase in BAL cell counts (**Fig. 14**) but a relatively minimal increase in lung collagen content (**Fig. 15**). No differences between the wild-type and *Mmp3-/-* mice were observed.

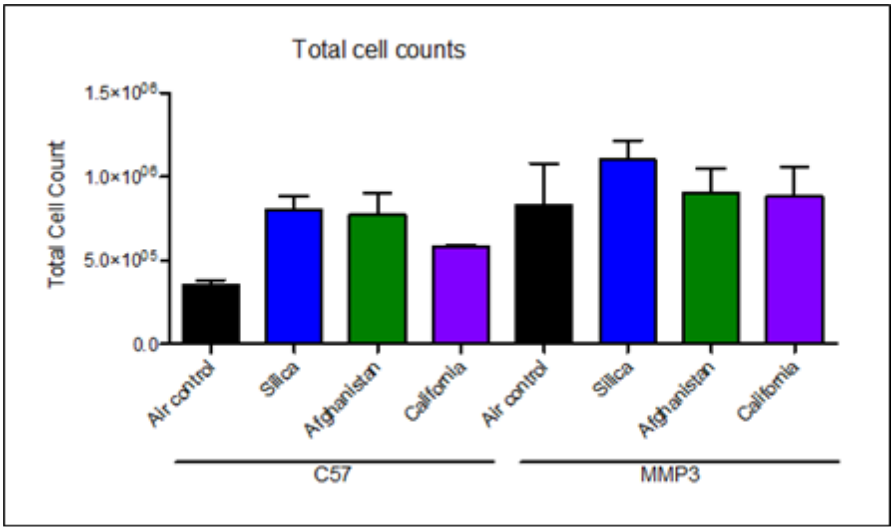

Fig. 14. Aerosol exposure to PM from Afghanistan or California (China Lake) or to purified crystalline silica resulted in lung inflammation by as measured increased total cells in BAL fluid.

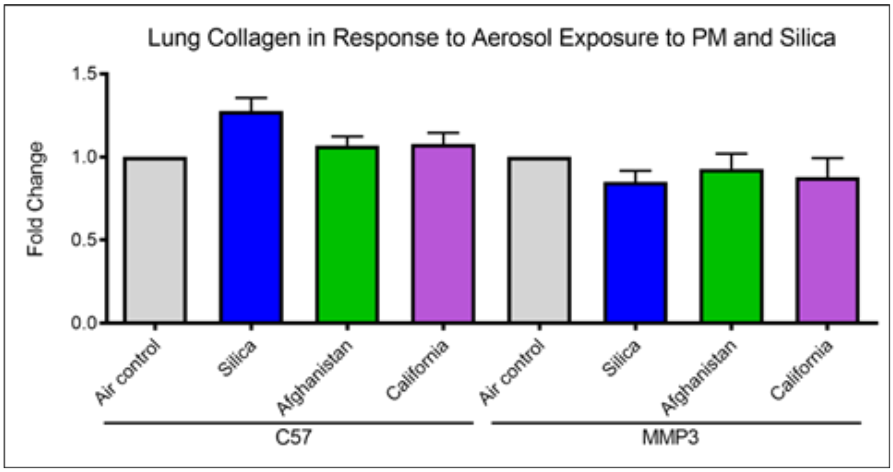

Fig. 15. Minimal increase in lung collagen content induced by aerosol exposure to silica as measured by hydroxyproline.

Given the absence in significant lung fibrosis from the initial protocol, we redesigned the exposure protocol based on published studies from other groups (using rats) who used a higher dose and allowed a longer period of time (up to 90 days) after the completion of exposures that would allow fibrosis to develop. A second aerosol exposure experiment using a higher concentration of PM (70 mg/m^3, 5 h/day, for 12 days) was conducted at NAMRU-Dayton and the mice were shipped to National Jewish Health for end point analysis. The mice were euthanized at 2, 4, and 8 weeks after exposure. We observed evidence of lung inflammation (increase in total cell counts in BAL fluid) but no evidence of lung fibrosis (**Fig. 16**). We interpreted this to mean that the efficiency of the mouse nasopharynx at removing aerosolized PM prevents much of the PM from accessing the lung and thus there was no measurable fibrotic response.

We again modified the protocol to include a 12-week time point based on the rationale that fibrosis may take longer to develop than 8 weeks in response to the aerosol exposure protocol. We conducted a third large experiment with aerosol exposure to PM (70 mg/m^3, 5 h/day, for 12

days) at NAMRU-Dayton and the mice were shipped to National Jewish Health for end point analysis. We euthanized the mice at 4, 8, and 12 weeks and conducted BAL to measure inflammation and assessed lung fibrosis using hydroxyproline. Again we observed evidence of lung inflammation (increase in total cell counts in BAL fluid) but no evidence of lung fibrosis even out to 12 weeks (not illustrated). Based on discussions with our program officer, we decided to use the oropharyngeal aspiration method for delivery to the lung for all future experiments.

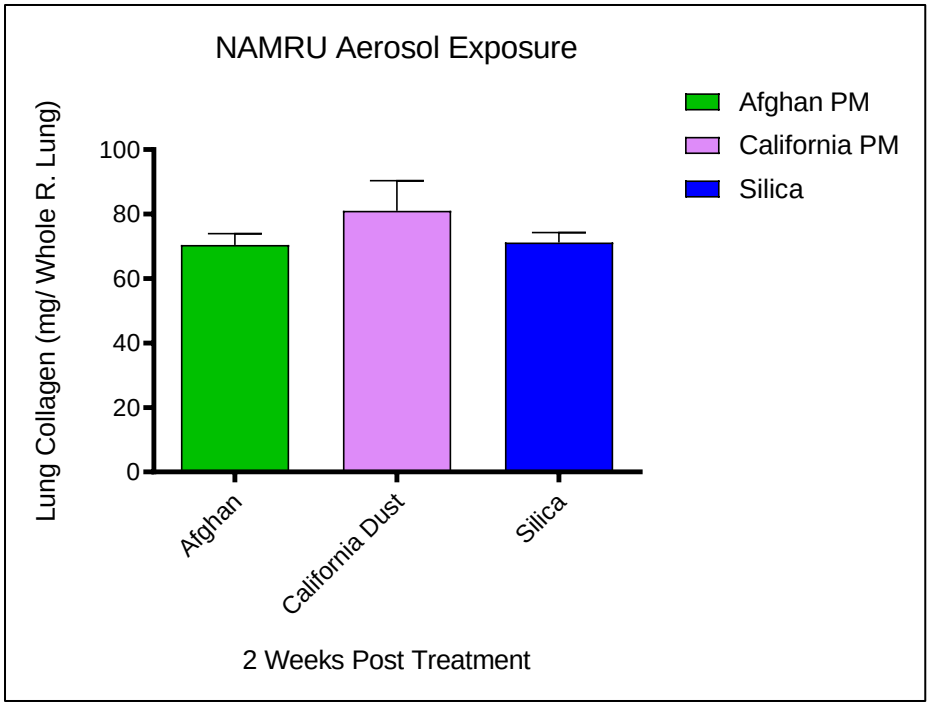

Fig. 16. No increase in lung collagen content induced by aerosol exposure to PM from Afghanistan or California or to purified silica as measured by lung hydroxyproline content.

Subtask 5. Assess osteopontin cleavage in PM-induced fibrosis.

We conducted experiments measuring cleaved fragments of osteopontin in the lungs of mice treated with bleomycin and PM from Southwest Asia. We were able to detect both intact osteopontin and several smaller Mr proteolytic fragments (not illustrated). There were no apparent differences in the abundance of the proteolytic fragments between WT and *Mmp3*$^{-/-}$ mice. Thus there appear to be other proteinases (i.e. besides MMP3) that are able to cleave osteopontin.

We have conducted a series of experiments looking at the potentially inflammatory and fibrogenic mediators released in mouse lung in response to silica exposure. We have been able to detect increased levels of interleukin-(IL)1β, tumor necrosis factor (TNF)α, and osteopontin mRNA after silica exposure (**Figs. 17, 18, and 19**). Responses were comparable or even amplified in *Mmp3*$^{-/-}$ compared to WT mice.

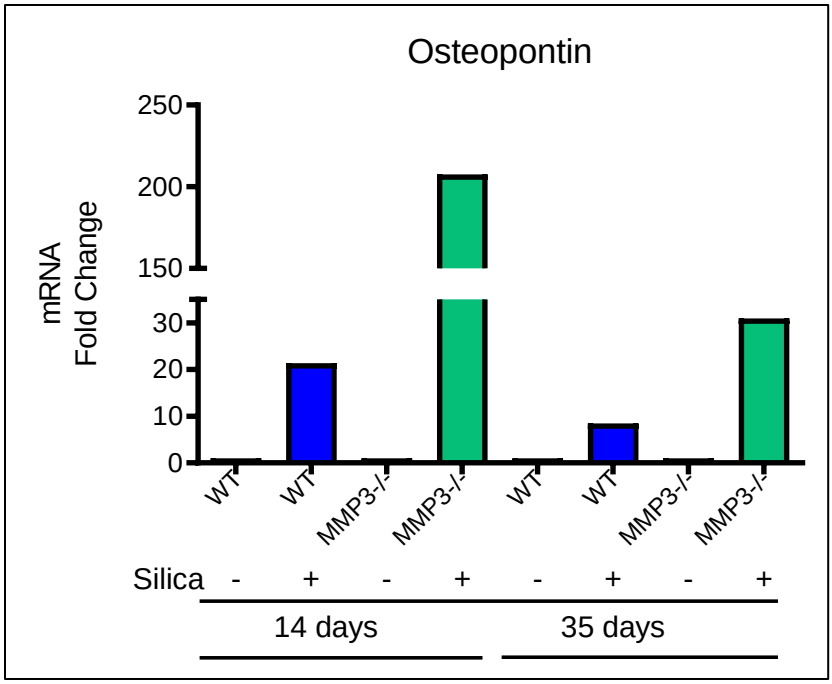

Fig. 17. Levels of osteopontin mRNA in whole lung extracts in WT and *Mmp3*$^{-/-}$ mice in response to silica exposure as determined by qPCR (TaqMan).

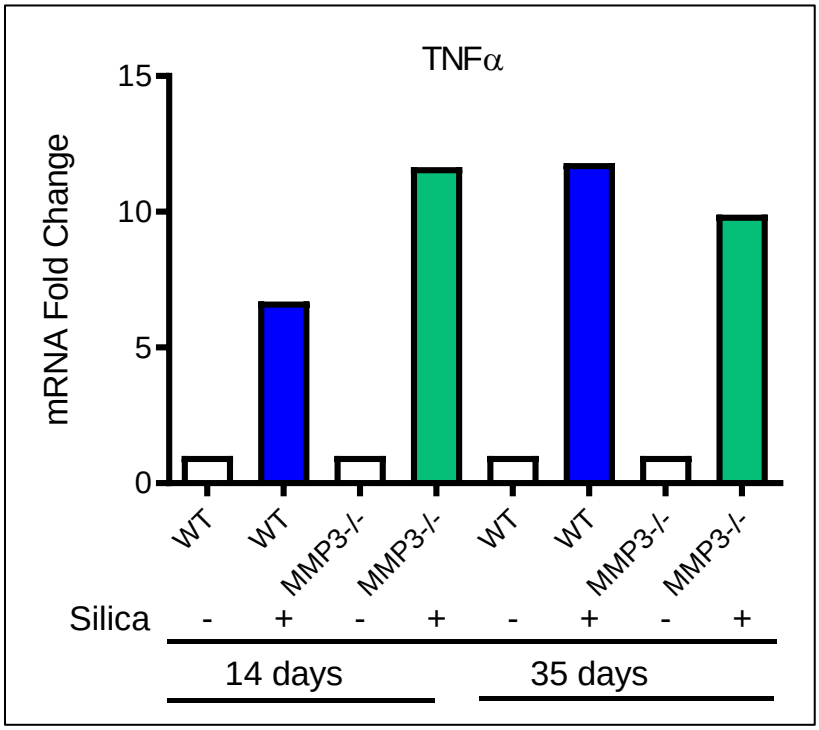

Fig. 18. Levels of TNFα mRNA in whole lung extracts in WT and *Mmp3*$^{-/-}$ mice in response to silica exposure as determined by qPCR (TaqMan).

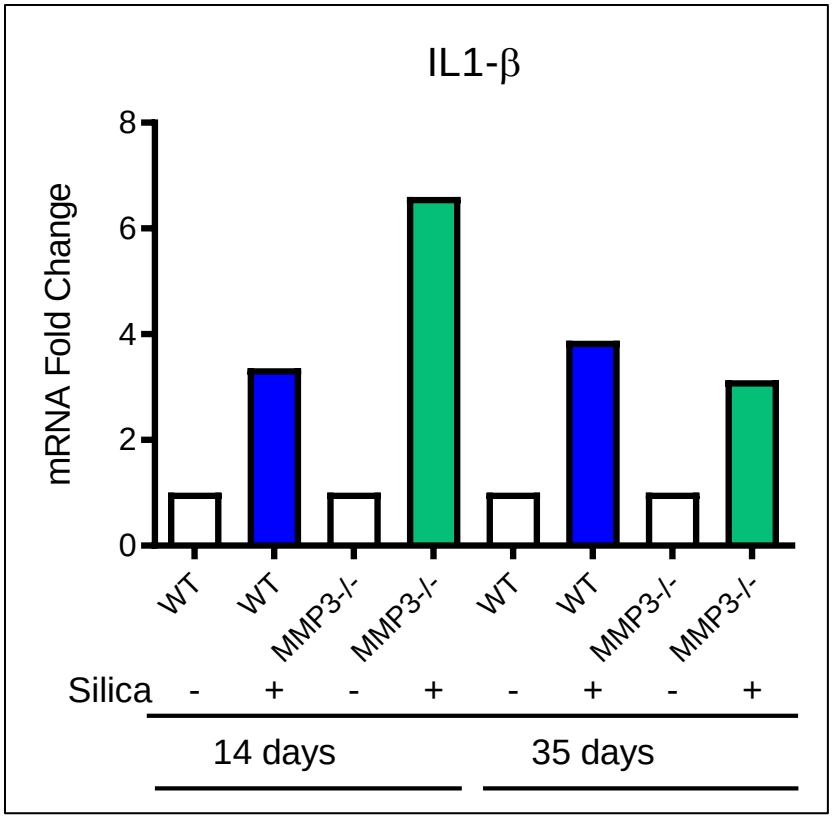

Fig. 19. Levels of IL-1β mRNA in whole lung extracts in WT and *Mmp3*$^{-/-}$ mice in response to silica exposure as determined by qPCR (TaqMan).

Subtask 6. Identify signaling pathways distinctly activated during PM-induced fibrosis by PCR arrays and RNAseq.

We first examined changes in global mRNA expression in whole lung extracts using in WT C57BL/6 mice in response to direct intrapulmonary instillation of multiple dose PM from Iraq and Afghanistan 35 days after the final instillation of PM. Saline was used as a control. **Fig. 20** illustrates that instillation of PM from Iraq and Afghanistan resulted in enhanced expression of a variety of inflammatory and fibrogenic genes including Ccl3 (MIP1α), MMP-13, TNFα, IL1α, IL-10, Lox, Mmp2, Tbfb1, Col3a1, CTGF, Mmp3, Il1β, Il13, Itgb6, and Mmp14.

At this juncture, given that there were no apparent differences in the degree of pulmonary fibrosis between WT and *Mmp3*$^{-/-}$ mice induced by instillation of silicate-containing PM from Southwest Asia or purified silica, we decided not to proceed with whole lung RNAseq analysis of WT and *Mmp3*$^{-/-}$ mice exposed to PM as we felt that this would not be informative

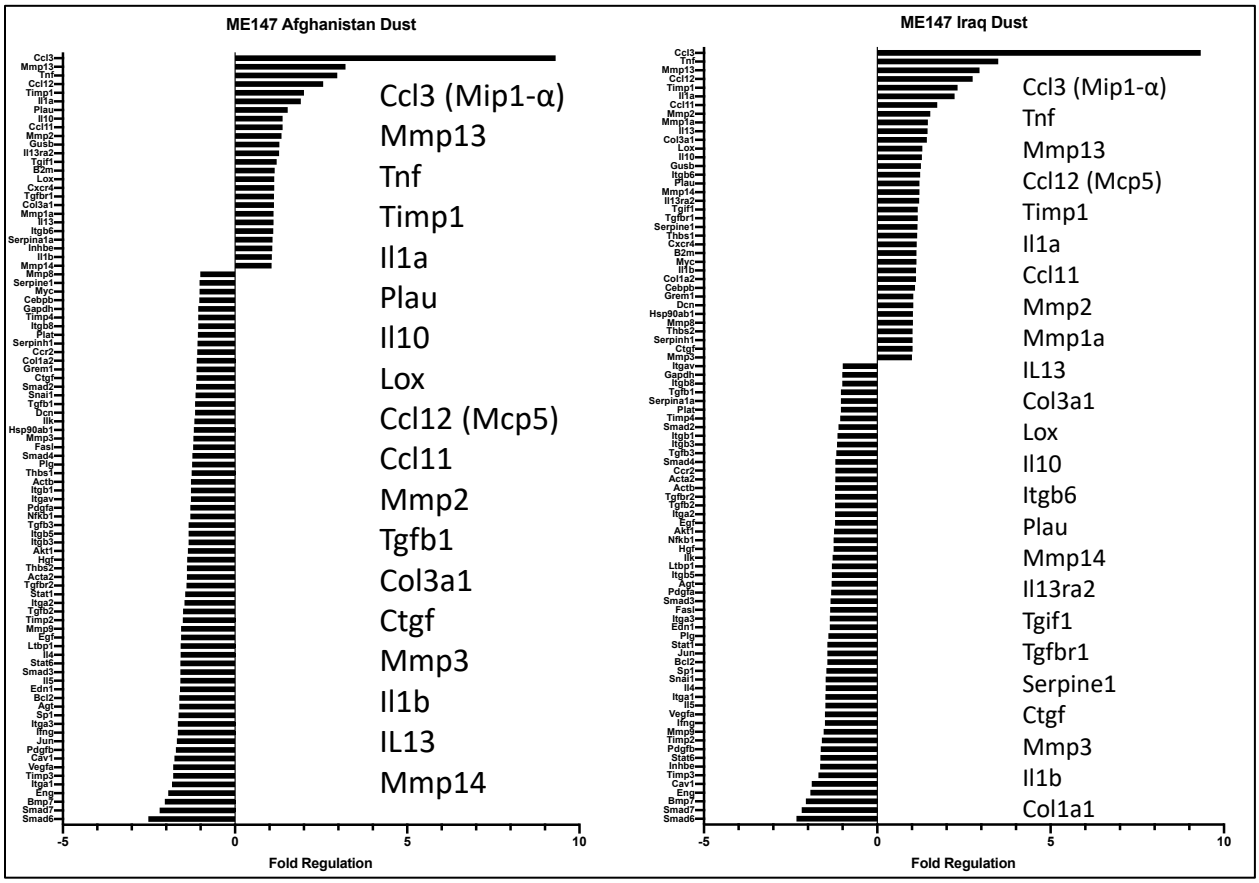

Fig. 20. Transcriptional alterations in whole mouse lung extracts in response to instillation of multiple dose PM (35-day time point) from Iraq and Afghanistan as determined by PCR arrays (QIAGEN).

Subtask 7. Assess fibrogenic response and matrix remodeling in PM-exposed lung fibroblasts.

We developed a reproducible and robust method of isolating fibroblasts from mouse and human lung using a combination of collagenase and Dispase to digest lung followed by negative selection using magnetic beads coated with anti-CD45 and anti-PECAM antibodies to remove hematopoietic cells and epithelial cells. We compared fibrogenic gene expression (Col1a1, EDA-fibronectin, Acta2, and Ccn2) in fibroblasts isolated from WT and *Mmp3*$^{-/-}$ mice at 14 and 35 days after PM and silica exposure. There were no apparent differences between lung fibroblasts isolated from WT and *Mmp3*$^{-/-}$ mice.

Subtask 8. Prepare and submit manuscripts for publication.

We submitted one abstract and published one manuscript related to these studies.

Abstract: Downey GP, Roybal H, Redente E, Aschner Y, Wong M. MMP3 Is Required for Bleomycin- but not Silica-Induced Pulmonary Fibrosis in Experimental Models. Submitted to the 2018 Annual International Conference of the American Thoracic Society.

Manuscript: Raeeszadeh-Sarmazdeh M, Greene KA, Sankaran B, Downey GP, Radisky D, Radisky Y. Directed evolution of metalloproteinase inhibitor TIMP-1 reveals cooperation between domains in matrix metalloproteinase recognition. *J Biol Chem* 2019;294(24):9476-9488. doi: 10.1074/jbc.RA119.008321).

Major Task 2: Develop an MMP-3-selective tissue inhibitor of metalloproteinase (TIMP) and evaluate its efficacy in animal models of PM-induced pulmonary fibrosis (Data in this task are from Dr. Radisky at the Mayo Clinic)

First generation MMP-3 inhibitors based on human TIMP-1. To improve the potency and selectivity of the natural MMP inhibitor TIMP-1 toward MMP-3, we used yeast surface display (YSD) to screen a diversity library of full-length human TIMP-1, as reported in detail in our publication (**Raeeszadeh-Sarmazdeh 2019**). The coding sequence of human TIMP-1 was C-terminally fused to the N-terminus of yeast surface protein Aga2p in the yeast expression vector pCHA. We demonstrated efficient expression and display of the fusion construct, and robust binding to the MMP-3 catalytic domain (MMP-3cd) (**Fig. 21A,B**). We next constructed a YSD diversity library of 5×10^6 independent variants, in which 17 residues located in five discontinuous loops of TIMP-1 (**Fig. 21C**) were partially degenerated, such that each clone contained an average of 4 mutations. We screened this library using fluorescence-activated cell sorting (FACS), identifying "ultra-binders" of MMP-3 possessing affinities enhanced by ~5-10-fold (**Fig. 22A**). Affinity improvements quantified in the YSD context were validated by MMP-3 inhibition studies using purified soluble recombinant TIMP variants, with consistent results showing improved inhibition constants in the low picomolar range. Sequencing of ultra-binder variants revealed that most contained 3-5 mutations, distributed among the diversified loops (**Fig. 22B**). Interestingly, we noted that frequent mutation L34G, located in the N-terminal domain, often co-occurred with mutations of residue Gly154, located >30 Å away in the C-terminal domain. We probed the functional interaction of these distant residues through mutagenesis, finding that while single mutations of Gly154 had no significant impact on MMP-3cd binding, substitutions at this position had a powerful synergistic effect when combined with the L34G mutation (**Fig. 22C-E**). To elucidate the structural basis for this synergistic effect, we co-crystallized ultra-binder TIMP-1 variants with MMP-3cd, and solved the crystal structures (**Fig. 22F**). We found that key mutation L34G brings the TIMP-1 AB-loop closer to MMP-3cd, cinching a reciprocal "tyrosine clasp" formed by Tyr35 of TIMP-1 and Tyr153 of MMP-3cd (**Fig. 22F**). Key mutation G154A promotes formation of an α-helical turn by TIMP-1 residues

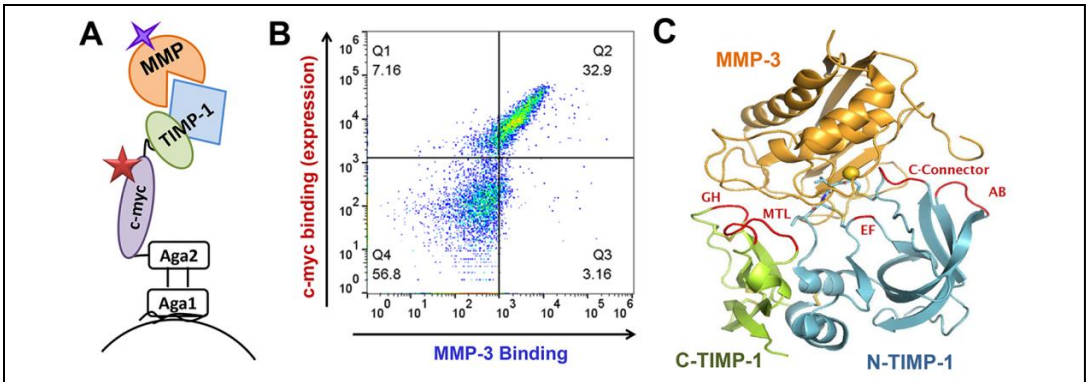

Figure 21. Yeast display of full-length TIMP-1 diversity library. (A) TIMP-1 is C-terminally fused to c-myc epitope and yeast surface protein Aga2p. TIMP-1 expression is detected with anti-c-myc and FITC-secondary antibody; MMP binding is detected with biotinylated MMP and APC-streptavidin. **(B)** Flow cytometry scatter plot shows yeast surface expression of TIMP-1 fusion construct (*y-axis*) and labeling by MMP-3 (*x-axis*). **(C)** Library diversity is focused in 17 residues of TIMP-1 (loops in red), located in both the N-terminal (*blue*) and C-terminal (*green*) domains, that interact with bound MMP-3cd (*orange*). Raeeszadeh-Sarmazdeh *et al. 2019*

154-157 at the interface between N- and C-terminal domains, creating a new H-bond between the TIMP-1 domains (**Fig. 22F**). Stabilization of TIMP-1 inter-domain interactions promotes structural and functional integration of the two TIMP domains and leads to stabilization of hydrophobic interactions between the TIMP-1 C-terminal domain and MMP-3cd, explaining synergy between the distant mutations. Our data reveal that the C-terminal domain cooperates with the N-terminal domain to shape TIMP-1 affinity toward MMP catalytic domains, showing that holistic engineering of the full-length protein can help us to develop stronger inhibitors.

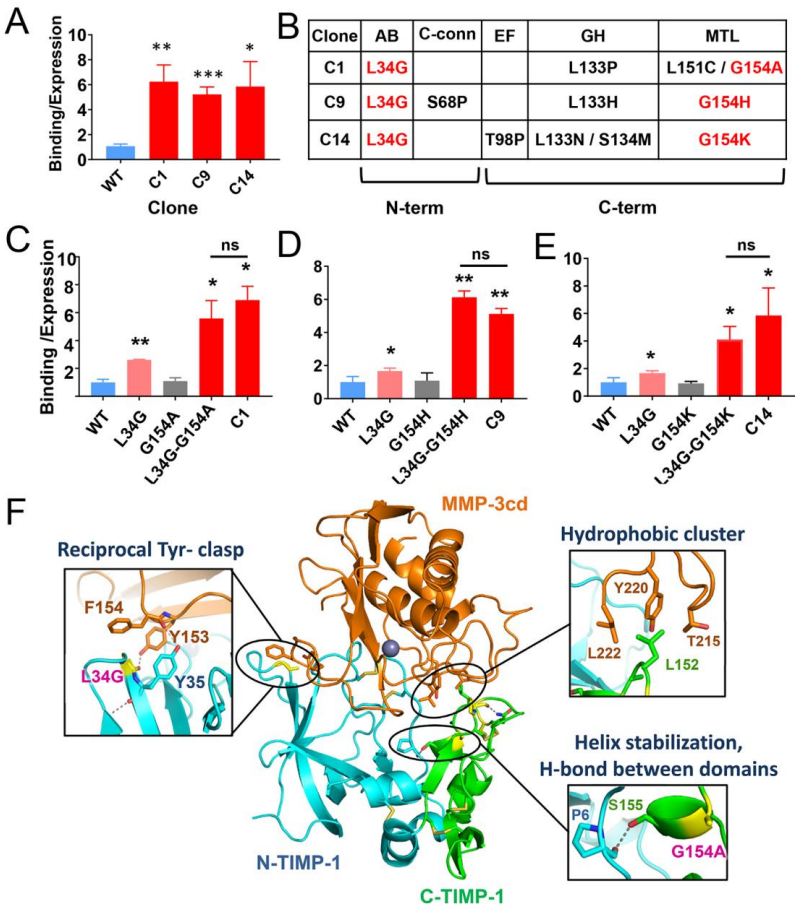

Figure 22. Distant mutations of TIMP-1 N- and C-terminal domains synergize to enhance MMP-3 binding. (A) Screening of our YSD library of TIMP-1 variants using FACS identified clones with enhanced MMP-3cd binding compared to WT-TIMP-1. **(B)** Sequencing showed that improved binders possessed 4-5 mutations spread across N- and C-terminal domains. **(C-E)** Analysis of single and double mutants showed that while L34G has a modest effect and mutations of Gly154 have no detectable effect in isolation, combining these mutations confers a synergistic enhancement of MMP-3cd binding. **(F)** Crystal structure of TIMP-1-C1 ultra-binder with MMP-3cd reveals optimized inter-domain and intermolecular interactions. L34G leads to tight cinching of a reciprocal "tyrosine clasp" (*left inset*) formed by Tyr35 of TIMP-1 and Tyr153 of MMP-3cd. G154A causes adoption of an α-helical turn by TIMP-1 residues at the interface between domains and formation of a new inter-domain H-bond (*lower right inset)*. Stabilization of TIMP-1 inter-domain interactions further leads to stabilization of hydrophobic interactions between the TIMP-1 C-terminal domain and MMP-3cd (*upper right inset*). Adapted from *Raeeszadeh-Sarmazdeh et al. 2019.*

Second generation MMP-3 inhibitors based on human TIMP-1. Our first-generation MMP-3 inhibitors very potently inhibited MMP-3, however they proved to be not yet highly selective, as assessed by comparing affinities for MMP-3 and -10, the two most closely related MMP catalytic domains by sequence homology (85% identity) and structural similarity. Although we found that the MMP-3cd ultra-binder variants, which were selected exclusively for enhanced binding to MMP-3cd, were also improved binders of MMP-10cd with little discrimination between the two enzymes, we subsequently adapted our screening protocols to achieve impressively selective binders. Using a novel counter-selection strategy in which we screened our library against biotinylated MMP-3 in the presence of incremental concentrations of unlabeled MMP-10 as a competing binder in sequential rounds of FACS (**Fig. 23A**), we isolated TIMP-1 variants showing up to 26-fold improvement in selectivity for MMP-3 versus MMP-10, relative to WT TIMP-1 in the YSD context (**Fig. 23B,**C), and >13-fold preference for MMP-3 corroborated by MMP inhibition kinetics studies of the soluble TIMP variants (**Fig. 24**). Our kinetics studies also demonstrated reduced off-target activity for inhibition of MMP-9, an alternative natural target for WT TIMP-1 (**Fig. 24**).

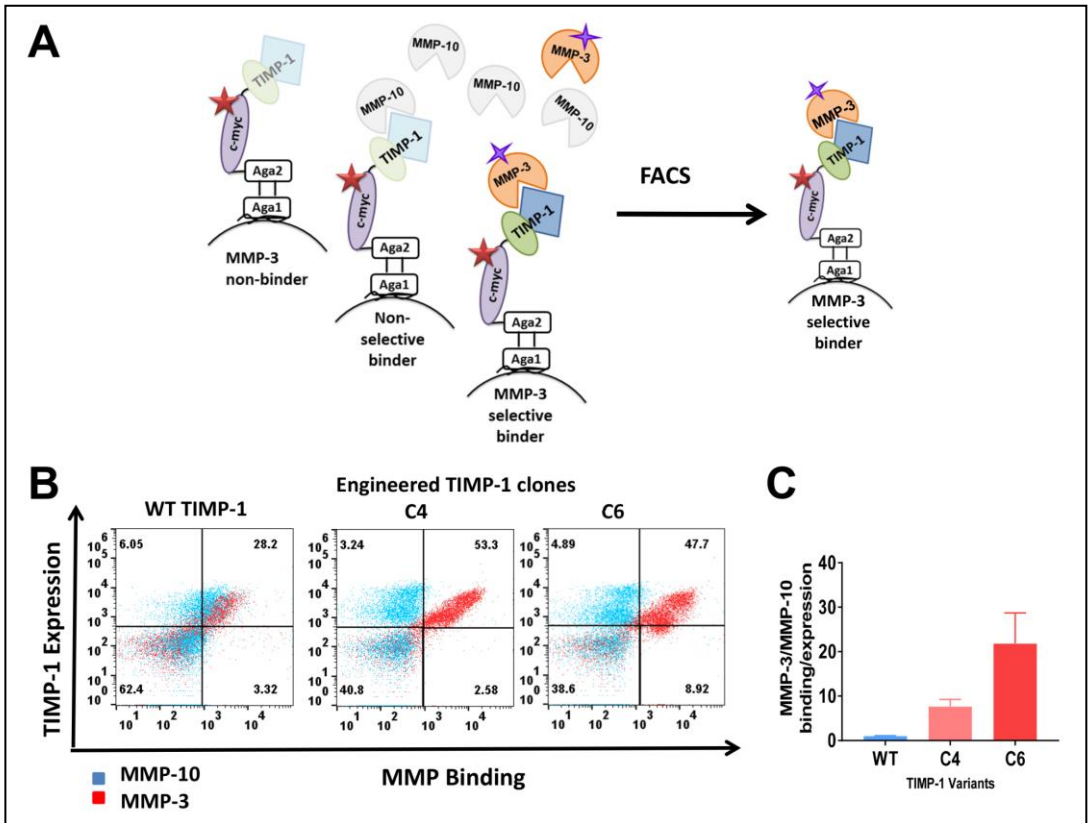

Figure 23. TIMP-1 YSD library screening yields variants selective for MMP-3 vs. MMP-10. (A) Yeast-displayed TIMP-1 library was enriched for MMP-3-selective binders by staining with biotinylated MMP-3 in the presence of increasing concentrations of unlabeled MMP-10 as a competing binder in sequential rounds of FACS. **(B)** Flow cytometry scatter plots for WT TIMP-1 (far left) show little discrimination in binding to MMP-3 (red) vs. MMP-10 (blue). Five rounds of library screening for MMP-3cd affinity in the presence of MMP-10cd competitor identified variants with highly improved selectivity, as shown by scatter plots for selective clones C4 and C6 (center and right). **(C)** Selectivity gains are quantified in bar graph.

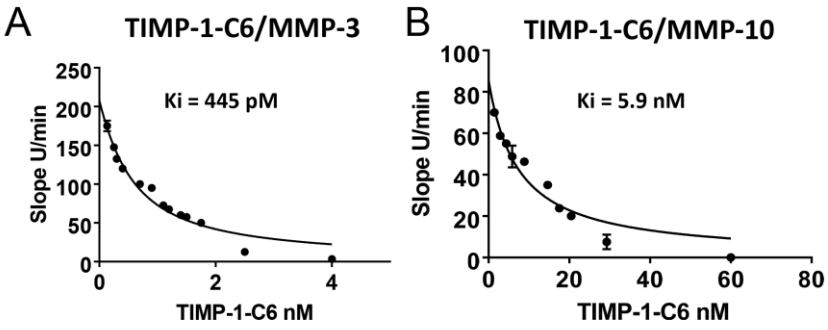

C

Ki, pM

	MMP-3	MMP-9	MMP-10
WT-TIMP1	96.4 ± 8.9	1640 ± 261	153 ± 11
TIMP-1-C6	444.7± 120.6	>> 10 nM	5947± 147.7
TIMP-1-C4	254.9 ± 18.05	>> 10 nM	4827 ± 31.5

Figure 24. MMP inhibition by soluble recombinant MMP-3-selective variants. (A) TIMP-1-C6 variant was evaluated for MMP-3 inhibition using a fluorometric substrate in the presence of increasing concentrations of the inhibitor. Data were fitted to Morrison's tight binding equation to determine an equilibrium inhibition constant (Ki) of 445 pM. **(B)** TIMP-1-C6 was found to inhibit MMP-10 with a Ki of 5.9 nM, showing >13-fold selectivity for MMP-3. **(C)** Inhibition constants (Ki) are summarized for selective variants compared to WT TIMP-1.

To elucidate the basis for specificity of selective TIMP-1 variants, we have examined sequences of variants to emerge from the selective screening protocol. We identified, in addition to the common L34G mutation found in our first-generation MMP-3 ultra-binders, the repeated presence of mutations of Met-66 (**Fig. 25A**). We have also co-crystallized TIMP-1-C6 with its target MMP-3, and solved the crystal structure at 2.3 Å resolution. This variant did not co-crystallize with the counter-target MMP-10, but we have used *in silico* mutagenesis and docking methods to model the complex, and have compared these structures to previously solved WT TIMP-1 complex structures to gain insight into selectivity. A major contributor to enhanced selectivity of TIMP-1-C6 appears to be the M66S mutation; this residue does not make critical contacts in the MMP-3cd complex, but its mutation disrupts crucial hydrophobic interactions with an MMP-10 exosite (**Fig. 25B**).

A

Clone	AB	C-conn	EF	GH	MTL
C4	L34G	M66D	T98G		Q153N
C5		M66G/E67N	T98D		S155L
C6	L34G	M66S/E67Y		L133N	
C9		M66G/E67H			
C10	L34G				S155L
C11	L34G	M66G/E67N			L151Q
C13	L34G	M66R			L152P/Q153C

B

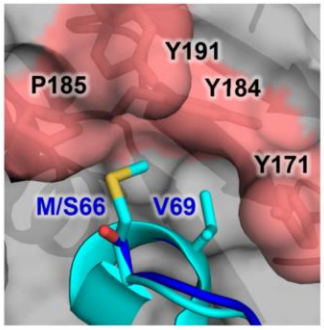

Figure 25. Loss of Met66 interactions with MMP-10 mediate improved selectivity for MMP-3. (A) Sequencing showed that selective binders possessed 2-4 mutations, with the most frequent being the common L34G mutation and various substitutions for Met66. **(B)** TIMP-1/MMP-10 crystal structure shows tight packing of TIMP-1 Met66 (*cyan*) with hydrophobic MMP-10 exosite residues (*salmon*), interactions that are lost in the model with MMP-3-selective TIMP-1-C6, featuring the M66S mutation (*blue*).

Major Task 3. Determine if levels of MMP-3 and MMP-3 proteolytic products are elevated in the lungs and blood of patients with pulmonary fibrosis and in military personnel previously deployed to Southwest Asia and can be used as a biomarker for disease progression. (This section is from Dr. Downey at National Jewish Health and Dr. Radisky at Mayo Clinic)

Subtask 1. Local IRB Approval

We obtained local (National Jewish Health) RRB approval on 11/29/2016 (NJH protocol # HS3012) to use archived blood and bronchoalveolar lavage samples.

We then obtained approval from the University of Colorado IRB (CoMIRB) on 1/19/2017 (CoMIRB protocol #16-2661) to use existing formalin-fixed lung biopsy samples (obtained by video-assisted thoracoscopic (VATS) biopsy) stored at the University of Colorado Hospital.

Subtask 2. USAMRMC IRB/HRPO Approval for human subjects.

We obtained USAMRMC IRB/HRPO approval on 03/2/2017 to conduct analysis on blood serum samples from idiopathic pulmonary fibrosis patients at the National Jewish Health and analysis of 10 archived lung biopsies samples from symptomatic military personnel previously deployed to Southwest Asia collected under standard care procedures at the University of Colorado Hospital.

Subtask 3. Determine if MMP-3 and osteopontin peptide levels are elevated in serum from patients with deployment lung disease.

We analyzed MMP-3 levels in blood samples from 10 normal human donors and 10 previously deployed military personnel (deployers) using an ELISA. The levels in both normal human donors and deployers were low (1.1 - 4.2 ng/ml) and there were no significant differences between the groups.

Subtask 4. Analyze the chemical and mineralogical composition and anatomic location of PM from VATS lung biopsies and alveolar macrophages obtained by BAL from deployed military personnel.

Over the last year, Dr. Geoff Plumlee and Ms. Heather Lowers at the United States Geological Survey (USGS) have continued to refine their methods to measure levels of particulate matter and chemical content of biological fluids and tissues including bronchoalveolar lavage fluid and whole lung tissue. This part of the project has encountered several hurdles and setbacks. Due to the COVID-19 pandemic, the USGS has either been closed or running on skeleton staff since March 2020. Despite these circumstances, they have made significant progress on developing methods to digest isolated lung lavage cells and lung tissue using highly purified hydrogen peroxide (H_2O_2). We found that most commercial preparations of H_2O_2 contained high levels of tin and other trace metals that were added to stabilize the H_2O_2 that is otherwise highly reactive and unstable in solution.

We reasoned that we would refine the methods to digest and analyze whole lung tissue using the lungs of mice that had been treated with PM from Afghanistan, Iraq, and California before using the valuable and limited surgical lung biopsies from previously deployed military personnel. Accordingly, the USGS completed a series of studies to measure the levels of PM and the elemental composition of the lungs of mice that had PM from Afghanistan and Iraq and California (China Lake) instilled by oropharyngeal instillation. For this analysis, they used inductively coupled plasma mass spectrometry (ICP-MS). These studies are summarized below in **Figure 26** and **Table 1**. Notably, the concentrations of some of the elements are very low in concentration and below the levels in the blanks (**Figure 26**). These studies indicate that silicate-containing PM can be detected in BAL fluid and lung tissue although the levels present for some metals are close to the limits of detection. We are awaiting the completion of methods development before using the human deployer VATS biopsy samples. This part of the analysis will be supported by our other DoD grant: 'Mechanisms and Treatment of Deployment-Related Lung Injury: Repair of the Injured Epithelium' (W81XWH-16-2-0018; PR150109).

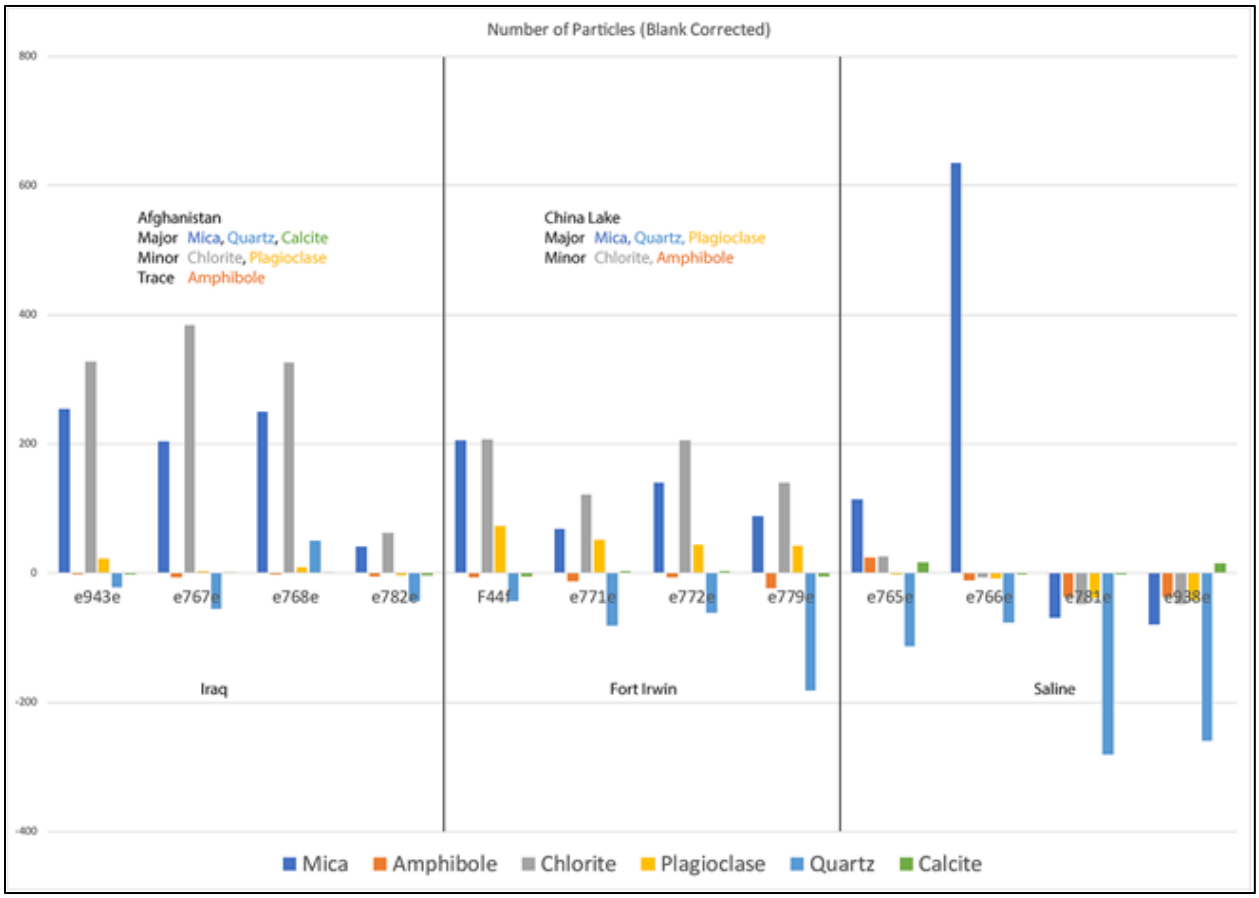

Figure 26. ICP-MS results from lungs of mice instilled with PM from Iraq, Afghanistan, or China Lake.

Slice_thickness_(um)	0	40	40	40	40	40	40	40	40	40	40	40	40
Slice_area_(cm2)	0.00	0.00	0.00	0.00	0.00	0.00	0.00	0.00	0.00	0.00	0.00	0.00	0.00
Slice_volume_(cm3)		1.0000	1.0000	1.0000	1.0000	1.0000	1.0000	1.0000	1.0000	1.0000	1.0000	1.0000	1.0000
Filter_(g)	0.0373	0.0381	0.0392	0.0414	0.0420	0.0422	0.0377	0.0382	0.0389	0.0401	0.0408	0.0424	0.0408
Tissue+Filter_(g)	0.0373	0.0456	0.0464	0.0555	0.0496	0.0502	0.0542	0.0459	0.0475	0.0471	0.0553	0.0503	0.0506
Filter_+_Tissue_(g)_after_xylene_and_dry_overnight	0.0367	0.0376	0.0388	0.0409	0.0415	0.0419	0.0372	0.0380	0.0386	0.0397	0.0402	0.0422	0.0404
Weight_of_tissue_(g)	-0.0006	0.0001	0.0002	0.0001	0.0001	0.0003	0.0001	0.0004	0.0003	0.0002	0.0000	0.0004	0.0002
Suspension_volume_(mL)	25	25	25	25	25	25	25	25	25	25	25	25	25
Aliquote_volume_(uL)	25000	25000	25000	25000	25000	25000	25000	25000	25000	25000	25000	25000	25000
Fraction_of_suspension_	1.0000	1.0000	1.0000	1.0000	1.0000	1.0000	1.0000	1.0000	1.0000	1.0000	1.0000	1.0000	1.0000
Active_area_filter_(mm2)	181	181	181	181	181	181	181	181	181	181	181	181	181
Field area (um)	48	48	48	48	48	48	48	48	48	48	48	48	48
Field height (um)	42	42	42	42	42	42	42	42	42	42	42	42	42
Field area (um)	2025	2025	2025	2025	2025	2025	2025	2025	2025	2025	2025	2025	2025
# of fields completed	56	18	20	7	12	26	22	26	44	34	19	55	54
Fraction of filter examined	0.0006	0.0002	0.0002	0.0001	0.0001	0.0003	0.0002	0.0003	0.0005	0.0004	0.0002	0.0006	0.0006
Total # particles	1089	973	913	976	314	986	745	919	827	913	957	352	470
Total #geologic material	692.0000	845.0000	780.0000	743.0000	197.0000	745.0000	422.0000	660.0000	579.0000	605.0000	831.0000	137.0000	156.0000
Totalparticles/cm3	#DIV/0!	4.8E+06	4.1E+06	1.2E+07	2.3E+06	3.4E+06	3.0E+06	3.2E+06	1.7E+06	2.4E+06	4.5E+06	5.7E+05	7.8E+05
Ag_phase	1	0	0	0	0	0	0	0	0	0	0	0	0
Al_oxide	41	1	1	6	0	18	2	3	6	15	2	5	9
Al_oxide_mix	15	2	2	0	0	3	0	0	1	17	5	0	2
Al_P_phase	0	1	0	0	1	0	1	0	0	0	3	0	0
Al_S_phase	0	0	0	1	0	1	0	0	0	0	0	0	0
Aluminosilicate_Al_gt_Si	15	3	3	7	2	10	0	1	3	29	231	3	3
Aluminosilicate_Al_lt_Si	68	137	146	186	26	168	67	97	84	116	430	23	13
Au_phase	2	0	0	0	0	0	0	0	2	2	1	0	0
Ba_phase	1	1	0	0	0	0	0	1	0	0	0	1	0
C_Cl	35	11	6	13	12	45	33	45	45	34	8	24	24
Ca_Al_oxide	0	0	1	0	0	0	0	0	0	3	0	0	0
Ca_Al_silicate	11	5	4	3	2	1	2	5	2	61	13	0	0
Ca_Mg_Al_Si	1	0	0	1	0	1	0	1	0	22	0	0	0
Ca_Mg_Fe_Al_silicate	11	2	0	0	0	2	1	0	1	2	0	0	0
Ca_Mg_Fe_silicate	9	2	0	0	1	3	1	3	2	4	2	0	0
Ca_Mg_phase	0	0	2	0	1	1	2	2	0	1	0	0	0
Ca_Mg_silicate	9	0	0	0	0	3	0	2	2	2	0	1	0
Ca_Mg_Ti_Al_Si	0	0	0	0	0	0	0	0	0	3	0	0	0
Ca_P_phase	0	0	0	1	1	2	8	0	1	0	0	0	0
Ca_P_phase_mix	1	0	1	0	1	1	2	1	0	1	0	0	0
Ca_phase	13	3	5	2	0	1	7	8	5	24	2	11	27
Ca_phase_mix	5	2	1	0	0	0	0	1	0	8	0	0	2
Ca_silicate	5	0	0	0	0	0	0	2	5	8	1	2	0
Ca_Ti_oxide	1	0	0	0	0	0	0	0	0	0	0	0	0
CaCl2	18	0	1	2	10	24	32	50	11	24	4	24	3
Carbonaceous	138	28	45	165	10	83	197	66	97	96	69	91	153
Carbonaceous_NoO	11	2	7	4	6	1	6	2	8	7	0	11	8
Cr_phase	4	2	0	0	0	2	6	3	2	2	3	3	2
Cu_phase	0	0	1	0	2	0	0	0	0	1	0	0	0
Fe_aluminosilicate	4	9	16	5	4	2	3	5	12	6	0	0	1
Fe_Cr	16	1	0	0	0	0	0	2	4	2	0	2	9
Fe_Ni	9	0	1	0	1	2	0	4	3	5	4	3	18
Fe_Ni_Cr	2	2	0	0	0	0	0	0	2	0	0	0	6
Fe_oxide	53	23	15	12	2	32	15	30	32	44	7	22	51
Fe_oxide_mix	32	50	42	29	18	24	20	38	23	41	14	16	5
Fe_silicate	6	3	2	1	1	3	1	4	2	1	1	1	0
Fe_Ti_oxide	0	0	0	0	0	1	0	0	0	3	0	0	0
Fe_Ti_oxide_mix	0	1	1	0	0	0	0	0	1	0	0	0	0
Feldspar_	1	0	0	0	0	0	0	0	0	0	0	0	0
Feldspar_K	15	25	13	11	3	73	50	45	50	13	6	8	5
Feldspar_Na	12	10	6	4	5	17	16	19	17	14	1	5	3
Feldspar_NaK	2	4	3	1	0	3	2	3	6	1	1	2	1
Feldspar_Plag	26	2	1	0	0	5	6	3	13	5	3	1	3
K_aluminosilicate	27	149	94	70	37	78	45	92	87	36	11	13	11
Mafic	9	7	7	3	3	3	1	6	2	18	0	0	0
Mg_aluminosilicate	5	85	128	128	19	105	65	76	42	13	2	3	2
Mg_Fe_aluminosilicate	46	238	251	190	49	119	70	144	127	39	9	10	6
Mg_Fe_phase	3	1	0	0	0	0	5	4	3	7	6	2	7
Mg_Fe_Silicate	8	1	0	2	0	3	0	3	5	1	4	0	1
Mg_phase	0	1	0	1	0	0	2	3	1	1	1	0	0
Mg_silicate	1	15	11	9	3	7	8	7	4	5	0	2	4
Mn_phase	0	1	0	0	0	0	0	0	0	0	0	0	0
Na_K_Ca_S_Cl	5	1	5	0	2	0	6	2	5	2	3	0	2
Na_P_phase	0	0	0	0	1	0	0	0	0	0	0	0	0
NaCl	1	0	1	0	0	0	0	6	0	0	0	0	2
Ni_phase	7	0	1	0	0	1	0	1	1	1	0	0	6
P_phase	1	0	0	0	0	0	0	0	0	0	0	0	0
REE	0	0	0	0	0	0	0	0	1	0	0	0	0
S_phase	0	0	1	0	0	0	0	0	0	0	0	0	0
Silica	226	59	45	70	24	79	35	60	58	69	30	31	54
Silica_mix	101	24	16	20	3	30	12	30	17	17	5	9	2
Sn_phase	1	0	0	0	51	4	1	1	5	2	2	14	12
Ti_Fe_oxide	0	4	0	1	0	0	1	1	1	3	8	0	2
Ti_Fe_oxide_mix	1	6	0	1	0	0	0	0	1	2	0	0	0
Ti_oxide	29	25	8	10	6	13	6	13	12	42	28	7	9
Ti_oxide_mix	23	22	18	13	6	10	6	19	12	33	36	2	2
Titanite	0	2	0	2	0	2	2	2	1	3	0	0	0
Zr_phase	2	0	1	2	1	0	0	3	0	2	1	0	0

Table 1. ICP-MS results from lungs of mice instilled with PM from Iraq, Afghanistan, or China Lake and the digested with H_2O_2 prior to analysis.

We have completed experiments examining the effects of *in vitro* exposure to particulate matter on fibrogenic gene expression in primary human alveolar macrophages isolated from the lungs or organ donors not used for transplant. We used RNASeq to quantify the fibrogenic gene expression in these alveolar macrophages exposed to particulate matter from Afghanistan and Iraq. These experiments were also supported in part by our other DoD grant: 'Mechanisms and Treatment of Deployment-Related Lung Injury: Repair of the Injured Epithelium' (W81XWH-16-2-0018; PR150109).

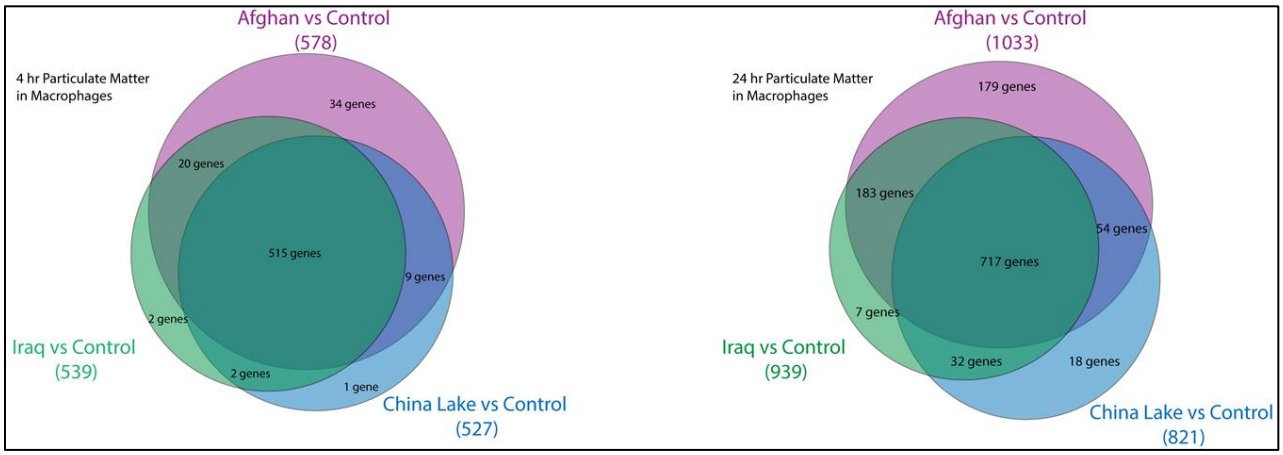

Figure 27. Analysis of differential gene expression in human primary alveolar macrophages exposed to PM (10 μg/cm^2) from Iraq, Afghanistan and California *in vitro*.

As illustrated in **Fig. 27**, exposure of human alveolar macrophages to PM from Iraq, Afghanistan, and China Lake induced differential expression of 500-1000 genes at 4 and 24 hr compared to control (saline). Of these genes, 515 were in common at 4 hr and 717 at 24 hr indicating common responses the PM independent of the geographic source of PM. By contrast, at 24 hr there were 179 unique genes expressed in response to PM from Afghanistan and 9 unique genes expressed in response to PM from Iraq.

Ingenuity Pathway Analysis revealed the macrophages responded to PM exposure by expression of a variety of acute inflammatory pathways including rheumatoid arthritis pathway (this is a pathway highly enriched in inflammatory signaling through IL-1β and TNFα) , TNFR1 and IL-6 signaling, acute phase response signaling (**Fig. 28**).

Figure 28. Pathway analysis of RNAseq using Ingenuity Pathway Analysis tool of differential gene expression in human primary alveolar macrophages exposed to PM (10 µg/cm^2) from Afghanistan *in vitro*.

Additional bioinformatics analysis revealed a strong signal in the NFκB pathway (**Fig. 29**) that is known to control signaling pathways involved on acute inflammatory responses and is a major target of glucocorticoids. This has important implications for potential therapeutic interventions for example with inhaled glucocorticoids that are currently used for a variety of human respiratory diseases such as asthma. We validated several of the genes most highly upregulated using qPCR to ensure that the signal in RNAseq was not an artifact.

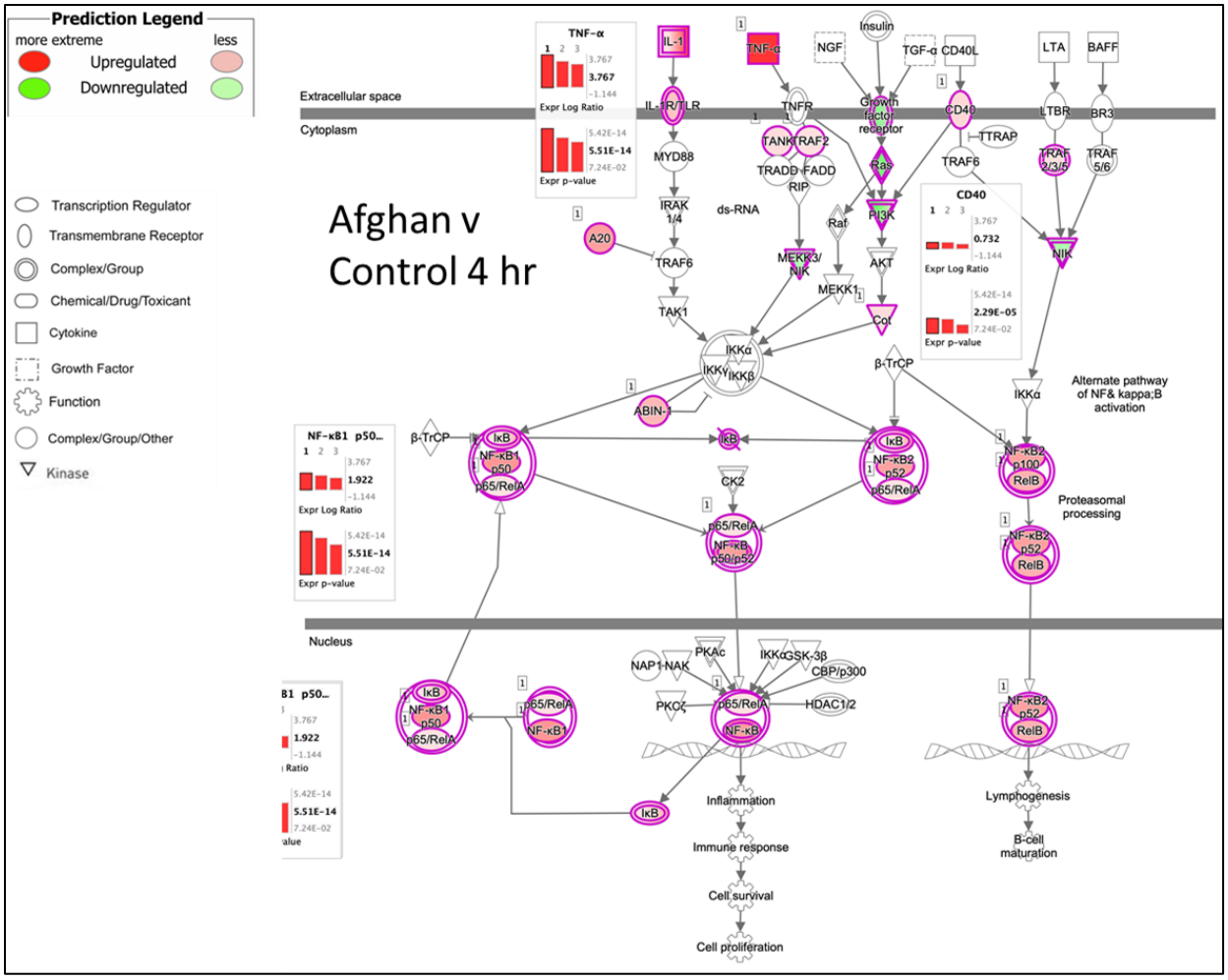

Figure 29. Pathway analysis of RNAseq using Ingenuity Pathway Analysis tool of differential gene expression in human primary alveolar macrophages exposed to PM (10 µg/cm^2) from Afghanistan *in vitro* reveals activation of the NFκB pathway that is a key controller of inflammation.

Subtask 5. Prepare and submit manuscripts for publication.

We have published two manuscripts to date:

1. Raeeszadeh-Sarmazdeh M, Greene KA, Sankaran B, **Downey GP**, **Radisky D**, Radisky Y. Directed evolution of metalloproteinase inhibitor TIMP-1 reveals cooperation between domains in matrix metalloproteinase recognition. J Biol Chem 2019;294(24):9476-9488. doi: 10.1074/jbc.RA119.008321

2. Garshick E, Abraham J, Baird C, Ciminera P, **Downey GP**, Falvo MJ, Hart JE, Jackson DA, Jerrett M, Kuschner W, Helmer DA, Jones KD, Krefft SD, Mallon T, Miller RF, Morris MJ, Proctor SP, Redlich CA, **Rose CS**, Rull, RP, Saers J, Schneiderman AI, Smith NL, Smith NL, Yiallouros P, Blanc PD. Respiratory Health after Military Service in Southwest Asia and Afghanistan. An Official American Thoracic Society Workshop Report. Ann Am Thorac Soc. 2019 Aug;16(8):e1-e16. doi: 10.1513/AnnalsATS.201904-344WS.

What opportunities for training and professional development has the project provided?

Dr. Maryam Raeeszadeh-Sarmazdeh, a postdoc in the E. Radisky laboratory working on the TIMP-1 engineering project, attended and her presented research at three conferences and has published one manuscript. Daniel Foster, a senior Research Associate in Dr. Downey's laboratory presented the bioinformatics analysis at the University of Colorado city-wide research rounds. Based on his interest in this area, Mr. Foster recently began his Ph.D. program in Toxicology at the University of Colorado Anschutz Campus.

How were the results disseminated to communities of interest?

Poster presentations and podium talks were presented at the annual MHSRS meetings in 2018 and 2019 in Orlando and Drs. Downey and Rose participated in a workshop at the annual meeting of the American Thoracic Society in 2018 on Deployment Lung Disease that lead to a publication in the Annals of the American Thoracic Society.

What do you plan to do during the next reporting period to accomplish the goals?

Nothing to report

4. IMPACT:

What was the impact on the development of the principal discipline(s) of the project?

We have demonstrated that exposure of mice to silicate-containing PM induces pulmonary fibrosis with initial inflammation in the terminal bronchioles and alveolar ducts followed by collagen deposition. We have demonstrated that human alveolar macrophages respond to inhaled particulate matter by producing an array of inflammatory and fibrogenic mediators that likely contribute to the respiratory symptoms and clinical illness frequently observed in military personnel previously deployed to Southwest Asia and Afghanistan.

What was the impact on other disciplines?

We have demonstrated the feasibility of engineering highly selective TIMP-based MMP inhibitors by yeast surface display. We expect this result to impact the field of protein engineering. Our efforts to uncover the sequence and structural determinants responsible for improvements in TIMP-1 selectivity will also impact the understanding of protein-protein interactions and binding specificity.

What was the impact on technology transfer?

Nothing to report

What was the impact on society beyond science and technology?

Nothing to report

5. CHANGES/PROBLEMS:

Changes in approach and reasons for change

Our method to expose mice to aerosolized silicate-containing PM or to purified silica resulted in low levels of inflammation and minimal fibrosis whereas bypass of the mouse nasopharynx using the technique of oropharyngeal aspiration to deliver materials directly to the lung results in in significant inflammation and fibrosis. Thus we have used oropharyngeal aspiration as our primary method of exposure. This has the advantage that the exposures can be done at our local institution instead of having to ship mice to and from Dayton, Ohio. We have also encountered difficulty in measuring the PM and metal content of lung tissue. In collaboration the US Geological Survey, we have developed novel ways to digest lung tissue using H_2O_2 that enables measurement of very low levels of particulates and metals in the lung.

Actual or anticipated problems or delays and actions or plans to resolve them

Transfer of funds from the DoD to NAMRU-Dayton was delayed both initially in 2016 and again in 2019. This led to short delays in obtaining local IACUC and then ACURO approval for the animal experiments involving inhalational exposure of mice to silicate-containing particulate matter (PM) and in conducting the experiments. We have now received funds and experiments have been completed.

Changes that had a significant impact on expenditures

The COVID-19 pandemic slowed down progress in the last 10 months. This was particularly severe for the studies with the US Geological Survey because their laboratories were either closed or on skeleton staffing for at least 6 months.

Significant changes in use or care of human subjects, vertebrate animals, biohazards, and/or select agents

Significant changes in use or care of human subjects

No significant changes

Significant changes in use or care of vertebrate animals.

No significant changes

Significant changes in use of biohazards and/or select agents

No significant changes

6. PRODUCTS:

- **Publications, conference papers, and presentations**

Journal publications.

1. Raeeszadeh-Sarmazdeh M, Greene KA, Sankaran B, Downey GP, Radisky D, Radisky E.S. Directed evolution of metalloproteinase inhibitor TIMP-1 reveals cooperation between domains in matrix metalloproteinase recognition. J Biol Chem 2019;294(24):9476-9488. doi: 10.1074/jbc.RA119.008321.

2. Garshick E, Abraham J, Baird C, Ciminera P, **Downey GP**, Falvo MJ, Hart JE, Jackson DA, Jerrett M, Kuschner W, Helmer DA, Jones KD, Krefft SD, Mallon T, Miller RF, Morris MJ, Proctor SP, Redlich CA, **Rose CS**, Rull, RP, Saers J, Schneiderman AI, Smith NL, Smith NL, Yiallouros P, Blanc PD. Respiratory Health after Military Service in Southwest Asia and Afghanistan. An Official American Thoracic Society Workshop Report. Ann Am Thorac Soc. 2019 Aug;16(8):e1-e16. doi: 10.1513/AnnalsATS.201904-344WS.

Books or other non-periodical, one-time publications.

Nothing to Report

Other publications, conference papers, and presentations.

1. Maryam Raeeszadeh-Sarmazdeh, Banumathi Sankaran, Derek C. Radisky, Evette S. Radisky. Structural Elucidation of Engineered Tissue Inhibitor of Metalloproteinases-1 (TIMP-1) Variants with Improved Binding Affinity toward Matrix Metalloproteinase-3 (MMP-3). ASBMB Annual Meeting, Orlando, FL, April 2019 (poster).
2. Maryam Raeeszadeh-Sarmazdeh, Matt Coban, Banumathi Sankaran, Radisky E.S. Structural elucidation of engineered tissue inhibitor of metalloproteinase -1 (TIMP-1) variants with improved binding affinity toward matrix metalloproteinase-3 (MMP-3). ACS Annual Meeting, Orlando, FL, April 2019 (oral presentation).
3. Maryam Raeeszadeh-Sarmazdeh, Matt Coban, Banumathi Sankaran, Radisky E.S. Directed evolution of the tissue inhibitor of metalloproteinases-1 (TIMP-1) scaffold for developing selective therapeutic agents. ACS Annual Meeting, Orlando, FL, April 2019 (poster and short talk).
4. Maryam Raeeszadeh-Sarmazdeh, Matt Coban, Banumathi Sankaran, Radisky E.S. Directed evolution of the metalloproteinase inhibitor TIMP-1 reveals cooperation between domains in matrix metalloproteinase recognition. Gordon Research Conference – Metalloproteases, Il Ciocco, Barga, Tuscany, Italy, May 2019 (poster).

- **Website(s) or other Internet site(s)**

Nothing to Report

- **Technologies or techniques**

We have developed and optimized protocols for selectivity screening of yeast surface displayed TIMP-1 libraries; this methodology will be shared in published research papers.

- **Inventions, patent applications, and/or licenses**

Nothing to Report

- **Other Products**

We have developed preclinical animal models of pulmonary fibrosis induced by exposure to silicate containing particulate matter that reflect deployment related exposures to military personnel.

7. PARTICIPANTS & OTHER COLLABORATING ORGANIZATIONS

What individuals have worked on the project?

Name:	Gregory Downey, MD
Project Role:	Principal Investigator
Researcher Identifier (e.g. ORCID ID):	0000-0003-3253-5862
Nearest person month worked:	1 (annually)

Contribution to Project: Dr. Downey is the PI at the National Jewish Site. as planned and overseen experiments including preclinical models of exposure to silicate-containing particulate matter.

Name:	Daniel Foster
Project Role:	Lab Researcher
Researcher Identifier (e.g. ORCID ID):	N/A
Nearest person month worked:	2 (annually year three)

Contribution to Project:

Name:	Geoffrey Plumlee
Project Role:	Site PI USGS
Researcher Identifier (e.g. ORCID ID):	N/A
Nearest person month worked:	<1 (annually)

Contribution to Project: Dr. Plumlee has been responsible for measurement of the particle size and content of silica and particulate matter from Iraq, Afghanistan and California.

Name: Heather Lowers
Project Role: Co-Investigator
Researcher Identifier (e.g. ORCID ID): N/A
Nearest person month worked: 1 month (annually)
Contribution to Project: This participant is responsible for sample handling and logistics, SEM analysis, XRD summary, particle size analysis, and report writing

Name: Bill Benzel
Project Role: Researcher
Researcher Identifier (e.g. ORCID ID): N/A
Nearest person month worked: 1 month (annually)
Contribution to Project: This participant is responsible for XRD analysis and particle size analysis

Name: Kate Campbell
Project Role: Researcher
Researcher Identifier (e.g. ORCID ID): N/A
Nearest person month worked: 1 month (annually)
Contribution to Project: This participant is responsible for sample handling and ICP-MS method development

Name: David Roth
Project Role: Researcher
Researcher Identifier (e.g. ORCID ID): N/A
Nearest person month worked: 1 month (annually)
Contribution to Project: This participant is responsible for ICP-MS method development and sample analysis

Name: Nour Hanandeh
Project Role: Contractor/Engineer
Nearest person month worked: 1 (annually)
Contribution to project: Operating wright dust feeder for generation/collection of sand/silica particles.

Name: Derek Radisky
Project Role: Partner PI
Researcher Identifier (e.g. ORCID ID):
Nearest person month worked: 2 (annually)
Contribution to Project: Dr. Downey is the partnering PI at the Mayo Clinic Jacksonville site. Dr. Radisky has been responsible for the planning and oversight of the experiments on the recombinant TIMP-1 variants.

Name: Evette S. Radisky
Project Role: Co-Investigator
Researcher Identifier (e.g. ORCID ID): N/A
Nearest person month worked: 1
Contribution to Project: Dr. E. Radisky supports the planning and execution of the recombinant TIMP-1 variants experiments.

Name: Maryam Raeeszadeh Sarmazdeh
Project Role: Postdoctoral Fellow
Researcher Identifier (e.g. ORCID ID): N/A
Nearest person month worked: 4
Contribution to Project: Performs TIMP selection, production, and characterization.

Name: Erin Miller
Project Role: Technician
Researcher Identifier (e.g. ORCID ID): N/A
Nearest person month worked: 1
Contribution to Project: Provides support for TIMP selection.

Name: Melody Stallings Mann
Project Role: Technician
Researcher Identifier (e.g. ORCID ID): N/A
Nearest person month worked: 1
Contribution to Project:

Has there been a change in the active other support of the PD/PI(s) or senior/key personnel since the last reporting period?

Nothing to report

What other organizations were involved as partners?

Organization Name: Mayo Clinic Jacksonville
Location of Organization: (if foreign location list country) Jacksonville, FL
Partner's contribution to the project (identify one or more) Partnering PI

- Dr. Radisky has been responsible for the design and generation of recombinant TIMP-1 variants.
- Dr. Radisky visited National Jewish Health on March 8, 2017 to discuss the project progress and future plans.

Organization Name: NAMRU Dayton
Location of Organization: (if foreign location list country) Dayton, Ohio
Partner's contribution to the project (identify one or more) Collaboration on inhalational toxicology

Organization Name: United States Geological Survey (USGS)
Location of Organization: (if foreign location list country) Reston, VA and Lakewood, CO
Partner's contribution to the project (identify one or more)

- The USGS has carried out mineralogical and particle size distribution analyses of the crystalline silica standard to be used in in vitro and in vivo tests by NJH
- The USGS is currently performing mineralogical and particle size distribution analyses of the Iraq dust sample to be used in in vitro and in vivo tests by NJH
- The USGS and NJH have worked together to develop a plan for chemical analyses of materials from *in vitro* dosing tests, to examine uptake of metals and other components from the dosing materials by the test cells.

8. SPECIAL REPORTING REQUIREMENTS

COLLABORATIVE AWARDS:

QUAD CHARTS:

Not applicable

9. APPENDICES:

AMERICAN THORACIC SOCIETY DOCUMENTS

Respiratory Health after Military Service in Southwest Asia and Afghanistan

An Official American Thoracic Society Workshop Report

Eric Garshick, Joseph H. Abraham, Coleen P. Baird, Paul Ciminera, Gregory P. Downey, Michael J. Falvo, Jaime E. Hart, David A. Jackson, Michael Jerrett, Ware Kuschner, Drew A. Helmer, Kirk D. Jones, Silpa D. Krefft, Timothy Mallon, Robert F. Miller, Michael J. Morris, Susan P. Proctor, Carrie A. Redlich, Cecile S. Rose, Rudolph P. Rull, Johannes Saers, Aaron I. Schneiderman, Nicholas L. Smith, Panayiotis Yiallouros, and Paul D. Blanc; on behalf of the American Thoracic Society Assembly on Environmental, Occupational and Population Health and the American Thoracic Society Environmental Health Policy Committee

This official workshop report of the American Thoracic Society was approved May 2019

Abstract

Since 2001, more than 2.7 million U.S. military personnel have been deployed in support of operations in Southwest Asia and Afghanistan. Land-based personnel experienced elevated exposures to particulate matter and other inhalational exposures from multiple sources, including desert dust, burn pit combustion, and other industrial, mobile, or military sources. A workshop conducted at the 2018 American Thoracic Society International Conference had the goals of: *1*) identifying key studies assessing postdeployment respiratory health, *2*) describing emerging research, and *3*) highlighting knowledge gaps. The workshop reviewed epidemiologic studies that demonstrated more frequent encounters for respiratory symptoms postdeployment compared with nondeployers and for airway disease, predominantly asthma, as well as case series describing postdeployment dyspnea, asthma, and a range of other respiratory tract findings. On the basis of particulate matter effects in other populations, it also is possible that deployers experienced reductions in pulmonary function as a result of such exposure. The workshop also gave particular attention to constrictive bronchiolitis, which has been reported in lung biopsies of selected deployers. Workshop participants had heterogeneous views regarding the definition and frequency of constrictive bronchiolitis and other small airway pathologic findings in deployed populations. The workshop concluded that the relationship of airway disease, including constrictive bronchiolitis, to exposures experienced during deployment remains to be better defined. Future clinical and epidemiologic research efforts should address better characterization of deployment exposures; carry out longitudinal assessment of potentially related adverse health conditions, including lung function and other physiologic changes; and use rigorous histologic, exposure, and clinical characterization of patients with respiratory tract abnormalities.

Keywords: deployment; particulate matter; constrictive bronchiolitis

Ann Am Thorac Soc Vol 16, No 8, pp e1–e16, Aug 2019

DOI: 10.1513/AnnalsATS.201904-344WS
Internet address: www.atsjournals.org

Contents

Overview

Land-based U.S. military personnel deployed to Afghanistan and Southwest Asia in support of military operations starting in 2001 experienced exposures to elevated levels of fine particulate matter (PM) as well as other, not well-characterized inhalational exposures, leading to concerns about potential adverse health effects (1). Workshop goals were to *1*) summarize and assess studies evaluating postdeployment respiratory health, *2*) update emerging research, and *3*) identify conflicting findings and knowledge gaps.

Iraq, Afghanistan, and other deployment locations include large arid and semiarid regions where there is frequent exposure to geologic dust (2, 3). Additional sources of PM include various military operations such as burn pit emissions from open-air waste burning, vehicular exhaust, and poorly regulated industrial point sources. The workshop reviewed epidemiologic studies analyzing health encounters during military service that have demonstrated increased deployment-associated encounters for respiratory symptoms and selected airway disease diagnoses (4–6). We also considered reports based on Veterans Health Administration (VHA) encounters for health care, suggesting that former deployers may be more frequently diagnosed with obstructive lung disease, particularly asthma (7). In addition, we reviewed case series describing the clinical assessment of postdeployment dyspnea, and we considered Millennium Cohort Study data relevant to postdeployment asthma as well as other abnormalities (8–10). Of particular note, constrictive bronchiolitis and other small airway abnormalities have been reported in lung biopsies from case referral series (11). Based on a review of the established pathologic features of constrictive bronchiolitis (12–14), opinions among workshop participants differed regarding the interpretation of the prevalence of disease reported.

On the basis of a review of the adverse health effects of exposure to particulate matter with an aerodynamic diameter <2.5 μm ($PM_{2.5}$) in general population studies (15, 16), the workshop concluded that it was plausible that deployers could have experienced particulate exposure–associated decrements in pulmonary function. It was recognized, however, that there have been no findings to date assessing long-term health effects in cohorts of U.S. military personnel exposed to high ambient $PM_{2.5}$ concentrations. The workshop was updated on ongoing research projects. The Department of Veterans Affairs (VA) Cooperative Studies Program is using National Aeronautics and Space Administration (NASA) satellite data and airport visibility data (17, 18) to estimate historical $PM_{2.5}$ concentrations and assess associations with pulmonary function and current asthma in a national cohort of veteran deployers. The Department of Defense (DoD) Serum Repository, which includes 60 million samples, may serve as a supplemental means to identify chemical compounds associated with combustion product–related environmental exposures (19). Prospective cohort studies (the Millennium Cohort Study [20] and a planned Comparative Health Assessment Interview Research Study) and follow-up of participants enrolled in the Airborne Hazards and Open Burn Pit Registry also may provide additional information regarding the development of deployment-related health conditions. Another study, based at National Jewish Health (NJH), assessing molecular effects of desert dust exposure in Southwest Asia may provide information regarding biologic mechanisms.

Key Conclusions

- Deployed military personnel were exposed to ambient PM and other air pollutants, with contributions from

ORCID IDs: 0000-0001-5931-5638 (E.G.); 0000-0001-9011-6098 (J.H.A.); 0000-0002-8024-9230 (C.P.B.); 0000-0003-3253-5862 (G.P.D.); 0000-0001-9348-6676 (M.J.F.); 0000-0002-0826-1163 (J.E.H.); 0000-0001-9263-6011 (D.A.J.); 0000-0002-9732-1366 (W.K.); 0000-0003-0385-432X (D.A.H.); 0000-0002-0275-3503 (K.D.J.); 0000-0003-4808-3549 (S.D.K.); 0000-0002-3312-5737 (T.M.); 0000-0002-6801-6506 (R.F.M.); 0000-0001-6486-6725 (C.A.R.); 0000-0002-8190-9886 (C.S.R.); 0000-0002-0181-5979 (J.S.); 0000-0002-5596-5040 (A.I.S.); 0000-0002-8339-9285 (P.Y.); 0000-0001-9043-175X (P.D.B.).

An Executive Summary of this document is available at http://www.atsjournals.org/doi/suppl/10.1513/AnnalsATS.201904-344WS.

The views expressed in this article are those of the authors and the contents do not represent the views of the U.S. Department of Veterans Affairs, the U.S. Department of Defense, the United States Army, or the United States government.

Correspondence should be addressed to Eric Garshick, M.D., M.O.H., Pulmonary, Allergy, Sleep, and Critical Care Medicine Section, VA Boston Healthcare System, 1400 VFW Parkway, West Roxbury, MA 02132. E-mail: eric.garshick@va.gov.

a variety of sources, including geologic dust; mobile and stationary sources; industrial sites; and various military operations, including burn pits.
- Studies of deployed military personnel reported to date have not included consistent assessment of self-reported or other estimated exposures potentially relevant to adverse respiratory effects.
- Findings derived from epidemiologic studies conducted in nonmilitary populations raise concern about the potential adverse effects of PM exposure on pulmonary function in deployers.
- On the basis of military health encounter data, returning military personnel had more frequent postdeployment health encounters than nondeployed personnel for respiratory symptoms and for airway disease, predominantly asthma.
- Postdeployment asthma has been described in case series and among deployers assessed in the Millennium Cohort Study (U.S. DoD).
- Other respiratory health conditions, including constrictive bronchiolitis and other small airway abnormalities, have been described in case series.
- Workshop participants had heterogeneous views regarding the interpretation of histologic changes of constrictive bronchiolitis and other small airway findings derived from case series of veterans undergoing lung biopsy for postdeployment dyspnea.
- There is a paucity of information regarding the long-term respiratory health status of postdeployment active military personnel and veterans.
- There is a need for further research better characterizing PM and other deployment-related exposures, to better characterize the respiratory health of postdeployment military personnel and veterans, and to identify associations between such exposures and adverse respiratory health outcomes.

Introduction

Since October 2001, more than 2.7 million U.S. military personnel have been deployed to Central Asia (Afghanistan and Kyrgyzstan), Southwest Asia (Iraq, Kuwait, Qatar, and United Arab Emirates), and Africa (Djibouti) in support of Operation Enduring Freedom (OEF), Operation Iraqi Freedom (OIF), Operation New Dawn, and continuing operations (21). Land-based personnel deployed to these countries experienced potential exposures to elevated concentrations of fine PM and other pollutants, leading to concerns about possibly associated adverse health effects.

The American Thoracic Society (ATS) sponsored an all-day workshop, titled "Respiratory Health after Military Service in Southwest Asia and Afghanistan," that took place at the 2018 ATS International Conference in San Diego, California. The workshop was initiated, in part, in response to reports of an increased prevalence of respiratory symptoms and lung disease among postdeployment veterans. In particular, reported findings of lung biopsy–defined constrictive bronchiolitis in symptomatic veterans have raised concern about a possible newly emerging pattern of lung injury in this population. Workshop goals were to *1*) summarize and critically assess published data relevant to postdeployment respiratory health, *2*) provide an update on emerging research on this question, and *3*) identify knowledge gaps that could be addressed by future research.

Understanding the nature of deployment-associated inhalational exposures and their potential adverse respiratory health effects among veterans is relevant not only to VA providers but also to the wider healthcare community, because many veterans receive medical care outside the VHA. Approximately 40% of veterans are enrolled in VA healthcare programs, and only 65% of those access care in a given year (22). Moreover, the proportion of veterans who receive care outside the VHA is likely to increase with new VA policy initiatives encouraging community-based care. Thus, non-VHA providers are very likely to encounter patients with prior deployment-associated exposures who are experiencing potentially related adverse respiratory health effects.

Methods

A cross-disciplinary group of 25 experts representing a range of perspectives and viewpoints participated in the workshop. Participants represented the disciplines of pulmonary medicine, occupational and environmental medicine, medical pathology, epidemiology and biostatistics, respiratory physiology, and translational and laboratory-based research. Areas of specific expertise included air pollution exposure assessment, geographic information systems, lung pathology, exercise physiology, survey research methodology, and epidemiologic study design and analysis. Institutional backgrounds included academic medical centers, the VA (including VHA and VA medical centers), and the DoD.

There were 16 invited oral presentations. These presentations included the following:

1. A review of surveys and epidemiologic studies performed among previously deployed military personnel, including non–U.S. military personnel;
2. A summary of clinical data reported for previously deployed military personnel, including veterans treated in the VHA;
3. A review of lung pathologic findings in postdeployment personnel, including biopsies interpreted as showing constrictive bronchiolitis;
4. A review of airborne pollution exposures that might occur during deployment and their potential adverse respiratory health effects, including dust storms and other sources of PM such as burn pits and other military activities;
5. An update on novel approaches to exposure assessment, including estimation of PM exposures using satellite technology and the use of biobanked DoD serum samples to assess biomarkers of exposure; and
6. A description of other ongoing or planned relevant studies.

There were group discussions with all panelists after each presentation or main topic and a final overarching discussion of the workshop findings as a whole. After the workshop, each speaker provided their presentation materials (typically the set of slides shown), supplementing this with a written summary and references when appropriate. A writing committee composed of a subset of workshop participants reviewed a summary of the presentations. This summary underwent editing and was circulated to all participants for further comment. Potential conflicts of interest of all participants were disclosed before the

workshop and updated before this publication. Conflict of interest disclosures were managed according to the policies and procedures of the ATS.

Exposure Overview

Exposure Assessment

Iraq, Afghanistan, and other deployment locations include large arid or semiarid regions where there is frequent exposure to desert dust and sand, including from frequent dust storms (23–25). In addition to mineral particles, dust storm particles include airborne bacteria, fungal spores, plant and grass pollens, and other agricultural pollen grains (26, 27). Additional sources of PM include military operations, vehicle exhaust, and underregulated industrial sources. Open-air waste burning (burn pits) was the primary means of solid-waste management at military bases in Iraq, Afghanistan, and Djibouti that also contributed to potential exposures (1). Materials burned included plastics, metals, wood, and numerous other combustible materials. To assess exposure levels, the DoD conducted the Enhanced Particulate Matter Surveillance Program (EPMSP) to characterize airborne exposures at 15 sites, mainly in Iraq and Afghanistan and mainly during 2006 and 2007 (3, 28). These efforts were difficult in an active war zone, and only a small number of samples at each site were collected. For example, sampling occurred approximately four times per month at each location for $PM_{2.5}$, raising concerns regarding the accurate assessment of exposure variability. In addition, the equipment was not designed to collect PM during the highest exposure days (including dust storms), a limitation that would have resulted in the overloading of the sampler particle impaction surface, leading to sampling error. Recognizing these limitations, the mean 24-hour $PM_{2.5}$ values observed were consistently high at each site (~40 $\mu g/m^3$ to nearly 120 $\mu g/m^3$) (Figure 1) with concentrations that considerably exceeded the current U.S. annual $PM_{2.5}$ exposure standard (12 $\mu g/m^3$), the 1-year military exposure guideline (solid blue line in Figure 1), and the 24-hour U.S. Environmental Protection Agency National Ambient Air Quality Standard (35 $\mu g/m^3$; dashed blue line in Figure 1).

Other exposure estimates indicated similarly elevated $PM_{2.5}$ concentrations. For example, in daily sampling conducted in Kuwait City in 2004–2005 using equipment suitable for a desert environment, the annual average $PM_{2.5}$ value was 53 $\mu g/m^3$ (2, 29), within the range of mean $PM_{2.5}$ concentrations found by EPMSP. As noted in this document (*see below* and Figure 2), the $PM_{2.5}$ levels estimated based on military airport visibility data in Iraq, Afghanistan, Kuwait, and other countries in Southwest Asia (18) were also similar to the EPMSP concentrations.

Institute of Medicine Report

There has been considerable discussion regarding the potential for adverse health effects of burn pit emissions, given the often-continuous combustion of military base waste. In 2006, 2007, and 2009, multiple air samples were collected by the U.S. Army at Joint Base Balad, the site of the largest burn pit in Iraq (30). $PM_{2.5}$ concentrations upwind and downwind of the burn pit were similar, indicating that off-base sources (representing ambient $PM_{2.5}$) significantly contributed to on-base exposures. Before the publication of subsequent studies reviewed at the workshop, the Institute of Medicine (IOM; currently the Health and Medicine Division of the National Academies of Sciences, Engineering, and Medicine) was charged by the VA with assessing whether burn pit–related exposures could contribute to long-term health effects after deployment. The 2011 IOM report titled "Long-Term Health Consequences of Exposure to Burn Pits in Iraq and Afghanistan," noted that "a broader consideration of air pollution than exposure only to burn pit emissions–might be associated with long-term health effects, particularly in highly exposed populations (such as those who worked at the burn pit) or susceptible populations (for example, those who have asthma), mainly because of the high ambient concentrations of PM from both natural and anthropogenic, including military, sources" (1). The conclusions of this IOM report support the importance of considering the occurrence of health effects from all sources that jointly contribute to the high PM concentrations and also other pollutants. As an example of the contribution of multiple sources to ambient $PM_{2.5}$, a source apportionment study from Kuwait estimated contributions of 54% from sand dust, 18% from oil combustion, 12% from the petrochemical industry, 11% from traffic, and 5% from other anthropogenic sources (2).

Findings derived from the EPMSP also indicate that multiple sources contribute to ambient PM exposures experienced during

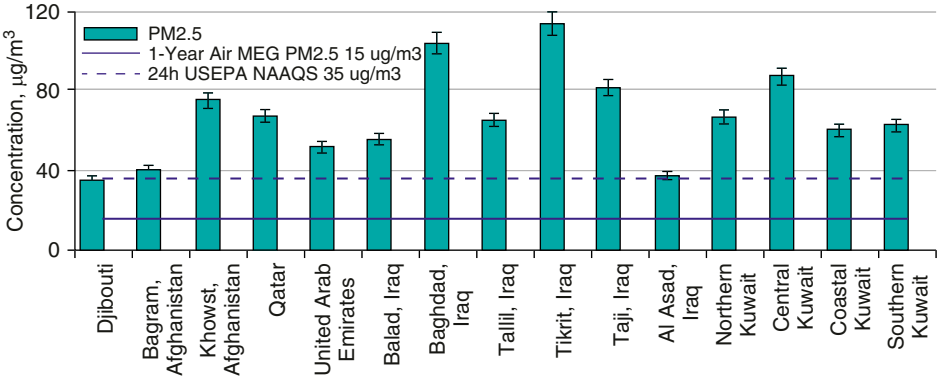

Figure 1. Mean particulate matter with an aerodynamic diameter less than or equal to 2.5 μm ($PM_{2.5}$) concentrations at 15 sites in Iraq, Afghanistan, Kuwait, and other sites in 2006 and 2007 (28). MEG = military exposure guideline; NAAQS = National Ambient Air Quality Standards; USEPA = U.S. Environmental Protection Agency.

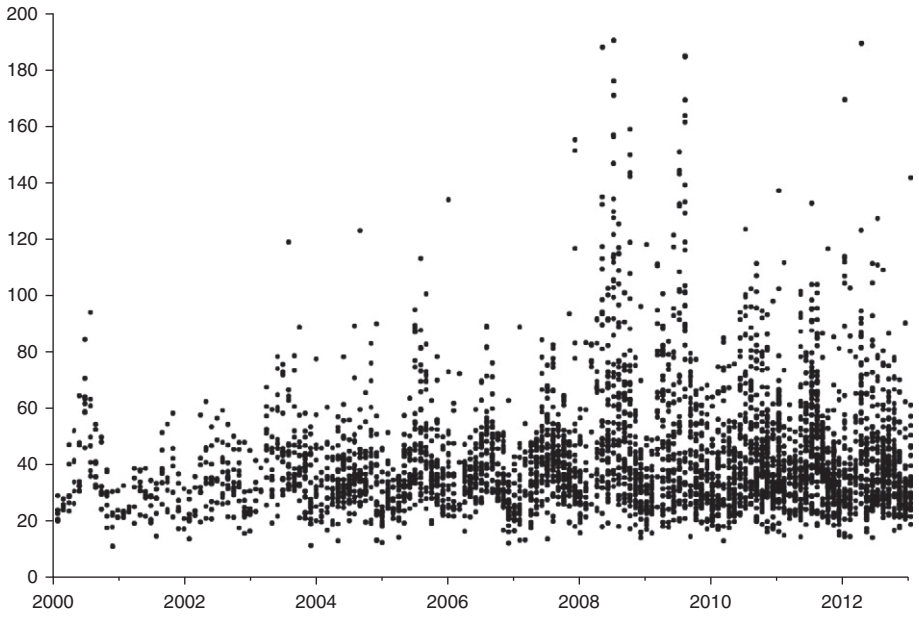

Figure 2. Monthly predictions of particulate matter with an aerodynamic diameter less than or equal to 2.5 μm in μg/m^3 (*y*-axis) by year (2000–2012) for sites in Afghanistan, Iraq, Kuwait, Kyrgyzstan, United Arab Emirates, Djibouti, and Qatar, based on military airport visibility data. Reprinted from Reference 18 by permission of Air & Waste Management Association, www.awma.org.

deployment (3). In addition to PM mass, the EPMSP characterized PM composition by conducting energy-dispersive X-ray fluorescence spectrometry for trace elements and scanning electron microscopy for particle filter samples. The major portion of PM was of geologic origin from local soils (31). Analysis also identified the contribution of industrial sources to PM that varied by location, such as lead, zinc, and other metals from nearby smelters and battery manufacturing, as well as from transportation activities, in particular due to the use of leaded gas. Carbon particles in samples were consistent with contributions from mobile and stationary combustion sources, including burn pits (1). At Joint Base Balad, polychlorinated dibenzo-*para*-dioxin/furans, polycyclic aromatic hydrocarbons, and volatile organic compounds were detected in both upwind and downwind air samples (1). The polycyclic aromatic hydrocarbon and volatile organic compound concentrations attributable to regional background sources, transportation emissions, and power generation were similar to concentrations noted in polluted environments outside the United States. The polychlorinated dibenzo-*para*-dioxin/furans concentrations were low and interpreted as most likely being attributable to burn pit emissions.

Effects of Desert Dust on Respiratory Illness

Despite the frequent occurrence of dust storms and the significant contribution of desert dust to ambient PM in the deployment region, a review of existing health studies presented at the workshop identified no large-scale epidemiologic studies assessing the cumulative effect of PM on pulmonary function or on risk of asthma or other chronic pulmonary diseases among exposed populations, although a few observational reports were available for review (P. Yiallouros, workshop presentation). Reports of adverse effects of dust storms on health have focused primarily on the description of short-term (acute and subacute) adverse respiratory effects. The first report of adverse effects of exposure to dust was reported in 1935 in response to a period of severe dust storms during the Dust Bowl period in the United States in Kansas, Colorado, New Mexico, Oklahoma, and Texas (32). These states experienced an increase in death rates attributable to acute respiratory infections, including bronchitis and pneumonia.

More recent studies have confirmed that desert dust exposures may have acute adverse health effects, both respiratory and nonrespiratory. There have been associations reported between desert dust events and increases in mortality of nonaccidental causes (33–35), cardiovascular mortality (36, 37), and respiratory mortality (38, 39). In Kuwait, dust storms also have been associated with emergency hospital admissions for asthma and for all respiratory causes; the association was strongest in children but also included adults (40). In studies that included younger adults of age comparable to that of deployed military personnel, days of desert dust exposure was associated with more emergency room visits for asthma and all respiratory causes in Athens (41); more asthma hospitalizations in El Paso, Texas (42); and an increase in asthma symptom scores in Japan resulting from transcontinental transport of dust (43). Desert dust also has been associated with more clinic visits for allergic rhinitis during dust storm events (44) and more allergic symptoms (45). Others have reported associations with respiratory infections, including hospital admissions for pneumonia (46–48) and chronic obstructive pulmonary disease (COPD) exacerbations (49, 50). Because dust storms include some quartz particles, it has been suggested that chronic exposure may result in nonoccupational silicosis on the basis of findings from surveys conducted in Himalayan villages (51, 52) and autopsy studies in Bedouins from the Negev region of Israel (53).

Surveys of military personnel that were conducted immediately after leaving deployment suggest that personnel could have experienced acute respiratory effects similar to those in the desert dust–exposed cohorts described above. Sanders and coworkers (54) surveyed 15,459 U.S. military personnel who had deployed to Iraq or Afghanistan during 2003–2004. Respiratory illnesses were reported by 69%. Of those with respiratory illness, 23% reported an allergy attack, 17% sought medical care, and 3.6% reported an asthma attack. In another survey conducted between April and July 2003, 95% of 1,250 consecutive service members returning from deployment completed a questionnaire assessing respiratory health retrospectively (55). The self-reported prevalence of wheezing in persons without a history of asthma was 19% during deployment compared with 6% before deployment, and it was 51% during deployment in persons with a history of asthma compared with 40% before deployment. Allergy symptoms,

defined as sneezing, rhinitis, or eye irritation, were reported by 55% of those without asthma during deployment compared with 27% before deployment, and they were reported by 62% among those with asthma during deployment compared with 44% before deployment. Surveys of Polish troops serving in Afghanistan also demonstrated high rates of acute respiratory illness (56, 57). A study of Soviet troops during the 1979–1989 war in Afghanistan found that 43% of service personnel had bronchitis and/or pneumonia within the first year of service in Afghanistan (58).

$PM_{2.5}$ and Long-Term Pulmonary Health Effects in Nonmilitary Cohorts

Population-based epidemiologic studies assessing exposure to ambient $PM_{2.5}$ have demonstrated that chronic exposure (10–14 yr in duration) at concentrations lower than those experienced during deployment results in reduced pulmonary function assessed by spirometry. These studies include the Framingham Heart Study in the United States (15) and the Taiwan MJ Cohort Study (16), in which $PM_{2.5}$ concentrations were estimated retrospectively at the participant's home address using aerosol optical depth (AOD) data available from NASA satellites. AOD is a measure of light extinction by particles in the atmosphere that can be calibrated using ground stations to estimate ground-level $PM_{2.5}$ (59–61). In the Taiwan MJ Cohort Study, there also was an increased risk of incident COPD attributable to greater exposure (16). Other cohort studies conducted in North America and Europe also suggest an association between ambient air pollution and the development of COPD (62–64). Small airway structural changes have also been described in association with ambient pollution in a comparison of lungs obtained at autopsy from nonsmoking Mexico City (high ambient air pollution) residents without lung disease and from Vancouver (low ambient air pollution) residents. The Mexico City residents had more fibrous tissue and smooth muscle in small airway walls (65).

The findings of these epidemiologic studies are consistent with the conclusions of the 2011 IOM report that considered the potential effects of exposure to burn pit emissions by reviewing effects in surrogate groups that included firefighters and incinerator workers (1). The IOM concluded that there was limited/suggestive evidence of an association between exposure to combustion products and long-term effects causing reduced pulmonary function. The IOM did not address the risk of asthma, but it considered those with preexisting asthma to be a susceptible subgroup. In contrast to studies demonstrating effects on pulmonary function, there is weaker evidence of an association between chronic PM exposure and new-onset asthma in adults (66–69).

An additional consideration that may impact health effects is the typical age of deployment at which military personnel are likely to be exposed to high concentrations of PM. As demonstrated by National Health and Nutrition Examination Survey data, lung growth as assessed by forced expiratory volume in 1 second (FEV_1) occurs through the mid-20s (70). Exposure to particulate pollution during periods of lung growth in children reduces their maximally attained FEV_1 (71). It is not known whether soldiers exposed to high concentrations of PM during their late teenage and early adult years are also more susceptible to adverse respiratory effects, given that they have not yet achieved their maximal FEV_1. It has been recognized that a lower FEV_1 in early adulthood is a risk factor for the development of future COPD (72). There is no comparable literature assessing pulmonary function in populations similar to previously deployed veterans who experienced high PM exposures over a relatively short duration based on total deployment time (typically lasting several months to several years among Southwest Asia and Afghanistan deployers, with an estimated mean [standard deviation (SD)] of 10.6 [6.6] mo) (E. Garshick, workshop presentation of unpublished data).

Epidemiologic and Observational Studies in Previously Deployed Military Personnel

DoD Healthcare Encounters

Asthma diagnosed at any age previously had been cause to be medically disqualified from enlistment in the U.S. military, although persons could apply for a medical waiver. Between 1997 and 2002, 15% of all U.S. Army medical waivers were for asthma. In 2004, the standards were relaxed to medically disqualify persons with asthma from military service only if diagnosed and symptomatic after age 13 (73, 74). Once in the military, persons are provided asthma medications if required, and fitness for duty is assessed on the basis of their ability to serve in their unit. It is likely that, since 2004, policy changes resulted in persons with a history of childhood asthma more likely to be inducted into the military and deployed.

Investigators from the U.S. Army Public Health Command reviewed clinical encounters using *International Classification of Diseases, Ninth Revision* (ICD-9), codes to categorize respiratory health–related conditions before and after deployment. Analysis of these data indicated a postdeployment increase in encounters for respiratory symptoms and obstructive lung diseases, predominantly asthma (4–6). In U.S. military personnel deployed as of December 31, 2005, pre- and postdeployment medical encounter rates 6 months before and 6 months after deployment were compared (4). Rates of encounters for asthma/COPD and allied conditions (ICD-9 codes 490–496) were significantly increased after deployment (rate ratio, 1.25; 95% confidence interval [CI], 1.13–1.39), although there was not a step-up in risk with multiple deployments. Respiratory symptom rates (ICD-9 code 786) also increased after deployment.

In another report (5), rates of respiratory encounters in U.S. Air Force and U.S. Army personnel deployed between 2005 and 2007 to two sites in Iraq with burn pits (Joint Base Balad and Taji) and two sites in Kuwait without burn pits were compared over up to 4 years, with further comparison with U.S.-based troops eligible for deployment but not deployed. Individuals with previous asthma or COPD encounters were excluded from the analysis. Adjusted for age, sex, and rank, rates for respiratory symptoms (ICD-9 code 786) and for asthma (ICD-9 code 493) were significantly elevated among the deployed compared with the nondeployed, with relative risks (RRs) of 1.25 (95% CI, 1.20–1.30) and 1.54 (95% CI, 1.33–1.78), for symptoms and asthma, respectively. There was no significant difference, however, in risk when individuals deployed to locations in Southwest Asia with and without burn pits were compared. In another study, personnel deployed to Kabul (Afghanistan) were

followed for up to 12 years after deployment (6). Compared with nondeployed U.S. personnel, deployment to Kabul was associated with more encounters for respiratory symptoms (RR, 1.54; 95% CI, 1.43–1.62) and asthma (RR, 1.61; 95% CI, 1.22–2.12), adjusted for covariates including age, sex, race, and rank. These associations were not observed for deployment to Kyrgyzstan or Bagram Air Base (Afghanistan) for asthma, although Bagram deployers had a higher risk of respiratory symptom encounters than nondeployed U.S. personnel (RR, 1.12; 95% CI, 1.05–1.19). The findings of this study support an interpretation that the effects of deployment may vary on the basis of ambient PM and other related exposures, a concern raised in light of relatively high levels of air pollution in Kabul (6).

VHA Healthcare Encounters

In an assessment of asthma prevalence among returning troops, Szema and colleagues (75) reviewed the records of U.S. soldiers discharged from military service and examined between March 2004 through May 2007 at the Northport VA Medical Center. They found that 61 of 920 (6.6%) soldiers deployed to Iraq or Afghanistan had been diagnosed with asthma. This rate was higher than that of soldiers who remained in the United States (age and sex adjusted odds ratio [OR], 1.88; 95% CI, 1.38–2.56). In a follow-up study, record review through 2010 noted an asthma diagnosis in 6.2% of previous deployers compared with 0.7% of nondeployed personnel in an analysis unadjusted for other factors that may have influenced asthma rates (76). Among deployers receiving VHA health care nationally from October 2002 through September 2011, the prevalence of encounters for chronic lung disease increased (7). During that time, 760,621 previously deployed veterans received VHA care, and 4.5% ($n = 34,228$) had at least one diagnosis of chronic lung disease, including COPD (0.8%), asthma (3.4%), or interstitial lung disease (0.3%). In analyses adjusting for demographics, multiple deployments, surrogates of tobacco use (i.e., smoking cessation treatment), and traumatic brain injury diagnosis, there was a statistically significant increased prevalence of asthma and COPD through 2011. In contrast, interstitial lung disease prevalence remained stable during this period. Factors associated with any of the three lung disease diagnoses included proxies for both tobacco use and traumatic brain injury (as a surrogate for blast injury). In contradistinction to these studies among veterans, rates of asthma and chronic bronchitis among active duty personnel decreased over the same time period (2001–2013) (77).

In another VA-based study of respiratory diagnoses, in which VHA medical records between 2001 and 2010 were used, deployed U.S. veterans who sought VHA care within 1 year of their last deployment and who had at least encounters per year for a minimum of 2 years were analyzed (78). The respiratory diagnoses studied were similar to those examined by Pugh and colleagues (7), but they also included codes for nonspecific respiratory encounters. Overall, 182,338 Iraq/Afghanistan veterans met inclusion criteria, of whom 14% had a respiratory diagnosis. Approximately 77% of veterans with a respiratory diagnosis also had a comorbid mental health diagnosis. A mental health diagnosis within the first year after deployment was associated with report of a respiratory diagnosis over 5 years of follow-up, adjusting for multiple demographic factors, multiple deployments, and tobacco use proxies (OR, 1.41; 95% CI, 1.37–1.46). Specific diagnoses with a statistically significant association included acute and chronic bronchitis (OR, 1.39; 95% CI, 1.21–1.60) and asthma (OR, 1.16; 95% CI, 1.08–1.25).

Prospective Cohort Studies

The Millennium Cohort Study was established by the DoD to prospectively study the short- and long-term self-reported health effects of military service and has since become the largest and longest-running health study in military history (20). Compared with 46,077 participants from the first enrollment panel who completed baseline questionnaires in 2001–2003, subsequent deployed persons more frequently self-reported respiratory symptoms (surveyed 2004–2006) than did nondeployers (14% vs. 10%) (79). Symptoms were defined by self-reported persistent or recurring cough or shortness of breath. Increased symptom reporting was not associated with sea-based deployment (i.e., U.S. Navy personnel would have had lower PM exposures when at sea). Compared with nondeployers, deployed personnel from the U.S. Army (OR, 1.73; 95% CI, 1.57–1.91) and the U.S. Marine Corps (OR, 1.49; 95% CI, 1.06, 2.08) had increased odds of symptom reporting, adjusted for smoking, age, rank, sex, military occupation, and education. Among U.S. Army personnel, the odds of respiratory symptoms also increased with deployment length. In a subsequent analysis of U.S. Army and U.S. Air Force deployers participating in the Millennium Cohort Study, deployment to a location near a burn pit, defined as a 3- or 5-mile radius (both were examined) from a burn pit, at three locations in Iraq was not statistically associated with new-onset respiratory symptoms (80). There was also no statistical association in this analysis with self-reported incident asthma, chronic bronchitis, or emphysema. Subsequent and longer follow-up of a larger number of Millennium Cohort Study participants followed through 2013 ($n = 77,770$) revealed an increased risk of respondent-reported new onset of health professional–diagnosed asthma for those with deployment-related combat experience compared with those who did not deploy (9). The RR of new-onset asthma was similar for men (RR, 1.30; 95% CI, 1.14–1.47) and women (RR, 1.24; 95% CI, 1.05–1.46) after adjustment for multiple covariates that included smoking, body mass index (BMI), rank, branch, and post-traumatic stress disorder status. There was no association with multiple deployments or deployment duration, and there was no increase in asthma in persons deployed but not in combat. Explanatory factors for the observed differences associated with combat experience were not identified in the study. Additional analyses of Millennium Cohort data based on deployment proximity to burn pits are in progress, including updated assessments of postdeployment asthma, COPD, and respiratory symptoms (R. P. Rull, workshop presentation of unpublished data).

The VA Post Deployment Health Services Epidemiology Program has conducted the Health Study for a New Generation of US Veterans, reporting on 20,563 OEF/OIF veterans who replied to a 2009–2011 survey eliciting a history of self-reported, physician-diagnosed asthma, sinusitis, and bronchitis (81). Adjusted for birth year, sex, service branch, unit component, race/ethnicity, education, and smoking status, the prevalence of asthma and bronchitis diagnosed after 2001 (the period of U.S. involvement in Southwest

Asia and Afghanistan) among the deployed veterans and nondeployed veterans was not significantly different. Deployed veterans, however, were more likely to report sinusitis (OR, 1.30; 95% CI, 1.13–1.49). The VA Post Deployment Health Services Epidemiology Program has completed data collection for a new epidemiologic study called the Comparative Health Assessment Interview Research Study. This study includes a population sample of 15,172 OEF/OIF/Operation New Dawn veterans, both deployed and nondeployed, and 4,654 civilians to assess a variety of health outcomes. The study plans to report on the prevalence of asthma and other lung diseases as well as to assess information on respiratory exposures from military, deployment, and occupational settings (A. I. Schneiderman, workshop presentation of unpublished data).

European Studies

A retrospective questionnaire-based study of Swedish military personnel who served primarily in Afghanistan (2008–2009) and who were surveyed 36 months to 5 years later found an increased prevalence of wheeze, wheeze without a cold, nocturnal coughing, and chronic bronchitis among soldiers compared with a referent group of civilians (82). A statistically significant relationship was found between months spent in a desert environment and wheeze, wheeze with breathlessness, and wheeze without a cold. Exposure to dust storms was also associated with report of nocturnal cough and chronic bronchitis. Studies of respiratory illness among Polish and Russian military personal soldiers while in service were cited previously (56–58), but there does not appear to be published data on postdeployment follow-up among these cohorts.

Findings in Clinical Assessments of Previously Deployed Military Personnel and Veterans

Four centers that regularly evaluate veterans and military personnel after deployment have published their clinical findings. These centers are the VA War Related Illness and Injury Study Center (WRIISC), NJH, Brooke Army Medical Center and other military medical facilities, and Vanderbilt University Medical Center. Their reported findings are summarized below.

Asthma and Airway Diseases

Assessment of active duty personnel and veterans at these four centers demonstrated that results of postdeployment spirometry were usually normal and that the most common specific diagnoses were asthma and nonspecific airway hyperresponsiveness. The VA WRIISC is a VHA national referral program (83) that provides comprehensive clinical evaluations of U.S. veterans with postdeployment health concerns. Among 124 veterans referred for evaluation to the New Jersey (NJ) WRIISC (both with and without respiratory symptoms), 26% had a positive bronchodilator response measured in spirometry. This was positively associated with deployment length, adjusted for smoking history (84). In a subsequent description of 138 veterans evaluated at the NJ WRIISC, 74.6% had normal pulmonary function, 19.6% had an obstructive deficit, and 5.8% had a restrictive deficit. These data, however, were not analyzed in regard to smoking history, BMI, clinical history, or the presence of respiratory symptoms (85).

At NJH, among 127 consecutive symptomatic military deployers referred for clinical evaluation, the most common symptoms were exertional dyspnea, 82%; cough, 77%; chest tightness, 74%; and wheezing, 67%. Only 2% were current smokers, and 36% were former smokers. Asthma was diagnosed in 31.5%, rhinitis/rhinosinusitis in 15%, and inducible laryngeal obstruction in 14.2% (S. D. Krefft, workshop presentation of unpublished data). Among 113 previously deployed, spirometry was normal in 70.8%, suggested restriction was present in 19.5%, obstruction was present in 5.3%, and a mixed pattern was present in 4.4%. At NJH, a pilot study exploring the utility of lung clearance index (LCI) testing as a marker of small airway dysfunction was conducted in 28 previously deployed veterans with respiratory symptoms evaluated at NJH. Compared with 24 referents without known lung disease, those previously deployed were found to have significantly higher mean LCI scores (86).

Brooke Army Medical Center investigators, in conjunction with other military treatment facilities, assessed the relationship between military deployment and chronic lung disease by electronic review of DoD medical records between 2005 and 2009. Additional direct clinical assessments were not performed as part of that study. There were 371 patients (52% previously deployed; 48% not deployed) with a minimum of three encounters for COPD/emphysema. There was no statistical difference in pulmonary function assessed by spirometry comparing deployers with nondeployers (87). Four hundred consecutive U.S. Army personnel undergoing medical discharge with a clinical diagnosis of asthma were also reviewed (previously deployed, 48.5%; nondeployers, 51.5%). Of 194 previously deployed with asthma, 52% had been diagnosed with asthma after deployment, whereas 48% had been diagnosed previously (10).

The STAMPEDE study (Study of Active Duty Military for Pulmonary Disease Related to Environmental Deployment Exposures) was conducted by the same investigators. STAMPEDE I prospectively evaluated 50 active duty military personnel with new-onset dyspnea during deployment (8). The primary findings in this study were that 42% had a nondiagnostic evaluation, whereas asthma and nonspecific bronchial hyperreactivity were the most common diagnoses, being present in 40%. There were frequent comorbid diagnoses, including sleep disorders (in 57%) and psychiatric conditions (in 68%). STAMPEDE II investigated the role of pre- and postdeployment spirometry in the clinical evaluation of postdeployment lung disease because spirometry is not routinely performed before deployment or as part of enlistment medical evaluations (88). In the predeployment phase, 1,693 soldiers from Fort Hood, Texas, participated. More than one-third of those surveyed reported a cigarette-smoking history, 73% had an elevated BMI, and 6.2% reported a history of asthma. Before deployment, abnormal spirometry was found in 22.3% of participants. Abnormal spirometry was more common in those with asthma (10.1% vs. 5.1%); those who failed physical fitness tests (9.0% vs. 4.6%); and those who had chronic respiratory symptoms, including wheezing, cough, or dyspnea (32.8% vs. 24.3%) (88). After deployment, 873 soldiers of the original cohort underwent repeat spirometry. A history of asthma and postdeployment wheezing was associated with airway obstruction after deployment, but an assessment of change in forced vital capacity and FEV_1 before and after

deployment using paired pulmonary function data was not conducted (89). In STAMPEDE III, an ongoing prospective study in which symptomatic military personnel undergo a comprehensive evaluation, the most common diagnoses in 310 participants included asthma (23%), nonspecific airway hyperresponsiveness (11%), gastroesophageal reflux (6%), and upper airway disorders (5%); 26% remained undiagnosed despite being symptomatic (M. J. Morris, workshop presentation of unpublished).

Reduction in Diffusing Capacity of the Lung for Carbon Monoxide

Among the four centers, the prevalence of a reduction in diffusing capacity of the lung for carbon monoxide (D_{LCO}) varied, depending on center, referral population, and choice of predicted values. Among patients evaluated at the NJ WRIISC, 30% of 130 previously deployed veterans had a reduction in D_{LCO} below the lower limit of normal, which was the only abnormality in 40.2% of patients with preserved spirometry and lung volumes (85). A reduction in D_{LCO} was found in 23% of 48 symptomatic deployers assessed in STAMPEDE I (8). Among 108 consecutive postdeployment veterans assessed at NJH after referral for symptoms, 18.3% had an abnormally decreased D_{LCO}. Among 38 active duty soldiers who were referred for assessment of dyspnea at Vanderbilt University Medical Center and who were reported to have constrictive bronchiolitis on lung biopsy, in 19 (50%), the only pulmonary function abnormality was an isolated reduction in D_{LCO} (11). In 82 postdeployment service members with unexplained cough and dyspnea assessed at Walter Reed National Military Medical Center and at Fort Belvoir Community Hospital (in Virginia), D_{LCO}, expressed as the mean percent predicted value, was 73.2% (SD, 12.1%), and 63.9% were below the fifth percentile using Crapo (90) predicted values (91). In contrast, only 9.8% had an abnormal diffusion value when Miller predicted values for D_{LCO} were used (92). Of note, the prevalence of D_{LCO} abnormalities from the VA WRIISC (30%) was based on Miller predicted values (85). The studies from Vanderbilt (11) and NJH used the Crapo reference equations (90), which predict higher normal values than Miller, potentially accounting for some of the differences among studies reporting D_{LCO} abnormalities.

Constrictive Bronchiolitis and Other Lung Biopsy Findings

Pathologic criteria for constrictive bronchiolitis. As a result of case series of constrictive bronchiolitis (which has also been called "obliterative bronchiolitis") reported after deployment, the workshop reviewed the standard pathologic criteria for assessing bronchiolitis in lung tissue samples (K. D. Jones, workshop presentation). The broad category of bronchiolitis refers to a range of disorders characterized by combinations of inflammation and fibrosis involving the small airways. The term "bronchiolitis obliterans" was noted to have a confusing history because of parallel definitions that existed until the ATS/European Respiratory Society classification agreed on a precise terminology (93, 94). Organizing pneumonia is the most common specific histologic finding to describe the entity previously referred to as "bronchiolitis obliterans organizing pneumonia." In that condition, rounded branching polypoid plugs of granulation tissue form in the distal airways (a proliferative pattern) and extend down into alveolar ducts and alveolar spaces, and this has been associated with nitrogen dioxide exposure. In contrast to bronchiolitis obliterans organizing pneumonia, constrictive bronchiolitis is a pattern of injury characterized by subepithelial scarring resulting in narrowing or obliteration of the bronchioles, without the presence of luminal plugs. This pathology is commonly observed in chronic rejection among lung transplant recipients or in chronic graft-versus-host disease after bone marrow transplant. Other conditions in which constrictive bronchiolitis may be observed include autoimmune connective tissue disease (e.g., scleroderma, rheumatoid arthritis, systemic lupus erythematosus), other systemic disorders (e.g., inflammatory bowel disease), drug reactions (e.g., due to penicillamine), ingested toxins (e.g., *Sauropus androgynus*), and infection (e.g., adenovirus) (12–14, 94). Constrictive bronchiolitis has also been reported after inhalational injury, including cases after sulfur mustard (gas) used in the Iran–Iraq War (95), and in food-flavoring workers exposed to the ketone butter flavoring diacetyl (13, 96–98).

As noted by Epler (13, 14), the characteristic histopathologic finding of constrictive bronchiolitis is subepithelial scarring that leads to narrowing of the airway. There is widening of the space between basement membrane and elastica, and the segment of the bronchiole that is sclerotic and narrowed is short compared with its total length. Therefore, it is possible to miss regions of fibrotic scarring on initial sections unless there is clinical suspicion leading to review of additional sections. Overdiagnosis is also possible. In particular, narrowing of bronchioles due to *ex vivo* smooth muscle contraction is well described (99). This is due to normal airway smooth muscle contraction coupled with loss of tethering resulting in narrowing of the bronchiolar lumen, accompanied by scalloping or undulation of the respiratory epithelium. This artifact, which may simulate pathologic bronchiolar narrowing, is less prominent in lobectomy or pneumonectomy specimens (when perfusion fixation through the bronchi is performed) than in specimens obtained by video-assisted thoracoscopic surgical (VATS) biopsy. It was noted during the workshop that in some publications, such as one by Leslie (100), smooth muscle hypertrophy has been included in the description of constrictive bronchiolitis in addition to fibrotic changes. Most recent descriptions, however, emphasize that constrictive bronchiolitis is a fibrotic airway disorder (14, 101) and requires subepithelial fibrosis to be present (K. D. Jones, workshop presentation).

Results of lung biopsy in symptomatic deployers. Investigators from Vanderbilt University Medical Center published the first biopsy series selected from among 80 postdeployment military personnel referred from Ft. Campbell, Kentucky, with unexplained shortness of breath and exercise limitation, cough, or chest tightness after deployment (11). These personnel had evaluations including inspiratory and expiratory high-resolution computed tomography of the chest; pulmonary function testing; cardiopulmonary exercise testing; and in some cases, nonspecific bronchial challenge testing. Forty-nine underwent VATS lung biopsy, and 38 (median age, 33 yr; range, 23–44 yr) had pathology interpreted as findings of constrictive bronchiolitis. The predominant bronchiolar tissue changes were reported to include smooth muscle in 7 cases, fibrous tissue in 3 cases, and mixed smooth muscle and fibrous tissue in 28 cases. Other small airway biopsy findings included respiratory

bronchiolitis (71.0% of biopsies), peribronchiolar inflammation (89.5%), pigment deposition (97.4%), polarizable material within pigment (94.7%), and bronchial-associated lymphoid tissue (50%). It has been suggested that past exposure to sulfur dioxide associated with the 2003 Mishraq Sulfur Mine fire (102) might explain these findings, although 10 of the 38 with constrictive bronchiolitis did not report this exposure history, and that condition has not been documented as associated with sulfur dioxide exposure. The 11 soldiers who underwent lung biopsy without findings of constrictive bronchiolitis did have other pathologic findings, including hypersensitivity pneumonitis, respiratory bronchiolitis, respiratory bronchiolitis–associated interstitial lung disease, and sarcoidosis. The original case series was updated to include 94 postdeployment personnel with dyspnea, of whom 75 had lung biopsies interpreted as findings of constrictive bronchiolitis (R. F. Miller, workshop presentation of unpublished data).

The other center with a similar clinical experience is NJH. In a series of 127 symptomatic military postdeployment personnel who underwent clinical evaluation at NJH, VATS lung biopsies from 52 were reported as having a range of overlapping abnormalities, including bronchiolitis (including constrictive bronchiolitis), emphysema with hyperinflation, and granulomatous pneumonitis (C. Rose, workshop presentation of unpublished data). At NJH, among 118 postdeployment referrals who underwent inspiratory and expiratory high-resolution computed tomography, air trapping was observed in approximately half and centrilobular nodularity in one-third, both of which suggest small airway disease but are not specifically diagnostic of constrictive bronchiolitis (S. D. Krefft, workshop presentation of unpublished data). There were differing views among workshop participants regarding the interpretation of the histologic changes considered as showing constrictive bronchiolitis.

In an ongoing study (C. Rose, workshop presentation of unpublished data), surgical lung biopsies from 50 deployers evaluated at either Vanderbilt or NJH were compared with 19 positive and 20 negative control lung tissue samples. Lung tissue samples were analyzed by a panel of four pulmonary pathologists blinded to sample status. Adjusting for smoking and age, and using subepithelial fibrosis as the primary histologic criterion, constrictive bronchiolitis was more common among deployers. Other abnormalities more prevalent among deployers included respiratory bronchiolitis, organizing pneumonia, hypersensitivity pneumonitis, and emphysema.

To investigate additional associations with nonmalignant pathologic pulmonary diagnoses, including small airway disease, DoD investigators at Brooke Army Medical Center and the Joint Pathology Center (JPC) conducted a retrospective review of 391 lung biopsy reports for nonneoplastic lung disease between 2005 and 2012 (137 in previous deployers). In that study, 45% of biopsies were obtained via transthoracic needle or via bronchoscopy (including some only with endobronchial biopsy samples), limiting the extent of tissue available for histologic review (103). Approximately 6% of deployers and nondeployers had small airway abnormalities, but none was interpreted as showing constrictive bronchiolitis. Deployed personnel were noted to have higher proportions of nonnecrotizing granulomas than nondeployed personnel (16.1% vs. 8.4%; $P = 0.04$). Findings were limited by the limited amount of lung tissue available in cases without VATS sampling and a paucity of information on clinical indications for biopsy. Future planned analyses at that center include a more in-depth histopathologic and radiologic review of surgical biopsies and lung resections in both deployed and nondeployed U.S. military personnel from 2002 to 2015 reviewed at the JPC. That study is planned to include additional cases from 2016 and 2017 and will have a subset of biopsy specimen cases analyzed by scanning electron microscopy and energy-dispersive X-ray spectroscopy (M. J. Morris, workshop presentation).

Eosinophilic Pneumonia

One of the earliest reported pulmonary diseases associated with deployment in Southwest Asia was acute eosinophilic pneumonia (AEP). This condition is usually idiopathic, but it has also been reported after inhalational exposures, including in smokers. First recognized by physicians at Landstuhl Regional Medical Center and based on bronchoalveolar lavage eosinophilia, the initial data on 18 patients was first reported in 2004 (104). An additional retrospective review of 43 patients with AEP (all deployed to Iraq, Afghanistan, Kuwait, or other locations, including the previous cases) between 2003 and 2010 was subsequently published. In that series, 91% were males; the mean age was 25.5 years; and cigarette smoking was reported in 91% of the patients (85% were recently new smokers) (105). AEP in deployed troops has not been associated with a particular exposure beyond cigarette smoking. In an observation potentially related to this syndrome, an elevated IgE (>100 kU/L) or peripheral eosinophilia (>2.8% or 300 cells/μl) was noted in 17 of 124 symptomatic deployers evaluated at NJH (Reference 86 and S. D. Krefft, workshop presentation of unpublished data).

Other Pulmonary Abnormalities

Diagnostic computed tomographic (CT) scans obtained in symptomatic deployers have generally been reported as normal or only subtly abnormal, showing mosaic attenuation consistent with air trapping and/or centrilobular nodules, consistent with small airway disease (Reference 86 and S. D. Krefft, workshop presentation of unpublished data). Among 49 postdeployers assessed during STAMPEDE I with CT scans, only 3 had air trapping on expiratory scans, and otherwise only minor nonspecific abnormalities were noted (8). In the lung biopsy series reported by Vanderbilt University Medical Center (11), CT scans were normal in 68%, and there was mild air trapping in 16%. Changes consistent with interstitial lung disease or other diffuse lung disease have not been observed, including in the review of biopsies from JPC (103).

Airborne Hazards and Open Burn Pit Registry

Public Law 112-260 Section 201, enacted in 2013, requires the VA to implement the Airborne Hazards and Open Burn Pit Registry to maintain a registry for those individuals who may have been exposed to burn pit emissions during their military service. The stated purpose is to monitor and ascertain adverse health effects from exposures and monitor the health care of veterans with concerns. There is an internet-based portal that allows veterans to

self-enroll, complete an exposure and health questionnaire, and request a clinical assessment. As of May 2018, 140,691 had participated. A recent analysis of registry participants reported a statistically significant association between self-reported blast injury with self-reported dyspnea and/or decreased ability to exercise, adjusted for smoking and other exposures, including burn pit smoke (106). An earlier publication analyzed symptoms and reported health conditions in a subset of registry participants deployed either to a location with a burn pit or to a location without a burn pit, reporting an association between proximity to a burn pit and self-reported respiratory conditions (107). The National Academies of Sciences, Engineering, and Medicine reviewed the function of the registry and suggested that efforts be made to improve participation and focus the scope of information gathered (108). It also suggested that the data should be used to explore the potential to conduct epidemiologic studies. It is possible that a benefit of the registry will be to track the incidence of various pulmonary conditions that occur over time in an effort to assess patterns of disease in relation to health and exposure information provided at entry and in conjunction with other sources of information, including the VHA medical record (D. A. Helmer, workshop presentation).

New Approaches to Assessment of Deployment-related Exposures and Health Effects

Assessment of Deployment $PM_{2.5}$ Exposures

A new study, VA Cooperative Studies Program #595, Pulmonary Health and Deployment to Southwest Asia and Afghanistan (NCT02825654; also called SHADE [Service and Health among Deployed Veterans]) has been designed to assess the respiratory health of previously deployed veterans. SHADE, which commenced recruitment in June 2018, is being conducted at six VA medical centers to enroll approximately 5,000 veterans with land-based deployments in Afghanistan and Southwest Asia. The primary objectives are to study whether greater cumulative exposure to $PM_{2.5}$ experienced during deployment is associated with lower lung function assessed by pre- and post-bronchodilator spirometry and to examine associations with healthcare provider–diagnosed asthma. A strength of SHADE is an exposure assessment approach that does not rely on self-reported exposure. Historical NASA satellite and military airport visibility (visual range assessment) records will be used to reconstruct deployment-related $PM_{2.5}$ at each veteran's deployment locations (17, 18). This approach integrates ground-level $PM_{2.5}$ data obtained from monitoring stations, airport visibility data in the countries where U.S. military personnel were deployed, and high-resolution AOD data available from NASA satellites (E. Garshick, workshop presentation).

On the basis of historical airport visibility data between 2000 and 2012 gathered from 104 military sites in Iraq, Afghanistan, Kuwait, Kyrgyzstan, United Arab Emirates, Djibouti, and Qatar calibrated with ground-level $PM_{2.5}$ stations, estimated monthly average $PM_{2.5}$ concentrations at these sites ranged from approximately 10 $\mu g/m^3$ to 365 $\mu g/m^3$, with values mainly between 50 $\mu g/m^3$ and nearly 200 $\mu g/m^3$ (Figure 2) (18). The feasibility of using land surface temperature determined by satellite-based remote sensing (109) to detect burn pit locations will also be assessed. A collaboration between the NASA Joint Propulsion Laboratory and the University of Southern California will use newly developed AOD data fractionated by particle characteristics. It is proposed that this information will be useful in determining the extent that various sources of pollution, such as burn pits or dust storms, contributed to the historical $PM_{2.5}$ concentrations (E. Garshick, workshop presentation). A limitation of this approach is that exposures to relatively brief but high concentrations of PM, vapors, and gases from various military-related exposures (such as burning vehicles or blasts) may not be assessed.

DoD Serum Repository and Metabolomics

The DoD Serum Repository started in the mid-1980s to store serum samples remaining after required human immunodeficiency virus testing. Serum samples are obtained from active military personnel during periodic medical examinations, before overseas assignments, and before and after major deployments (19). As of June 30, 2016, the repository included 60 million samples stored at −30°C collected from about 10 million service members (110). These samples have been linked electronically to the Defense Medical Surveillance System. The Defense Medical Surveillance System can be used to select records for review on the basis of medical encounters and outcomes, demographics, deployment history, and military job codes. The repository is housed at the Defense Health Agency, Armed Forces Health Surveillance Branch, in Silver Spring, Maryland (111).

DoD and various university collaborators have conducted a series of pilot studies to assess the suitability of the sample repository for use in research. After confirmation that the samples were of sufficient quality to permit study (112), analysis of various chemicals believed to be associated with exposure was conducted using high-resolution mass spectrometry in deidentified samples. Serum samples collected from 200 persons before and after deployment were compared with those of nondeployed control subjects. Naphthalene was found to be elevated after deployment, and four dioxin/furan compounds were measurable in 38% of the samples and elevated after deployment (111, 113). Other exploratory analyses have found miRNAs differentially expressed in previous deployers, as have correlations with dioxin and dibenzofuran concentrations (114, 115). These analyses demonstrate that high-resolution metabolomic, gene expression, and other approaches may be used to identify associations between deployment, specific chemical compounds and/or altered gene expression, and eventually adverse health outcomes

Mechanisms of Lung Epithelial Injury

A 5-year DoD-funded study newly underway at NJH, titled "Mechanisms and Treatment of Deployment-Related Lung Injury: Repair of the Injured Epithelium," will focus on understanding mechanisms by which exposure to PM may predispose the lung epithelium to injury after a second stimulus, with the long-term goal of developing strategies to promote lung repair. This investigation will test the hypothesis that exposure to respirable PM from Southwest Asia triggers inflammatory signaling pathways in respiratory epithelial cells, which, after a second stimulus (e.g., blast injury, tobacco smoke, allergens, viruses), leads to dysregulated production of proinflammatory mediators that drive lung epithelial cell injury. The project will apply transcriptomic and genetic analyses to

in vivo and *in vitro* airway epithelial cells from postdeployment study participant patients and will include study of airway epithelial cytokines, growth factor expression, and markers of oxidative stress. It will also assess noninvasive clinical markers of small airway findings in symptomatic veterans, including computed tomography and LCI testing.

Summary and Key Questions

Deployment-associated Exposures

As described in the 2011 IOM report (1), military personnel deployed to Afghanistan and Southwest Asia (including Kuwait and Iraq) experienced a complex mixture of exposures. Most notable and widespread have been the ambient $PM_{2.5}$ exposures known to be greater than U.S. concentrations. Sources contributing to $PM_{2.5}$ included desert dust with a mix of organic and inorganic constituents, waste incineration from burn pits, and poorly regulated or unregulated local industrial and vehicular pollution. The quantitative assessment of $PM_{2.5}$ over each deployment using airport visibility and NASA satellite AOD data, as proposed in the new SHADE study, represents an advance in exposure assessment that should reduce misclassification compared with self-reported exposure intensities. Future studies should include efforts to characterize more specific exposures that are based on job duties or deployment locations (using estimates of $PM_{2.5}$ or other pollutants) rather than simply considering deployment status as a single exposure, because exposure may vary on the basis of job duties, location, and time in theater. The use of banked serum samples to characterize exposures using selected biomarkers related to burn pit or other military exposures may be feasible in the future to better characterize exposure status.

Adverse Respiratory Health Effects

Previous deployers with respiratory symptoms. Studies conducted by DoD analyzing military encounter data suggest that more encounters occur for respiratory symptoms and for obstructive lung disease, predominantly asthma, after deployment (4–6). A study in Swedish troops deployed to Afghanistan also documented the persistence of symptoms several years after deployment (82). Case series describing the evaluation of symptomatic military personnel do not note any single etiology, emphasizing the importance of a comprehensive clinical assessment, but asthma has been a common finding (References 8 and 75 and S. D. Krefft, workshop presentation of unpublished data). This is consistent with epidemiologic findings from the Millennium Cohort Study that demonstrate an increased risk of new-onset asthma (by self-report) related to combat exposure during deployment (9) and the observational findings in which approximately half of the deployed persons discharged with asthma after deployment did not have a previous known diagnosis (10). Nonetheless, a number of questions remain regarding the drivers of increased healthcare use for respiratory conditions and potential under- and overdiagnosis of specific conditions. The relationship of asthma after deployment with specific exposures, such as burn pit work, is not known, nor is the relationship with previous pulmonary function test abnormality or previous asthma diagnosis. A study underway at NJH designed to elucidate the molecular effects of desert dust PM exposures on airway epithelial cells may provide insights into the mechanisms and the potential for airway damage.

Constrictive bronchiolitis. Centers performing VATS lung biopsies in a selected group of previously deployed service members undergoing evaluation for dyspnea have reported constrictive bronchiolitis, other small airway abnormalities, and granulomas (Reference 11 and presentation of unpublished data, S. D. Krefft and C. Rose). Review of histologic criteria defining constrictive bronchiolitis indicated that these criteria have not been applied consistently across case series. Because the histologic criteria for diagnosis of constrictive bronchiolitis have varied, in particular the presence of bronchiolar subepithelial scarring, it has been difficult to compare results across centers. There was a heterogeneity of views among workshop participants regarding the interpretation of the findings of constrictive bronchiolitis and its potential relationship with dyspnea and related respiratory symptoms after deployment.

Future lung disease. The findings summarized in this workshop regarding estimated $PM_{2.5}$ concentrations during deployment raise concerns about the future respiratory health of previously deployed military personnel (active duty and veterans), especially given that adverse respiratory health effects have been observed at PM concentrations much lower than those experienced during deployment (15, 16). Although multiple sources contributed to PM during deployment, the predominant contribution was desert dust. Epidemiologic studies have demonstrated an association between acute desert dust exposure and increased hospitalization for asthma, pneumonia, and other respiratory causes (40–42, 46–50). Desert dust exposure may also have contributed to the acute respiratory illness experienced during deployment, as reported retrospectively in postdeployment surveys (54, 55). There is little currently available data, however, to guide the assessment of long-term effects of repeated PM or other air pollutant exposures during deployment, nor is there prior literature quantifying chronic pulmonary health effects attributable to the substantially higher but much shorter exposures (usually months to up to several years).

Key Questions

Suggestions to further understanding of the health effects of PM and other potential exposures during deployment include the following:

1. Better characterization of respiratory symptoms and clinical respiratory disease after deployment, including airway diseases in previous deployers presenting for health care and the potential exposures they experienced during deployment.
2. Improved assessment of long-term clinical consequences and outcomes of former deployers with respiratory symptoms and with respiratory disease, because there is a lack published information regarding follow-up among such persons. Many do not receive a conclusive respiratory diagnosis when symptomatic. Population-based nonmilitary studies have demonstrated that chronic respiratory symptoms are associated with reduced pulmonary function and an increased risk of future pulmonary disease (116–118).
3. More consistent characterization of specific histologic abnormalities, including the prevalence of constrictive bronchiolitis and other small airway abnormalities, established through review of biopsy material using standardized criteria comparable across

studies and delineating the relationship of such pathologic abnormalities with PM and other exposures.
4. Determination of the cross-sectional associations among cumulative exposures (in particular PM) and respiratory conditions (in particular asthma) and pulmonary function deficits, adjusted for smoking and other covariates.
5. Evaluation of the long-term longitudinal effects of deployment-related exposures (such as self-reported exposures in the Airborne Hazards and Open Burn Pit Registry, externally estimated cumulative PM exposures in the SHADE study, or biomarkers in the DoD Serum Repository) on the incidence of adverse respiratory health conditions or pulmonary function decline over time. ■

This official workshop report was prepared by an *ad hoc* subcommittee of the ATS Assembly on Environmental, Occupational and Population Health and the ATS Environmental Health Policy Committee.

Members of the subcommittee are as follows:

Eric Garshick, M.D., M.O.H. (*Co-Chair*)[1,2,3*]
Susan P. Proctor, D.Sc. (*Co-Chair*)[1,6]
Paul D. Blanc, M.D., M.S.P.H. (*Co-Chair*)[4,5]
Joseph H. Abraham, Sc.D.[7*]
Coleen P. Baird, M.D., M.P.H.[7‡]
Paul Ciminera, M.D., M.P.H.[8‡]
Gregory P. Downey, M.D.[9,10‡]
Michael J. Falvo, Ph.D.[11,12*]
Jaime E. Hart, Sc.D.[13,14*]
Drew A. Helmer, M.D.[11,12*]
David A. Jackson, Ph.D.[15‡]
Michael Jerrett, Ph.D.[16‡]
Kirk D. Jones, M.D.[5*]
Ware Kuschner, M.D.[17,18‡]
Silpa D. Krefft, M.D., M.P.H.[9,10,19*]
Timothy Mallon, M.D., M.P.H.[20*]
Robert F. Miller, M.D.[21*]
Michael J. Morris, M.D.[22*]
Carrie A. Redlich, M.D., M.P.H.[23‡]
Cecile S. Rose, M.D., M.P.H.[9,10*]
Rudolph P. Rull, Ph.D., M.P.H.[24*]
Johannes Saers, M.D.[25*]
Aaron I. Schneiderman, Ph.D., M.P.H., R.N.[26*]
Nicholas L. Smith, Ph.D.[27,28‡]
Panayiotis Yiallouros, M.D., Ph.D.[29*]

[1]VA Boston Healthcare System, Boston, Massachusetts; [2]Brigham and Women's Hospital, Boston, Massachusetts; [3]Harvard Medical School, Boston, Massachusetts; [4]San Francisco VA Health Care System, San Francisco, California; [5]University of California San Francisco School of Medicine, San Francisco, California; [6]U.S. Army Research Institute of Environmental Medicine, Natick, Massachusetts; [7]U.S. Army Public Health Center, Aberdeen Proving Ground, Maryland; [8]Office of the Assistant Secretary of Defense for Health Affairs, Health Services Policy and Oversight, Washington, District of Columbia; [9]National Jewish Health, Denver, Colorado; [10]University of Colorado, Denver, Colorado; [11]VA New Jersey Health Care System, East Orange, New Jersey; [12]Rutgers New Jersey Medical School, Newark, New Jersey; [13]Brigham and Women's Hospital and Harvard Medical School, Boston, Massachusetts; [14]Harvard T.H. Chan School of Public Health, Boston, Massachusetts; [15]Walter Reed Army Institute of Research, Silver Spring, Maryland; [16]Fielding School of Public Health, University of California, Los Angeles, Los Angeles, California; [17]VA Palo Alto Health Care System, Palo Alto, California; [18]Stanford University School of Medicine, Palo Alto, California; [19]VA Eastern Colorado Health Care System, Aurora, Colorado; [20]Uniformed Services University, Bethesda, Maryland; [21]Vanderbilt University, Nashville, Tennessee; [22]Brooke Army Medical Center, JBSA Fort Sam Houston, Texas; [23]Yale University School of Medicine, New Haven, Connecticut; [24]Deployment Health Research Department, Naval Health Research Center, San Diego, California; [25]Swedish Army (Reserve), Örebro University Hospital, Örebro, Sweden; [26]Veterans Health Administration, Washington, District of Columbia; [27]Seattle Epidemiologic Research and Information Center, Department of Veterans Affairs Office of Research and Development Studies Program, Seattle, Washington; [28]Department of Epidemiology, University of Washington, Seattle, Washington; and [29]University of Cyprus Medical School, Nicosia, Cyprus

*Workshop presenters.
‡Workshop discussants.

Author Disclosures: S.D.K. provided medicolegal consulting on exposure-related lung disease; developed podcast reviews of articles on occupational and exposure-related lung disease for Oakstone Medical Reviews; received support from the Sergeant Sullivan Foundation associated with the Center for Deployment-Related Lung Disease, National Jewish Health, for previous research on lung clearance index testing cited in this report. M.J.M. served as a speaker for Janssen Pharmaceuticals. E.G., J.H.A., C.P.B., P.C., G.P.D., M.J.F., J.E.H., D.A.J., M.J., W.K., D.A.H., K.D.J., T.M., R.F.M., S.P.P., C.A.R., C.S.R., R.P.R., J.S., A.I.S., N.L.S., P.Y., and P.D.B. reported no relevant commercial relationships.

References

1 Institute of Medicine, Board on the Health of Select Populations, Committee on the Long-Term Health Consequences of Exposure to Burn Pits in Iraq and Afghanistan. Long-term health consequences of exposure to burn pits in Iraq and Afghanistan. Washington, DC: National Academies Press; 2011.
2 Alolayan MA, Brown KW, Evans JS, Bouhamra WS, Koutrakis P. Source apportionment of fine particles in Kuwait City. *Sci Total Environ* 2013;448:14–25.
3 Engelbrecht JP, McDonald EV, Gillies JA, Jayanty RK, Casuccio G, Gertler AW. Characterizing mineral dusts and other aerosols from the Middle East—part 1: ambient sampling. *Inhal Toxicol* 2009;21: 297–326.
4 Abraham JH, DeBakey SF, Reid L, Zhou J, Baird CP. Does deployment to Iraq and Afghanistan affect respiratory health of US military personnel? *J Occup Environ Med* 2012;54:740–745.
5 Abraham JH, Eick-Cost A, Clark LL, Hu Z, Baird CP, DeFraites R, *et al*. A retrospective cohort study of military deployment and postdeployment medical encounters for respiratory conditions. *Mil Med* 2014;179:540–546.
6 Sharkey JM, Abraham JH, Clark LL, Rohrbeck P, Ludwig SL, Hu Z, *et al*. Postdeployment respiratory health care encounters following deployment to Kabul, Afghanistan: a retrospective cohort study. *Mil Med* 2016;181:265–271.
7 Pugh MJ, Jaramillo CA, Leung KW, Faverio P, Fleming N, Mortensen E, *et al*. Increasing prevalence of chronic lung disease in veterans of the wars in Iraq and Afghanistan. *Mil Med* 2016;181:476–481.
8 Morris MJ, Dodson DW, Lucero PF, Haislip GD, Gallup RA, Nicholson KL, *et al*. Study of Active Duty Military for Pulmonary Disease Related to Environmental Deployment Exposures (STAMPEDE). *Am J Respir Crit Care Med* 2014;190:77–84.
9 Rivera AC, Powell TM, Boyko EJ, Lee RU, Faix DJ, Luxton DD, *et al*.; Millennium Cohort Study Team. New-onset asthma and combat deployment: findings from the Millennium Cohort Study. *Am J Epidemiol* 2018;187:2136–2144.
10 DelVecchio SP, Collen JF, Zacher LL, Morris MJ. The impact of combat deployment on asthma diagnosis and severity. *J Asthma* 2015;52: 363–369.
11 King MS, Eisenberg R, Newman JH, Tolle JJ, Harrell FE Jr, Nian H, *et al*. Constrictive bronchiolitis in soldiers returning from Iraq and Afghanistan. *N Engl J Med* 2011;365:222–230.
12 Lewin-Smith MR, Morris MJ, Galvin JR, Harley RA, Franks TJ. The problems with constrictive bronchiolitis: histopathological and radiological perspectives. In: Baird CP, Harkins DK, editors. Airborne hazards related to deployment. Fort Sam Houston, TX: Borden Institute, U.S. Army Medical Department and School; 2015. pp. 153–161.
13 Epler GR. Diagnosis and treatment of constrictive bronchiolitis. *F1000 Med Rep* 2010;2:32.
14 Epler GR. Constrictive bronchiolitis obliterans: the fibrotic airway disorder. *Expert Rev Respir Med* 2007;1:139–147.

15 Rice MB, Ljungman PL, Wilker EH, Dorans KS, Gold DR, Schwartz J, *et al*. Long-term exposure to traffic emissions and fine particulate matter and lung function decline in the Framingham Heart Study. *Am J Respir Crit Care Med* 2015;191:656–664.

16 Guo C, Zhang Z, Lau AKH, Lin CQ, Chuang YC, Chan J, *et al*. Effect of long-term exposure to fine particulate matter on lung function decline and risk of chronic obstructive pulmonary disease in Taiwan: a longitudinal, cohort study. *Lancet Planet Health* 2018;2:e114–e125.

17 Masri S, Garshick E, Coull BA, Koutrakis P. A novel calibration approach using satellite and visibility observations to estimate fine particulate matter exposures in Southwest Asia and Afghanistan. *J Air Waste Manag Assoc* 2017;67:86–95.

18 Masri S, Garshick E, Hart J, Bouhamra W, Koutrakis P. Use of visual range measurements to predict fine particulate matter exposures in Southwest Asia and Afghanistan. *J Air Waste Manag Assoc* 2017;67: 75–85.

19 Perdue CL, Cost AA, Rubertone MV, Lindler LE, Ludwig SL. Description and utilization of the United States Department of Defense Serum Repository: a review of published studies, 1985-2012. *PLoS One* 2015;10:e0114857.

20 Ryan MA, Smith TC, Smith B, Amoroso P, Boyko EJ, Gray GC, *et al*. Millennium cohort: enrollment begins a 21-year contribution to understanding the impact of military service. *J Clin Epidemiol* 2007; 60:181–191.

21 Wenger JW, O'Connell C, Cottrell L. Examination of recent deployment experience across the services and components. Santa Monica, CA: Rand Corporation; 2018.

22 Bagalman E. The number of veterans that use VA health services: a fact sheet. Washington, DC: Congressional Research Service; 2014.

23 Sissakian V, Al-Ansari N, Knutsson S. Sand and dust storm events in Iraq. *J Nat Sci* 2013;5:1084–1094.

24 Goudie AS. Desert dust and human health disorders. *Environ Int* 2014; 63:101–113.

25 Goudie AS. Dust storms: recent developments. *J Environ Manage* 2009;90:89–94.

26 Al-Dabbas M, Abbas MA, Al-Khafaji R. The mineralogical and micro-organisms effects of regional dust storms over Middle East region. *Int J Water Resour Arid Environ* 2011;1:129–141.

27 Polymenakou PN, Mandalakis M, Stephanou EG, Tselepides A. Particle size distribution of airborne microorganisms and pathogens during an intense African dust event in the eastern Mediterranean. *Environ Health Perspect* 2008;116:292–296.

28 National Research Council. Review of the Department of Defense enhanced particulate matter surveillance program report. Appendix D - Final report of the Department of Defense enhanced particulate matter surveillance program. Washington, DC: National Academies Press; 2010.

29 Brown KW, Bouhamra W, Lamoureux DP, Evans JS, Koutrakis P. Characterization of particulate matter for three sites in Kuwait. *J Air Waste Manag Assoc* 2008;58:994–1003.

30 U.S. Army Center for Health Promotion and Preventative Medicine. Maryland; May 2008. USACHPPM Report No. 47-MA-08PV-08/ AFIOH Report No. IOH-RS-BR-TR-2008-0001.

31 Engelbrecht JP, McDonald EV, Gillies JA, Jayanty RK, Casuccio G, Gertler AW. Characterizing mineral dusts and other aerosols from the Middle East—part 2: grab samples and re-suspensions. *Inhal Toxicol* 2009;21:327–336.

32 Brown EG, Gottlieb S, Latbourn RL. Dust storms and their possible effect on health. *Public Health Rep* 1935;50:1369–1383.

33 Samoli E, Kougea E, Kassomenos P, Analitis A, Katsouyanni K. Does the presence of desert dust modify the effect of PM_{10} on mortality in Athens, Greece? *Sci Total Environ* 2011;409: 2049–2054.

34 Crooks JL, Cascio WE, Percy MS, Reyes J, Neas LM, Hilborn ED. The association between dust storms and daily non-accidental mortality in the United States, 1993-2005. *Environ Health Perspect* 2016;124: 1735–1743.

35 Renzi M, Forastiere F, Calzolari R, Cernigliaro A, Madonia G, Michelozzi P, *et al*. Short-term effects of desert and non-desert PM_{10} on mortality in Sicily, Italy. *Environ Int* 2018;120: 472–479.

36 Stafoggia M, Zauli-Sajani S, Pey J, Samoli E, Alessandrini E, Basagaña X, *et al*.; MED-PARTICLES Study Group. Desert dust outbreaks in Southern Europe: contribution to daily PM_{10} concentrations and short-term associations with mortality and hospital admissions. *Environ Health Perspect* 2016;124:413–419.

37 Neophytou AM, Yiallouros P, Coull BA, Kleanthous S, Pavlou P, Pashiardis S, *et al*. Particulate matter concentrations during desert dust outbreaks and daily mortality in Nicosia, Cyprus. *J Expo Sci Environ Epidemiol* 2013;23:275–280.

38 Perez L, Tobias A, Querol X, Künzli N, Pey J, Alastuey A, *et al*. Coarse particles from Saharan dust and daily mortality. *Epidemiology* 2008; 19:800–807.

39 Mallone S, Stafoggia M, Faustini A, Gobbi GP, Marconi A, Forastiere F. Saharan dust and associations between particulate matter and daily mortality in Rome, Italy. *Environ Health Perspect* 2011;119: 1409–1414.

40 Thalib L, Al-Taiar A. Dust storms and the risk of asthma admissions to hospitals in Kuwait. *Sci Total Environ* 2012;433:347–351.

41 Trianti SM, Samoli E, Rodopoulou S, Katsouyanni K, Papiris SA, Karakatsani A. Desert dust outbreaks and respiratory morbidity in Athens, Greece. *Environ Health* 2017;16:72.

42 Grineski SE, Staniswalis JG, Bulathsinhala P, Peng Y, Gill TE. Hospital admissions for asthma and acute bronchitis in El Paso, Texas: do age, sex, and insurance status modify the effects of dust and low wind events? *Environ Res* 2011;111:1148–1155.

43 Watanabe M, Noma H, Kurai J, Shimizu A, Sano H, Kato K, *et al*. Association of sand dust particles with pulmonary function and respiratory symptoms in adult patients with asthma in western Japan using light detection and ranging: a panel study. *Int J Environ Res Public Health* 2015;12:13038–13052.

44 Chang CC, Lee IM, Tsai SS, Yang CY. Correlation of Asian dust storm events with daily clinic visits for allergic rhinitis in Taipei, Taiwan. *J Toxicol Environ Health A* 2006;69:229–235.

45 Kanatani KT, Hamazaki K, Inadera H, Sugimoto N, Shimizu A, Noma H, *et al*.; Japan Environment & Children's Study Group. Effect of desert dust exposure on allergic symptoms: a natural experiment in Japan. *Ann Allergy Asthma Immunol* 2016;116:425–430.e7.

46 Kang JH, Keller JJ, Chen CS, Lin HC. Asian dust storm events are associated with an acute increase in pneumonia hospitalization. *Ann Epidemiol* 2012;22:257–263.

47 Cheng MF, Ho SC, Chiu HF, Wu TN, Chen PS, Yang CY. Consequences of exposure to Asian dust storm events on daily pneumonia hospital admissions in Taipei, Taiwan. *J Toxicol Environ Health A* 2008;71:1295–1299.

48 Meng Z, Lu B. Dust events as a risk factor for daily hospitalization for respiratory and cardiovascular diseases in Minqin, China. *Atmos Environ* 2007;41:7038–7048.

49 Tam WW, Wong TW, Wong AH, Hui DS. Effect of dust storm events on daily emergency admissions for respiratory diseases. *Respirology* 2012;17:143–148.

50 Vodonos A, Friger M, Katara I, Avnon L, Krasnov H, Koutrakis P, *et al*. The impact of desert dust exposures on hospitalizations due to exacerbation of chronic obstructive pulmonary disease. *Air Qual Atmos Health* 2014;7:433–439.

51 Saiyed HN, Sharma YK, Sadhu HG, Norboo T, Patel PD, Patel TS, *et al*. Non-occupational pneumoconiosis at high altitude villages in central Ladakh. *Br J Ind Med* 1991;48:825–829.

52 Norboo T, Angchuk PT, Yahya M, Kamat SR, Pooley FD, Corrin B, *et al*. Silicosis in a Himalayan village population: role of environmental dust. *Thorax* 1991;46:341–343.

53 Bar-Ziv J, Goldberg GM. Simple siliceous pneumoconiosis in Negev Bedouins. *Arch Environ Health* 1974;29:121–126.

54 Sanders JW, Putnam SD, Frankart C, Frenck RW, Monteville MR, Riddle MS, *et al*. Impact of illness and non-combat injury during Operations Iraqi Freedom and Enduring Freedom (Afghanistan). *Am J Trop Med Hyg* 2005;73:713–719.

55 Roop SA, Niven AS, Calvin BE, Bader J, Zacher LL. The prevalence and impact of respiratory symptoms in asthmatics and nonasthmatics during deployment. *Mil Med* 2007;172:1264–1269.

56 Korzeniewski K, Brzozowski R. Sickness profile among Polish troops deployed to Afghanistan in the years 2003-2005. *Int Marit Health* 2011;62:63–70.
57 Korzeniewski K, Nitsch-Osuch A, Konarski M, Guzek A, Prokop E, Bieniuk K. Prevalence of acute respiratory tract diseases among soldiers deployed for military operations in Iraq and Afghanistan. *Adv Exp Med Biol* 2013;788:117–124.
58 Novozhenov VG, Gembitskiĭ EV. Pneumonia in young males in extreme conditions [in Russian]. *Klin Med (Mosk)* 1998;76:18–20.
59 Kloog I, Koutrakis P, Coull BA, Lee HJ, Schwartz J. Assessing temporally and spatially resolved $PM_{2.5}$ exposures for epidemiological studies using satellite aerosol optical depth measurements. *Atmos Environ* 2011;45:6267–6275.
60 Kloog I, Ridgway B, Koutrakis P, Coull BA, Schwartz JD. Long- and short-term exposure to $PM_{2.5}$ and mortality: using novel exposure models. *Epidemiology* 2013;24:555–561.
61 Lee HJ, Coull BA, Bell ML, Koutrakis P. Use of satellite-based aerosol optical depth and spatial clustering to predict ambient $PM_{2.5}$ concentrations. *Environ Res* 2012;118:8–15.
62 Adam M, Schikowski T, Carsin AE, Cai Y, Jacquemin B, Sanchez M, *et al*. Adult lung function and long-term air pollution exposure. ESCAPE: a multicentre cohort study and meta-analysis. *Eur Respir J* 2015;45:38–50.
63 Garshick E. Effects of short- and long-term exposures to ambient air pollution on COPD. *Eur Respir J* 2014;44:558–561.
64 Schikowski T, Adam M, Marcon A, Cai Y, Vierkötter A, Carsin AE, *et al*. Association of ambient air pollution with the prevalence and incidence of COPD. *Eur Respir J* 2014;44:614–626.
65 Churg A, Brauer M, del Carmen Avila-Casado M, Fortoul TI, Wright JL. Chronic exposure to high levels of particulate air pollution and small airway remodeling. *Environ Health Perspect* 2003;111:714–718.
66 Künzli N, Bridevaux PO, Liu LJ, Garcia-Esteban R, Schindler C, Gerbase MW, *et al*.; Swiss Cohort Study on Air Pollution and Lung Diseases in Adults. Traffic-related air pollution correlates with adult-onset asthma among never-smokers. *Thorax* 2009;64: 664–670.
67 Jacquemin B, Siroux V, Sanchez M, Carsin AE, Schikowski T, Adam M, *et al*. Ambient air pollution and adult asthma incidence in six European cohorts (ESCAPE). *Environ Health Perspect* 2015;123: 613–621.
68 Young MT, Sandler DP, DeRoo LA, Vedal S, Kaufman JD, London SJ. Ambient air pollution exposure and incident adult asthma in a nationwide cohort of U.S. women. *Am J Respir Crit Care Med* 2014; 190:914–921.
69 Fisher JA, Puett RC, Hart JE, Camargo CA Jr, Varraso R, Yanosky JD, *et al*. Particulate matter exposures and adult-onset asthma and COPD in the Nurses' Health Study. *Eur Respir J* 2016;48:921–924.
70 Hankinson JL, Odencrantz JR, Fedan KB. Spirometric reference values from a sample of the general U.S. population. *Am J Respir Crit Care Med* 1999;159:179–187.
71 Gauderman WJ, Vora H, McConnell R, Berhane K, Gilliland F, Thomas D, *et al*. Effect of exposure to traffic on lung development from 10 to 18 years of age: a cohort study. *Lancet* 2007;369:571–577.
72 Lange P, Celli B, Agustí A, Boje Jensen G, Divo M, Faner R, *et al*. Lung-function trajectories leading to chronic obstructive pulmonary disease. *N Engl J Med* 2015;373:111–122.
73 Martin BL, Engler RJM, Klote MM, With CM, Krauss MR, Nelson MR. Asthma and its implications for military recruits. In: DeKoning BL, editor. Recruit medicine (Textbooks of Military Medicine series). Washington, DC: Department of the Army, Office of the Surgeon General, Borden Institute; 2006. p. 89–108.
74 Millikan AM, Niebuhr DW, Brundage M, Powers TE, Krauss MR. Retention of mild asthmatics in the navy (REMAIN): a low-risk approach to giving mild asthmatics an opportunity for military service. *Mil Med* 2008;173:381–387.
75 Szema AM, Peters MC, Weissinger KM, Gagliano CA, Chen JJ. New-onset asthma among soldiers serving in Iraq and Afghanistan. *Allergy Asthma Proc* 2010;31:67–71.
76 Szema AM, Salihi W, Savary K, Chen JJ. Respiratory symptoms necessitating spirometry among soldiers with Iraq/Afghanistan war lung injury. *J Occup Environ Med* 2011;53:961–965.
77 Abraham JH, Clark LL, Sharkey JM, Baird CP. Trends in rates of chronic obstructive respiratory conditions among US military personnel, 2001-2013. *US Army Med Dep J* 2014 Jul-Sep:33–43.
78 Slatore CG, Falvo MJ, Nugent S, Carlson K. Afghanistan and Iraq war veterans: mental health diagnoses are associated with respiratory disease diagnoses. *Mil Med* 2018;183:e249–e257.
79 Smith B, Wong CA, Smith TC, Boyko EJ, Gackstetter GD, Ryan MAK; the Millennium Cohort Study Team. Newly reported respiratory symptoms and conditions among military personnel deployed to Iraq and Afghanistan: a prospective population-based study. *Am J Epidemiol* 2009;170:1433–1442.
80 Smith B, Wong CA, Boyko EJ, Phillips CJ, Gackstetter GD, Ryan MA, *et al*.; Millennium Cohort Study Team. The effects of exposure to documented open-air burn pits on respiratory health among deployers of the Millennium Cohort Study. *J Occup Environ Med* 2012;54:708–716.
81 Barth SK, Dursa EK, Peterson MR, Schneiderman A. Prevalence of respiratory diseases among veterans of Operation Enduring Freedom and Operation Iraqi Freedom: results from the National Health Study for a New Generation of U.S. Veterans. *Mil Med* 2014; 179:241–245.
82 Saers J, Ekerljung L, Forsberg B, Janson C. Respiratory symptoms among Swedish soldiers after military service abroad: association with time spent in a desert environment. *Eur Clin Respir J* 2017;4: 1327761.
83 Lincoln AE, Helmer DA, Schneiderman AI, Li M, Copeland HL, Prisco MK, *et al*. The war-related illness and injury study centers: a resource for deployment-related health concerns. *Mil Med* 2006;171: 577–585.
84 Falvo MJ, Abraham JH, Osinubi OY, Klein JC, Sotolongo AM, Ndirangu D, *et al*. Bronchodilator responsiveness and airflow limitation are associated with deployment length in Iraq and Afghanistan veterans. *J Occup Environ Med* 2016;58:325–328.
85 Falvo MJ, Helmer DA, Klein JC, Osinubi OY, Ndirangu D, Patrick-DeLuca LA, *et al*. Isolated diffusing capacity reduction is a common clinical presentation in deployed Iraq and Afghanistan veterans with deployment-related environmental exposures. *Clin Respir J* 2018; 12:795–798.
86 Krefft SD, Strand M, Smith J, Stroup C, Meehan R, Rose C. Utility of lung clearance index testing as a noninvasive marker of deployment-related lung disease. *J Occup Environ Med* 2017;59:707–711.
87 Matthews T, Abraham J, Zacher LL, Morris MJ. The impact of deployment on COPD in active duty military personnel. *Mil Med* 2014;179:1273–1278.
88 Skabelund AJ, Rawlins FA III, McCann ET, Lospinoso JA, Burroughs L, Gallup RA, *et al*. Pulmonary function and respiratory health of military personnel before Southwest Asia deployment. *Respir Care* 2017;62: 1148–1155.
89 Morris MJ, Skabelund AJ, Rawlins FA III, Gallup RA, Aden JK, Holley AB. Study of Active Duty Military Personnel for Environmental Deployment Exposures: Pre- and Post-Deployment Spirometry (STAMPEDE II). *Respir Care* 2019;64:536–544.
90 Crapo RO, Morris AH. Standardized single breath normal values for carbon monoxide diffusing capacity. *Am Rev Respir Dis* 1981;123: 185–189.
91 Holley AB, Sobieszczyk M, Perkins M, Cohee BM, Costantoth CB, Mabe DL, *et al*. Lung function abnormalities among service members returning from Iraq or Afghanistan with respiratory complaints. *Respir Med* 2016;118:84–87.
92 Miller A, Thornton JC, Warshaw R, Anderson H, Teirstein AS, Selikoff IJ. Single breath diffusing capacity in a representative sample of the population of Michigan, a large industrial state: predicted values, lower limits of normal, and frequencies of abnormality by smoking history. *Am Rev Respir Dis* 1983;127:270–277.
93 Meyer KC, Raghu G, Verleden GM, Corris PA, Aurora P, Wilson KC, *et al*.; ISHLT/ATS/ERS BOS Task Force Committee; ISHLT/ATS/ERS BOS Task Force Committee. An international ISHLT/ATS/ERS clinical practice guideline: diagnosis and management of bronchiolitis obliterans syndrome. *Eur Respir J* 2014;44:1479–1503.

94 Burgel PR, Bergeron A, de Blic J, Bonniaud P, Bourdin A, Chanez P, *et al*. Small airways diseases, excluding asthma and COPD: an overview. *Eur Respir Rev* 2013;22:131–147.

95 Ghanei M, Tazelaar HD, Chilosi M, Harandi AA, Peyman M, Akbari HM, *et al*. An international collaborative pathologic study of surgical lung biopsies from mustard gas-exposed patients. *Respir Med* 2008;102: 825–830.

96 Akpinar-Elci M, Travis WD, Lynch DA, Kreiss K. Bronchiolitis obliterans syndrome in popcorn production plant workers. *Eur Respir J* 2004; 24:298–302.

97 Rose CS. Early detection, clinical diagnosis, and management of lung disease from exposure to diacetyl. *Toxicology* 2017;388:9–14.

98 Kreiss K. Occupational causes of constrictive bronchiolitis. *Curr Opin Allergy Clin Immunol* 2013;13:167–172.

99 Thunnissen E, Blaauwgeers HJ, de Cuba EM, Yick CY, Flieder DB. Ex vivo artifacts and histopathologic pitfalls in the lung. *Arch Pathol Lab Med* 2016;140:212–220.

100 Leslie KO. My approach to interstitial lung disease using clinical, radiological and histopathological patterns. *J Clin Pathol* 2009;62: 387–401.

101 Allen TC. Pathology of small airways disease. *Arch Pathol Lab Med* 2010;134:702–718.

102 Baird CP, DeBakey S, Reid L, Hauschild VD, Petruccelli B, Abraham JH. Respiratory health status of US Army personnel potentially exposed to smoke from 2003 Al-Mishraq sulfur plant fire. *J Occup Environ Med* 2012;54:717–723.

103 Madar CS, Lewin-Smith MR, Franks TJ, Harley RA, Klaric JS, Morris MJ. Histological diagnoses of military personnel undergoing lung biopsy after deployment to Southwest Asia. *Lung* 2017;195: 507–515.

104 Shorr AF, Scoville SL, Cersovsky SB, Shanks GD, Ockenhouse CF, Smoak BL, *et al*. Acute eosinophilic pneumonia among US military personnel deployed in or near Iraq. *JAMA* 2004;292:2997–3005.

105 Sine CR, Hiles PD, Scoville SL, Haynes RL, Allan PF, Franks TJ, *et al*. Acute eosinophilic pneumonia in the deployed military setting. *Respir Med* 2018;137:123–128.

106 Jani N, Falvo MJ, Sotolongo A, Osinubi OY, Tseng CL, Rowneki M, *et al*. Blast injury and cardiopulmonary symptoms in U.S. veterans: analysis of a national registry. *Ann Intern Med* 2017;167:753–755.

107 Liu J, Lezama N, Gasper J, Kawata J, Morley S, Helmer D, *et al*. Burn pit emissions exposure and respiratory and cardiovascular conditions among airborne hazards and open burn pit registry participants. *J Occup Environ Med* 2016;58:e249–e255.

108 National Academies of Sciences, Engineering, and Medicine. Assessment of the Department of Veterans Affairs Airborne Hazards and Open Burn Pit Registry. Washington, DC: National Academies Press; 2017.

109 Kloog I, Chudnovsky A, Koutrakis P, Schwartz J. Temporal and spatial assessments of minimum air temperature using satellite surface temperature measurements in Massachusetts, USA. *Sci Total Environ* 2012;432:85–92.

110 Lushniak B, Mallon CT, Gaydos JC, Smith DJ. Utility of the Department of Defense Serum Repository in assessing deployment exposure. *J Occup Environ Med* 2016;58(8, Suppl 1):S1–S2.

111 Mallon CT, Rohrbeck MP, Haines MK, Jones DP, Utell M, Hopke PK, *et al*. Introduction to Department of Defense research on burn pits, biomarkers, and health outcomes related to deployment in Iraq and Afghanistan. *J Occup Environ Med* 2016;58(8, Suppl 1):S3–S11.

112 Walker DI, Mallon CT, Hopke PK, Uppal K, Go YM, Rohrbeck P, *et al*. Deployment-associated exposure surveillance with high-resolution metabolomics. *J Occup Environ Med* 2016;58(8, Suppl 1):S12–S21.

113 Xia X, Carroll-Haddad A, Brown N, Utell MJ, Mallon CT, Hopke PK. Polycyclic aromatic hydrocarbons and polychlorinated dibenzo-*p*-dioxins/dibenzofurans in microliter samples of human serum as exposure indicators. *J Occup Environ Med* 2016;58(8, Suppl 1): S72–S79.

114 Dalgard CL, Polston KF, Sukumar G, Mallon CT, Wilkerson MD, Pollard HB. MicroRNA expression profiling of the Armed Forces Health Surveillance Branch cohort for identification of "enviro-miRs" associated with deployment-based environmental exposure. *J Occup Environ Med* 2016;58(8, Suppl 1):S97–S103.

115 Woeller CF, Thatcher TH, Van Twisk D, Pollock SJ, Croasdell A, Hopke PK, *et al*. MicroRNAs as novel biomarkers of deployment status and exposure to polychlorinated dibenzo-*p*-dioxins/dibenzofurans. *J Occup Environ Med* 2016;58(8, Suppl 1):S89–S96.

116 Jaakkola MS, Jaakkola JJ, Ernst P, Becklake MR. Respiratory symptoms in young adults should not be overlooked. *Am Rev Respir Dis* 1993;147:359–366.

117 Sunyer J, Basagaña X, Roca J, Urrutia I, Jaen A, Antó JM, *et al*.; ECRHS study. Relations between respiratory symptoms and spirometric values in young adults: the European Community Respiratory Health Study. *Respir Med* 2004;98:1025–1033.

118 Kalhan R, Dransfield MT, Colangelo LA, Cuttica MJ, Jacobs DR Jr, Thyagarajan B, *et al*. Respiratory symptoms in young adults and future lung disease: the CARDIA Lung Study. *Am J Respir Crit Care Med* 2018;197:1616–1624.

Directed evolution of the metalloproteinase inhibitor TIMP-1 reveals that its N- and C-terminal domains cooperate in matrix metalloproteinase recognition

Received for publication, March 6, 2019, and in revised form, April 23, 2019 Published, Papers in Press, April 30, 2019, DOI 10.1074/jbc.RA119.008321

Maryam Raeeszadeh-Sarmazdeh[‡], Kerrie A. Greene[‡], Banumathi Sankaran[§], Gregory P. Downey[¶‖], Derek C. Radisky[‡], and Evette S. Radisky[‡1]

From the [‡]Department of Cancer Biology, Mayo Clinic, Jacksonville, Florida 32224, [§]Berkeley Center for Structural Biology, Lawrence Berkeley National Laboratory, Berkeley, California 94720, [¶]Departments of Medicine, Pediatrics, and Biomedical Research, National Jewish Health, Denver, Colorado 80206, and [‖]Departments of Medicine, Immunology, and Microbiology, University of Colorado, Aurora, Colorado 80045

Edited by Norma M. Allewell

Tissue inhibitors of metalloproteinases (TIMPs) are natural inhibitors of matrix metalloproteinases (MMPs), enzymes that contribute to cancer and many inflammatory and degenerative diseases. The TIMP N-terminal domain binds and inhibits an MMP catalytic domain, but the role of the TIMP C-terminal domain in MMP inhibition is poorly understood. Here, we employed yeast surface display for directed evolution of full-length human TIMP-1 to develop MMP-3–targeting ultra-binders. By simultaneously incorporating diversity into both domains, we identified TIMP-1 variants that were up to 10-fold improved in binding MMP-3 compared with WT TIMP-1, with inhibition constants (K_i) in the low picomolar range. Analysis of individual and paired mutations from the selected TIMP-1 variants revealed cooperative effects between distant residues located on the N- and C-terminal TIMP domains, positioned on opposite sides of the interaction interface with MMP-3. Crystal structures of MMP-3 complexes with TIMP-1 variants revealed conformational changes in TIMP-1 near the cooperative mutation sites. Affinity was strengthened by cinching of a reciprocal "tyrosine clasp" formed between the N-terminal domain of TIMP-1 and proximal MMP-3 interface and by changes in secondary structure within the TIMP-1 C-terminal domain that stabilize interdomain interactions and improve complementarity to MMP-3. Our protein engineering and structural studies provide critical insight into the cooperative function of TIMP domains and the significance of peripheral TIMP epitopes in MMP recognition. Our findings suggest new strategies to engineer TIMP proteins for therapeutic applications, and our directed evolution approach may also enable exploration of functional domain interactions in other protein systems.

The majority of eukaryotic proteins consist of at least two domains, and these multidomain proteins can perform elaborate tasks, often employing a binding or active site located at the domain interface (1). The separate domains of a multidomain protein fold independently, and yet the interplay between protein domains has an important role in protein structure, stability, and function (2). Efforts to understand the cooperative impact of individual protein domains on function of multidomain proteins can provide deeper insight into natural protein function and regulation and can also inform new strategies for rational design and engineering of multidomain proteins (3).

Tissue inhibitors of metalloproteinases (TIMPs),[2] a family of four proteins in vertebrates, are endogenous inhibitors of matrix metalloproteinases (MMPs) that regulate MMP function and activity (4, 5). TIMPs comprise two domains that pack side by side. The N-terminal domain is widely recognized as the primary inhibitory domain that blocks MMP enzymatic activity by binding at the active site and interacting with the catalytic zinc (5–7). The TIMP C-terminal domain in some cases regulates MMP activation through interactions with noncatalytic MMP hemopexin domains (8) or stimulates MMP-independent cell signaling by binding to membrane receptors (9, 10). Although the TIMP C-terminal domain may also contribute to the binding interface with an MMP catalytic domain, conferring a degree of binding affinity (11, 12), the significance of this interaction and mechanism by which it contributes to MMP recognition have been largely overlooked. Here, we sought to probe the role of the TIMP C-terminal domain and of cooperativity between TIMP domains in MMP recognition.

Directed evolution of proteins is commonly used to improve or alter protein function toward desired properties but, importantly, can also be used to uncover insights relating sequence to function (13–15). Yeast surface display (YSD) is a directed evolution platform for engineering protein binders, including anti-

This work was supported by National Institutes of Health Grant R21 CA205471 (to E. S. R.) and United States Department of Defense Grant W81XWH-16-2-0030 (to G. P. D. and D. C. R.). The authors declare that they have no conflicts of interest with the contents of this article. The content is solely the responsibility of the authors and does not necessarily represent the official views of the National Institutes of Health.

The atomic coordinates and structure factors (codes 6MAV and 6N9D) have been deposited in the Protein Data Bank (http://wwpdb.org/).

[1] To whom correspondence should be addressed: Dept. of Cancer Biology, Mayo Clinic, 310 Griffin Bldg., 4500 San Pablo Rd., Jacksonville, FL 32224. Tel.: 904-953-6372; E-mail: radisky.evette@mayo.edu.

[2] The abbreviations used are: TIMP, tissue inhibitor of metalloproteinases; MMP, matrix metalloproteinase; YSD, yeast surface display; MMP-3cd, MMP-3 catalytic domain; MTL, multiple-turn loop; FN3, fibronectin type III domain; TLS, translation/libration/screw; PDB, Protein Data Bank; Bis-Tris, 2-[bis(2-hydroxyethyl)amino]-2-(hydroxymethyl)propane-1,3-diol.

bodies (16, 17) or other scaffolds (18), and benefits from eukaryotic secretion machinery that provides quality control for displaying full-length, stable, and properly folded proteins (17, 19), making it a suitable platform for engineering multidomain proteins. YSD has typically been applied to evolve single protein domains for altered binding characteristics, as in the recent engineering of the TIMP-2 N-terminal domain for selectivity toward MMP-9 and -14 (20–22). We hypothesized that by simultaneously applying directed evolution to both domains of a full-length TIMP on the yeast surface, we might probe the roles of each individual domain as well as any cooperative dynamic in MMP recognition; by evolving the intact multidomain protein holistically, we could optimize functional domain interplay.

Here, by creating a YSD library incorporating diversity into both domains of TIMP-1 and analyzing mutations of variants selected for improved binding to an already extremely high-affinity natural target, the MMP-3 catalytic domain (MMP-3cd), we aimed to evaluate the potential contributions of each TIMP domain to MMP affinity. The results of our analyses identify an unsuspected role for the TIMP-1 C-terminal domain in evolving MMP-3 affinity, mediated through synergistic effects between distant sites on the opposing TIMP domains. Protein structures of TIMP-1 mutants cocrystallized with MMP-3cd provide insights into the domain cooperativity of TIMP-1 variants with improved MMP-3cd binding. Our results have important implications for development of therapeutic TIMPs with optimized MMP-binding characteristics, while our conceptual approach may be more widely applicable to the application of directed evolution as a tool to probe domain interplay in other multidomain proteins.

Results

Screening of full-length TIMP-1 surface-displayed library identifies variants with improved binding to MMP-3

To explore the roles of each TIMP-1 domain in modulating MMP binding and inhibition, we first developed a platform for YSD of full-length human TIMP-1. The free, exposed N terminus of TIMP-1 is required for MMP binding and inhibition (6, 23); accordingly, we designed a fusion construct connecting the C terminus of TIMP-1 to the N terminus of yeast cell wall protein Aga2p, with secretion directed by the yeast α-factor signal sequence (Fig. 1*A*). Display of TIMP-1 bearing the correctly processed, mature N terminus was optimized by deletion of Glu-Ala residues from the signal sequence, which otherwise were inefficiently removed by yeast STE13 protease (Fig. 1). The optimized construct was N-terminally processed by yeast protease Kex2, resulting in efficient display of a functional TIMP-1 fusion that demonstrated robust MMP binding, as detected using biotinylated MMP-3cd (Figs. 1*C* and 2, *A* and *D*). MMP-3cd was selected as a model for the TIMP-1/MMP interaction as it offers a well-studied, well-behaved minimal MMP catalytic domain, and its interaction with TIMP-1 has been structurally characterized (6). We also evaluated the potential benefit of codon optimization of the human TIMP-1 gene for yeast but found minimal impact on efficiency of display (Fig. 1*D*).

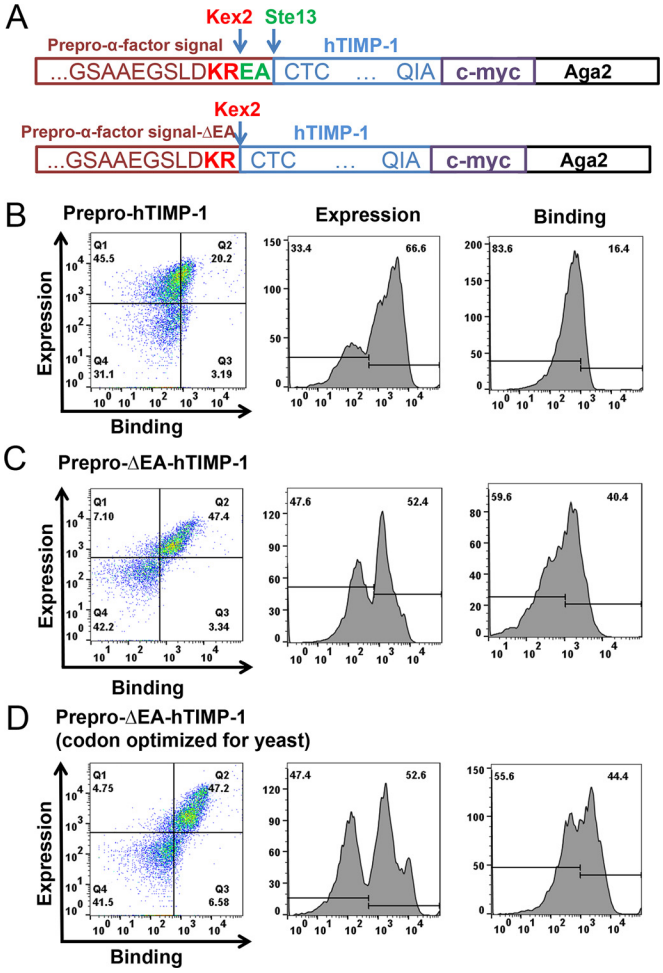

Figure 1. TIMP-1 yeast display and MMP-3cd binding optimization. *A*, TIMP-1 yeast surface display constructs in pCHA vector. *Top* construct (prepro-hTIMP-1), prepro-α-factor yeast signal with Kex2 (*KR*) and Ste13 (*EA*) cleavage sites fused to the mature N terminus of TIMP-1 followed by c-myc epitope tag fused to the N terminus of Aga2. *Bottom* construct (prepro-ΔEA-hTIMP-1), prepro-α-factor yeast signal with Kex2 (*KR*) cleavage site fused to the mature N terminus of TIMP-1 followed by c-myc epitope tag fused to the N terminus of Aga2. *B–D*, flow cytometry results for MMP-3cd binding to TIMP-1 constructs displayed on the yeast surface. *Left panels*, dual scatter plot representing MMP-3cd binding on the *x axis* and TIMP-1 expression (c-myc binding) on the *y axis*; *Q2* represents the cell population dually labeled by biotinylated MMP-3cd and anti-c-myc binding. *Middle panels*, histograms of TIMP-1 expression (detected by anti-c-myc). *Right panels*, histograms of MMP-3cd binding. *B*, yeast display of human TIMP-1 (*hTIMP-1*) with Kex2 and Ste13 cleavage sites (prepro-hTIMP-1) shows high expression but only modest MMP-3cd binding, suggesting inefficient processing by Ste13. *C*, yeast display of human TIMP-1 with Kex2 cleavage site only (prepro-ΔEA-hTIMP-1) shows high expression and MMP-3dc binding, indicating more efficient processing of the mature N terminus of TIMP-1. *D*, yeast display of human TIMP-1, codon-optimized for yeast, with Kex2 cleavage site only shows expression and MMP-3cd binding similar to the noncodon-optimized construct.

We next generated a targeted library of TIMP-1 mutants, incorporating diversity into MMP contact zones located on both domains of TIMP-1, including 8 residues within the N-terminal domain and 9 residues within the C-terminal domain (Fig. 2, *B* and *C*). The TIMP-1 mutant library was constructed aiming to achieve on average three to four mutations per variant through incorporation of degenerate codons and yielded a library size of $\sim 5 \times 10^6$ independent TIMP-1 variants

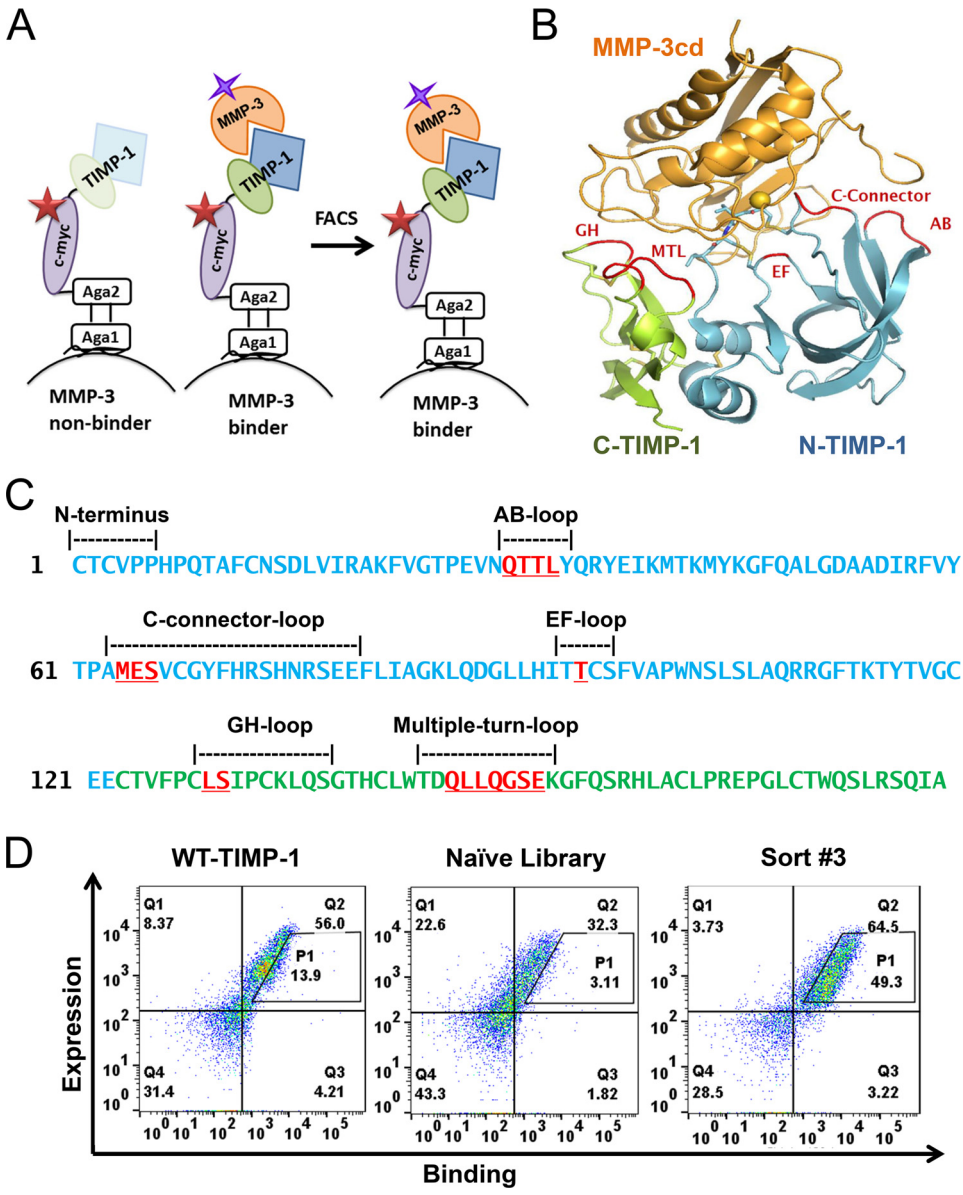

Figure 2. Screening a library of TIMP-1 mutants for MMP-3 binding. *A*, schematic diagram illustrates how a library of TIMP-1 mutants (*blue*/*green*) was displayed on the yeast surface. TIMP-1 expression was measured using fluorescent conjugated c-myc antibody (*red star*), and MMP-3 binding was measured using biotinylated MMP-3cd (*orange*) and fluorescent conjugated streptavidin (*purple star*). TIMP-1 variants with improved MMP-3cd binding were screened using FACS. *B*, library diversity was focused in 17 residues of TIMP-1 (loops in *red*), located in both the N-terminal (*blue*) and C-terminal (*green*) domains, that interact with bound MMP-3cd (*orange*) in PDB structure 1UEA. Targeted residues are located in the AB-loop, C-connector, and EF-loop of the N-terminal domain, and the GH-loop and MTL of the C-terminal domain. *C*, the WT TIMP-1 N- and C-terminal domain sequences are shown, colored in *blue* and *green*, respectively. Segments that interact with MMP-3cd in crystal structure 1UEA are annotated in *black text* above the sequence, including the N terminus and AB-loop, C-connector, EF-loop, GH-loop, and MTL. TIMP-1 residues diversified in the targeted library are highlighted in *red* and *underlined*. *D*, flow cytometry scatter plots of dually labeled yeast cells show lower MMP-3cd binding signal (*x axis*) for naïve library (*center panel*) relative to WT TIMP-1 (*left panel*); the population after three rounds of FACS sorting (*right panel*) shows greatly increased MMP-3 binding signal. *P1*, the diagonal sort gate, represents a population of yeast cells with a high ratio of MMP-3cd binding relative to TIMP-1 expression.

in yeast upon transformation. The YSD TIMP-1 library was screened using fluorescence-activated cell sorting (FACS) by incrementally decreasing the concentration of biotinylated MMP-3cd in successive rounds of sorting, selecting for clones with enhanced affinity toward MMP-3cd (Fig. 2, *A* and *D*). After several rounds of FACS to enrich the pool for variants with highest MMP-3 binding relative to TIMP-1 expression, the enriched pool showed significant enhancement in MMP-3 binding compared with both the naïve library and WT TIMP-1 (Fig. 2*D*). The further enriched TIMP-1 variants isolated after six rounds of FACS screening, representing a total of four unique sequences, showed up to 10-fold binding improvement compared with WT TIMP-1 (Fig. 3, *A*–*C*).

Analysis of TIMP-1 single and double mutants reveals cooperative impact of N- and C-terminal domain mutations on MMP-3 binding

The high-affinity MMP-3-binding TIMP-1 variants obtained from library screening contained four to five mutations per gene; notably, all sequences contained mutations in both the N-terminal and C-terminal domains (Fig. 3*C*). To identify the mutations directly responsible for affinity improvements, we

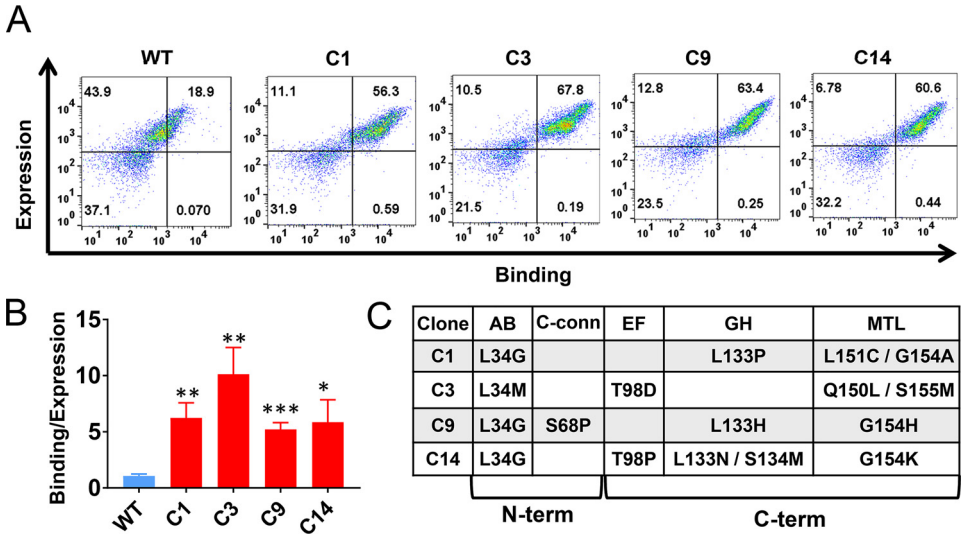

Figure 3. TIMP-1 variants with improved MMP-3 binding. *A*, flow cytometry scatter plots of dually labeled yeast cells are shown for four yeast-displayed TIMP-1 variants with improved MMP-3cd–binding activity; WT TIMP-1 is shown for reference on the *left*. The *x axis* (APC channel) represents biotinylated MMP-3cd binding (250 nM); the *y axis* (FITC channel) represents TIMP-1 expression. *B*, median fluorescence MMP-3cd binding signal, corrected for background and normalized to TIMP-1 expression, is plotted for each yeast-displayed TIMP-1 variant stained with 250 nM biotinylated MMP-3cd. Flow cytometry binding experiments were repeated at least twice; plotted values represent average ± S.D. (*error bars*). *C*, mutations found in TIMP-1 variants with improved MMP-3 binding are shown, along with their locations in the five targeted MMP-3–interacting loops of TIMP-1 (AB-loop, C-connector (*C-conn*), EF-loop, GH-loop, and MTL). *, $p \leq 0.05$; **, $p \leq 0.01$; ***, $p \leq 0.001$.

next generated single-mutant constructs representing the most prevalent mutations and assessed MMP-3cd binding on the yeast surface. Mutations L34G located in the AB-loop and T98D located in the EF-loop of the TIMP-1 N-terminal domain each conferred significant improvement (Fig. 4*A*), and yet the binding enhancements of these single mutants were modest by comparison with the composite mutants selected from the library (Fig. 3*B*). Interestingly, the L34G mutation co-occurred repeatedly in combination with Gly-154 mutations in the multiple-turn loop (MTL) of the C-terminal domain located ~30 Å away. To evaluate the potential functional interaction of these distant residues, we next generated and evaluated several TIMP-1 double-mutant constructs. We found that although TIMP-1 single mutations affecting Gly-154 in isolation had no significant impact on MMP-3 binding (Fig. 4*A*), several substitutions at this position (Ala, His, and Lys) had a powerful synergistic effect when combined with the L34G mutation (Fig. 4, *B–D*). In each case examined, the L34G/G154*X* double mutants showed binding improvements indistinguishable from those of the corresponding library clones, suggesting that mutations at these two sites were sufficient to confer the full functional improvements of selected clones C1, C9, and C14. By contrast, TIMP-1 double mutants combining G154A/H with T98D did not demonstrate similar augmentation of MMP-3 binding affinity above that of the T98D single mutant (Fig. 4, *E* and *F*), suggesting that Gly-154 mutations modify MMP affinity in a context-dependent fashion rather than conferring an independent and additive effect.

To extend our findings and quantitatively evaluate protease-inhibitory activity of TIMP-1 variants in solution, we next cloned, expressed, and purified soluble forms of several of the mutant TIMP-1 proteins using a human cell expression system. We then assessed inhibition of MMP-3cd activity by soluble WT TIMP-1 and TIMP-1 variants L34G, L34G/G154A, and C1 using an enzyme inhibition assay that measured the reduced rate of cleavage of a fluorometric substrate in the presence of increasing concentrations of the inhibitor. Data were fitted to Morrison's tight binding equation (Equation 1) to determine equilibrium inhibition constants (K_i) (Fig. 5 and Table 1). Importantly, these solution studies corroborated the YSD findings; variant C1 showed >5-fold improvement compared with WT TIMP-1, an effect fully recapitulated by theTIMP-1-L34G/G154A variant (Table 1). Thus, we find consistent evidence from both solution studies and YSD demonstrating that TIMP-1 C-terminal domain mutations can act cooperatively with N-terminal domain mutations to modulate MMP binding and inhibition.

Crystal structures of TIMP-1 variants in complex with MMP-3 show conformational changes that stabilize interdomain interactions and MMP-3 binding

To gain structural insights into the effect of amino acid substitutions on the binding mechanism of TIMP-1 with MMP-3cd, we cocrystallized the TIMP-1-L34G and TIMP-1-C1 (L34G/L151C/L133P/G154A) mutants in complex with MMP-3cd and solved the crystal structures of the complexes. The TIMP-1-L34G/MMP-3cd and TIMP-1-C1/MMP-3cd structures were solved by molecular replacement and refined against diffraction data extending to resolutions of 2.37 and 2.67 Å, respectively. Data collection and refinement statistics are summarized in Table 2. Each complex shows the expected protein architecture of TIMP-1 and MMP-3cd as described previously for the complex with WT TIMP-1 (PDB code 1UEA) (6); however, notable deviations are seen in the vicinity of the mutated residues that can account for the observed improvements in binding and inhibition.

A striking feature observed in both mutant structures, proximal to the L34G mutation at the enzyme/inhibitor

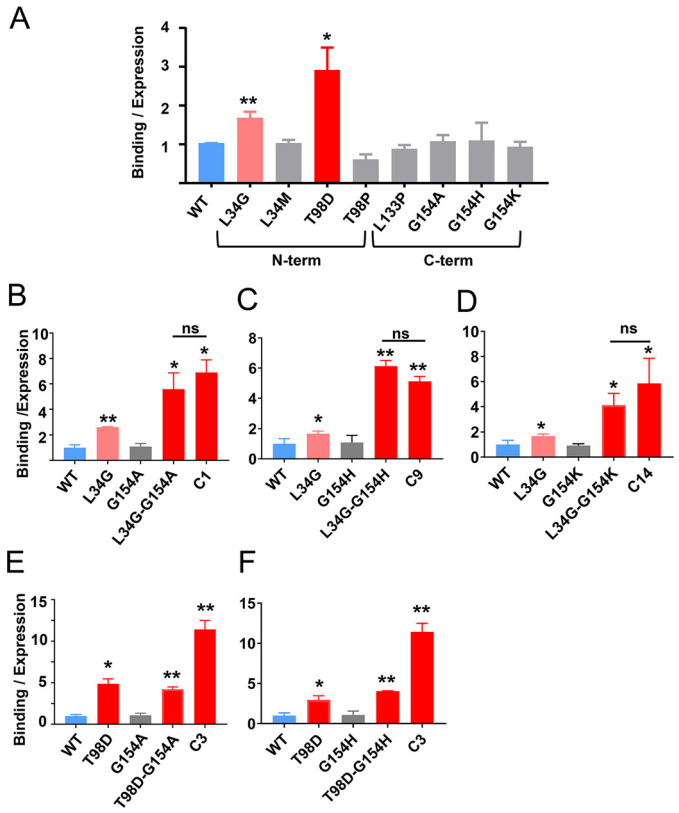

Figure 4. Dissecting functionally important mutations of TIMP-1 variants. *A*, among tested mutations found in the library-selected TIMP-1 variants with improved MMP-3cd–binding affinity, only L34G and T98D show functional enhancement as single mutations. *B–D*, Gly-154 mutations to Ala, His, or Lys cooperatively enhance MMP-3cd binding when combined with L34G. *B*, although not function-enhancing as a single mutation, G154A combined with L34G increases MMP-3cd binding nearly to the level of the composite library-selected variant C1 (L34G/L133P/L152C/G154A). *C*, likewise, G154H has no significant functional effect as a single mutation but cooperatively enhances MMP-3cd binding in combination with L34G, up to the level of the composite library-selected variant C9 (L34G/S68P/L133H/G154H). *D*, similarly, G154K offers functional benefit only in combination with L34G where it cooperatively enhances MMP-3cd binding nearly to the level of the composite library-selected variant C14 (L34G/T98P/L133N/S134M/G154K). *E*, by contrast, the G154A mutation does not confer further enhancement of MMP-3cd binding when combined with the T98D mutation. *F*, the G154H mutation likewise does not significantly improve MMP-3cd binding in the double T98D/G154H variant. Graphs show MMP-3cd binding to TIMP-1 expression ratio, based on median fluorescence corrected to background signal, for yeast-displayed TIMP-1 mutants stained with 250 nM biotinylated MMP-3cd. Flow cytometry binding experiments were repeated at least twice; plotted values represent average ± S.D. (*error bars*). *, $p \leq 0.05$; **, $p \leq 0.01$; *ns*, not significant.

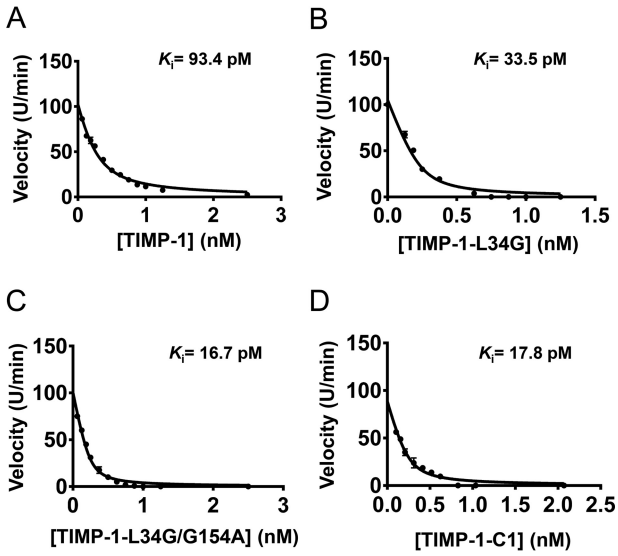

Figure 5. K_i determination using Morrison fits of inhibition assays. Equilibrium inhibition constants (K_i) of purified soluble TIMP-1 and variants toward MMP-3cd were measured by the reduction in cleavage rates of a fluorogenic substrate in the presence of increasing concentration of the inhibitors. Data were plotted as initial velocities *versus* TIMP variant concentration and fitted by multiple regression to Morrison's tight binding inhibition equation as shown. The K_i value determined for each TIMP-1 variant is indicated on the plot and in Table 1. *A*, WT TIMP-1. *B*, TIMP-1-L34G. *C*, TIMP-1-L34G/G154A. *D*, TIMP-1-C1 (L34G/L133P/L151C/G154A).

Table 1
K_i values for TIMP-1 variants

TIMP-1 mutant	K_i
	*p*M
WT	93.4 ± 8.1
L34G	33.5 ± 4.2
L34G/G154A	16.7 ± 1.5
C1	17.8 ± 1.8

interface, is a reciprocal "clasp" formed by Tyr-35 of TIMP-1 and Tyr-153 of MMP-3 (Fig. 6, *A* and *B*). The two Tyr rings, one from each protein, stretch across the interface to form H-bonds with the partner protein, TIMP-1 Tyr-35 with the MMP-3 Phe-154 backbone carbonyl and MMP-3 Tyr-155 with the TIMP-1 Gly-34 backbone carbonyl. Additionally, the two Tyr aromatic rings form hydrophobic and edge-to-face π interactions bridging the interface. Formation of this reciprocal tyrosine clasp is facilitated by substantial backbone displacements in the TIMP-1-L34G AB-loop and the MMP-3 S-loop compared with the WT TIMP-1/MMP-3cd complex (Fig. 6*C*). In the WT TIMP-1 structure, bulkier Leu-34 pushes these two loops apart, preventing Tyr-35 of TIMP-1 from H-bonding to the Phe-154 carbonyl, whereas in the L34G mutant structure the distance between oxygens is shortened from 3.5 to 3 Å. The H-bond between MMP-3 Tyr-155 and TIMP-1 Gly-34 is already present in the WT TIMP-1 complex with a distance of 2.6 Å between oxygens; however, the shift of the MMP-3 S-loop in the mutant complexes enables this short H-bond to be cinched even tighter in the TIMP-1 mutant complexes (Fig. 6).

The TIMP-1-C1/MMP-3cd crystal structure reflects near-identical conformational changes in the TIMP-1 AB-loop and MMP-3cd S-loop, resulting from the L34G mutation, with consequent cinching of the reciprocal tyrosine clasp. In addition, mutations in the C-terminal domain of TIMP-1 produce significant conformational changes in this domain, the effect of which is to strengthen interactions both with the TIMP-1 N-terminal domain and with MMP-3cd. TIMP-1-C1 mutation G154A results in adoption of an α-helical conformation by residues 154–157 of the multiple-turn loop at the interface between the TIMP-1 N- and C-terminal domains (Fig. 7, *A*, *D*, and *E*). Glycine, the native TIMP-1 residue at this position, is known to destabilize α-helical secondary structures (24), and each of the mutations of this residue identified in our library screen, to Ala, His, and Lys, are predicted to confer greater propensity for α-helix formation (25, 26), explaining the surprising array of varied substitutions selected at this position. This alteration

Table 2
X-ray crystallographic data collection and refinement statistics
r.m.s.d., root mean square deviation.

Crystal data		
Structure name	TIMP-1-L34G/MMP-3cd	TIMP-1-C1/MMP-3cd
PDB code	6MAV	6N9D
Data collection		
Resolution range (Å)	52.59–2.37 (2.46–2.37)	43.99–2.67 (2.77–2.67)
Space group	P 6_5 2 2	P 6_5 2 2
a, *b*, *c* (Å)	69.70, 69.70, 321.33	70.03, 70.03, 319.51
α, β, γ (°)	90, 90, 120	90, 90, 120
R_{merge}	0.066 (0.791)	0.247 (1.838)
R_{meas}	0.069 (1.180)	0.253 (1.882)
R_{pim}	0.028 (0.328)	0.055 (0.402)
CC1/2	0.999 (0.933)	0.982 (0.668)
Multiplicity	12.1 (12.7)	20.4 (21.1)
Completeness (%)	99.9 (100.0)	99.5 (89.3)
Mean $I/\sigma(I)$	19.1 (3.1)	18.8 (2.2)
Refinement		
Unique reflections used in refinement	19,911	14,162
R_{work}/R_{free}	0.217/0.298	0.184/0.258
Number of non-hydrogen atoms	2,681	2,675
Macromolecules	2,643	2,624
Ligands	5	5
Solvent	33	46
Protein residues	335	336
r.m.s.d. bonds (Å)	0.010	0.009
r.m.s.d. angles (°)	1.35	1.30
Ramachandran favored (%)	91	94
Ramachandran outliers (%)	1.2	0.3
Average B-factor	77.60	55.10
Macromolecules	77.70	55.20
Ligands	69.80	51.60
Solvent	71.30	49.20

in secondary structure allows the two domains of TIMP-1 to pack together more tightly and introduces a new H-bond stabilizing the interdomain interaction (Fig. 7*D*). Additional conformational alterations in the TIMP-1-C1 structure result in closer contact with MMP-3cd, including hydrophobic contacts of TIMP-1-C1 Leu-152 with MMP-3 Thr-215, Tyr-220, and Leu-222 side chains (Fig. 7*B*) and a new intradomain H-bond between TIMP-1 residues Gln-150 and Pro-133 (Fig. 7*C*). In sum, the stabilizing effects of the mutations on TIMP-1 C-terminal domain secondary structure and on interdomain interactions serve to integrate the domains of this multidomain protein, producing functional cooperativity, which in turn improves MMP-3cd binding.

Discussion

Despite the common belief that the N-terminal domain of a TIMP is solely responsible for MMP binding and inhibition, here we have found that the C-terminal domain of TIMP-1 and the interplay between the two domains play a significant role in MMP-3 binding. We further have shown that not only the MMP-contacting interface but also the interactions between TIMP domains can be optimized in an integral fashion to achieve desired binding characteristics. Prior studies seeking to define and reshape the protease-inhibitory function of TIMPs have focused on the N-terminal domain due to the early finding that the isolated N-TIMP domain is independently capable of MMP inhibition with only modest loss of affinity compared with full-length TIMPs (7, 12). Site-directed mutagenesis experiments identified several key amino acid residues, mutation of which can shift the inhibition specificity of N-TIMPs (27–35). More recently, directed evolution efforts have employed phage display or YSD screening of N-TIMP-2 libraries to more broadly scan the sequence determinants of binding specificity at the N-TIMP/MMP interface (20–22, 36). These studies have shown TIMPs to be malleable scaffolds, tolerant of mutation and relatively easy to reengineer for an altered spectrum of protease-inhibitory activity. However, prior work has overlooked the potential functional role of the TIMP C-terminal domain, which can contribute up to a third of the contact surface area at the TIMP/MMP interface (11). Furthermore, the more complex tertiary structures of multidomain proteins are often accompanied by more complex functional capabilities (1) where cooperation between domains renders an intact protein as more than the sum of its parts. Here, by applying evolutionary pressure to a library of full-length TIMP-1 variants, diversified in both domains, we have uncovered such functional cooperativity between TIMP domains.

Our structural analyses of TIMP-1 variants lend insight into how TIMP mutations at the periphery of the interface with an MMP, in both the N- and C-terminal domains, can stabilize binding interactions. Within the N-terminal domain AB-loop, we identified the L34G mutation, which facilitates tighter cinching of a reciprocal tyrosine clasp involving Tyr-35 of TIMP-1 and Tyr-153 of MMP-3. Our structures demonstrate shortening of one intermolecular H-bond and formation of a new additional H-bond. H-bonds have long been appreciated as major contributors to protein–protein binding affinity and specificity (37, 38), where the strength of H-bonds generally correlates well with interatomic distance between the proton donor and acceptor (39). Tyrosine residues in particular are highly represented in protein/protein interaction hot spots (40, 41), likely due to the ability to form aromatic π interactions as well as H-bonds, both of which are evidenced in our structures.

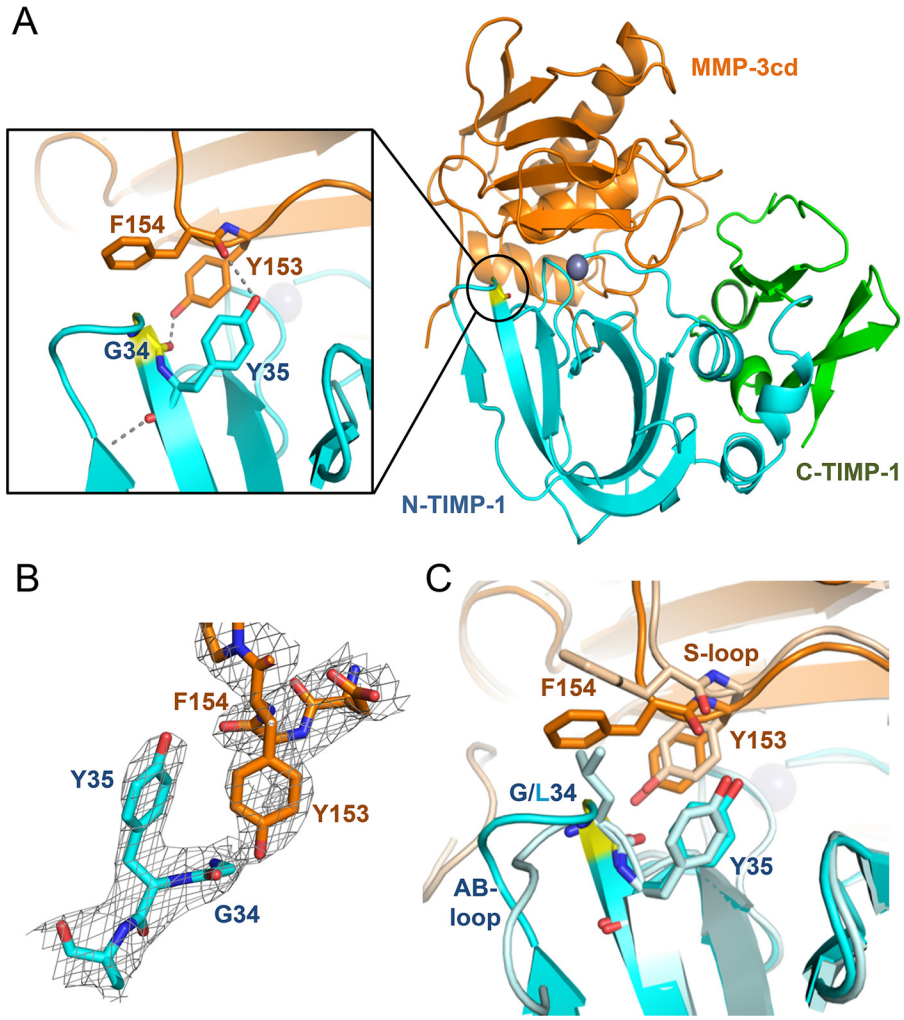

Figure 6. Crystal structure of TIMP-1-L34G mutant bound to MMP-3cd. *A*, cartoon representation of the TIMP-1-L34G/MMP-3cd complex crystal structure is shown (*right*); TIMP-1-L34G is in *blue* (N-terminal domain) and *green* (C-terminal domain) with the mutated residue in *yellow*, and MMP-3cd is in *orange* with the catalytic zinc ion shown as a *gray sphere*. The *inset panel* (*left*) shows interactions of TIMP-1-L34G Tyr-35 and MMP-3cd Tyr-153, which form a reciprocal tyrosine clasp at the binding interface. *B*, stick representation of the protein environment surrounding the reciprocal tyrosine clasp with $2F_o - F_c$ map contoured at 1.5σ. *C*, superposition of the mutant TIMP-1-L34G/MMP-3cd crystal structure (colored as above) with the WT TIMP-1/MMP-3cd structure (PDB code 1UEA; shown in *pale blue/pale orange*) highlights the conformational changes in the AB-loop of TIMP-1-L34G, which result in the cinching of the reciprocal tyrosine clasp.

Within the C-terminal domain, we identified the G154A mutation, responsible for conformational changes in the multiple-turn loop that impact both the binding interface with MMP-3cd and the interface between the TIMP domains. The interface with MMP-3cd gains new hydrophobic stabilizing contacts, while the interdomain interface is stabilized by the defined α-helical secondary structure adopted by TIMP residues 154–157 and by a new interdomain H-bond. Interestingly, TIMP-1 Gly-154, a residue with low helical propensity, was found mutated to Ala, Lys, and His, residues with higher helical propensities (25, 26), in three of four isolated clones with enhanced MMP-3cd– binding affinity. Given that we observed a function-enhancing role for these substitutions only in combination with the L34G mutation, it may be that a G154*X* mutation alone is insufficient to fully stabilize the helical turn but requires additional structural stability conferred by the reciprocal tyrosine clasp on the opposite side of the intermolecular interface.

Because MMPs represent high-value but challenging therapeutic targets, our results suggest new avenues for engineering MMP-targeted therapeutic proteins. Many human MMPs contribute to pathology of cancer, fibrosis, arthritis, cardiovascular, pulmonary, and other diseases when improperly expressed (23, 42, 43), but clinical trials of broad-spectrum MMP inhibitors in cancer and arthritis proved disappointing (44, 45). Engineered designer TIMPs have been viewed as a possible pathway to achieve greater selectivity and efficacy (23, 46, 47), and recent campaigns to develop such selectivity have employed YSD platforms for directed evolution of N-TIMP-2 aided by computational library design (20–22). Our present findings suggest that future TIMP engineering efforts may benefit from employing a full-length TIMP scaffold and, further, that maximum advantage of the multidomain scaffold may be best achieved through simultaneous optimization to capture cooperative mutations across domains.

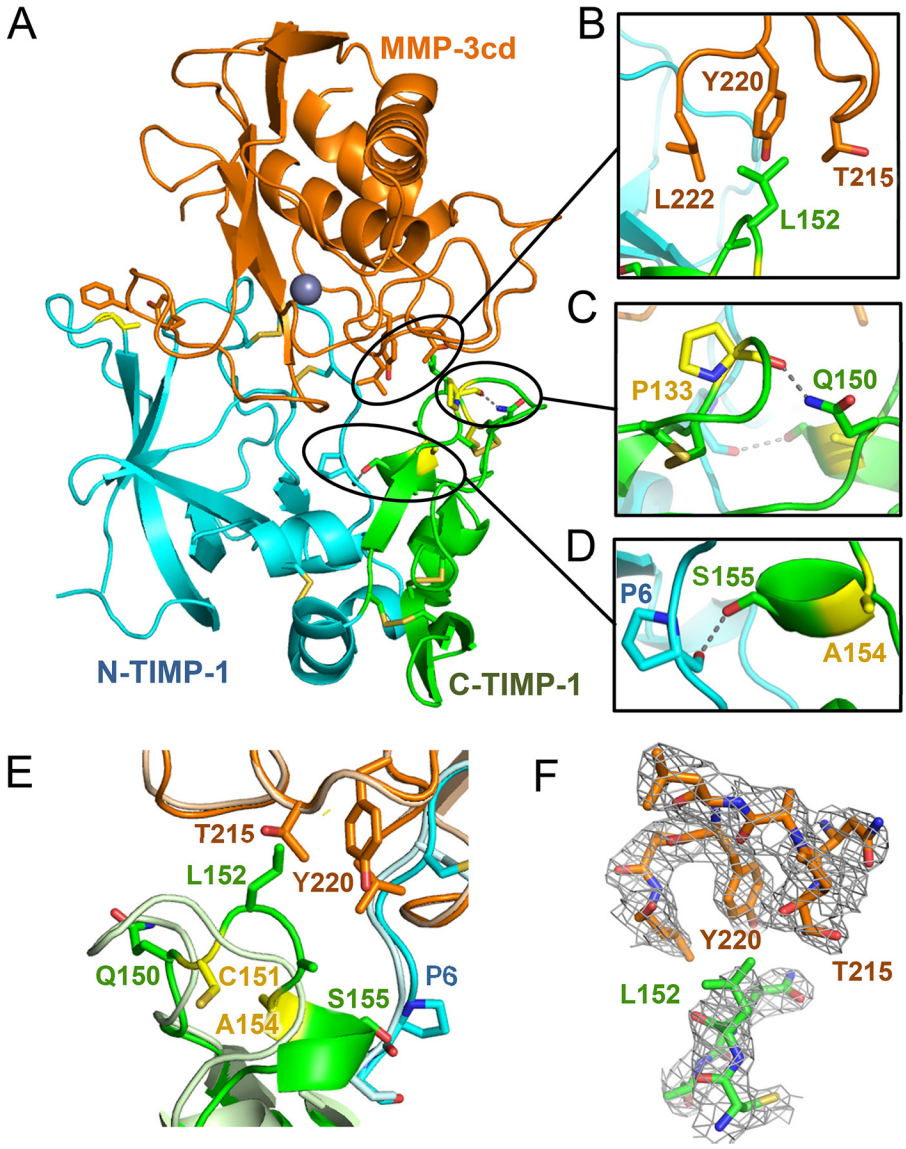

Figure 7. Crystal structure of TIMP-1-C1 variant bound to MMP3cd. *A*, cartoon representation of the TIMP-1-C1/MMP-3cd complex crystal structure is shown using the same color scheme described for Fig. 6. Altered inter- and intramolecular interactions attributable to TIMP-1-C1 mutations are highlighted in *B–D*. *B*, a hydrophobic cluster is formed at the intermolecular interface between TIMP-1 Leu-152 and MMP-3cd residues Thr-215, Tyr-220, and Leu-222. *C*, a new H-bond within the TIMP-1-C1 C-terminal domain is formed between the carbonyl of Pro-133 and the side chain of Gln-150. *D*, as a consequence of the G154A mutation, residues 154–157 adopt an α-helical conformation, and a new interdomain H-bond is formed between the side chain of Ser-155 in the C-terminal domain and the carbonyl of Pro-6 in the N-terminal domain. *E*, superposition of the TIMP-1-C1/MMP-3cd crystal structure (colored as above) with the WT TIMP-1/MMP-3cd structure (PDB code 1UEA; shown in *pale blue/pale orange*) highlights conformational changes in the multiple-turn loop of TIMP-1-C1, which facilitate stabilizing interdomain interactions within TIMP-1 as well as favorable hydrophobic interactions at the interface with MMP-3cd. *F*, stick representation of the protein environment surrounding the hydrophobic cluster at the intermolecular interface with $2F_o - F_c$ map contoured at 1.0σ.

Finally, the utility of our approach for identifying and engineering domain cooperativity may extend beyond the TIMP family and have relevance for other systems. Prior studies have demonstrated how connectivity and cooperativity of multiple domains contribute to protein folding, stability, and function (2, 48, 49). Dynamic interactions between individual domains orchestrate folding pathways, determining kinetic and equilibrium properties of cooperative folding (49). Favorable interactions between domains can dictate the stability of individual domain structures (48), and thus interdomain interactions have been critical in the natural evolution of function in multidomain proteins. Directed evolution can recapitulate this natural evolution of multidomain functionality, *e.g.* when a low-affinity peptide-binding PDZ domain was linked to an unrelated, functionally inert fibronectin type III domain (FN3), optimization of FN3 led to a highly selective domain-interdependent "affinity clamp" (1). To date, however, the ability to pinpoint specific sequence and structural determinants of domain cooperativity has been limited. Here, directed evolution simultaneously targeting residues within both domains of TIMP-1 enabled us to search for and identify pairs of residues responsible for interdomain cooperativity in TIMP-1 function. This strategy may be more broadly useful to detect domain cooperativity, probing the structure–function paradigm, and to engineer enhanced synergistic function into other multidomain proteins for varied practical applications.

Experimental procedures

Strains and plasmids

The yeast *Saccharomyces cerevisiae* strain EBY100 (*MATa AGA1::GAL1-AGA1::URA3 ura3–52 trp1 leu2-Δ200 his3-Δ200 pep4::HIS3 prb11.6R can1 GAL*) was used for yeast surface display of human TIMP-1 protein and its variants. Yeast display plasmids for displaying WT TIMP-1 and TIMP-1 mutants at the N terminus of Aga2p protein on the yeast surface were derived from the pCHA backbone, pCHA-VRC01 vector (50) purchased from Addgene.

Yeast surface display of TIMP-1

pCHA-TIMP-1 plasmids (the yeast display vectors) were transformed into the yeast strain EBY100 by electroporation using a Bio-Rad Gene Pulser and 2-mm electroporation cuvettes. The yeast cells were grown in minimal SD-CAA medium, pH 6 (20 g/liter dextrose, 6.7 g/liter yeast nitrogen base lacking amino acids, 5.4 g/liter Na_2HPO_4, 8.6 g/liter $NaH_2PO_4{\cdot}H_2O$, and 5 g/liter Bacto casamino acids). After 16 h growth at 30 °C, cells were pelleted at 3000 × *g* and resuspended in SGR-CAA medium (20 g/liter galactose, 6.7 g/liter yeast nitrogen base lacking amino acids, 5.4 g/liter Na_2HPO_4, 8.6 g/liter $NaH_2PO_4{\cdot}H_2O$, 5 g/liter Bacto casamino acids, and 20 g/liter raffinose) for induction. Cells were grown in SGR-CAA medium at 30 °C for 16 h before harvesting. The yeast cells displaying TIMP-1 variants were collected at an OD_{600} of 0.2 and washed with cold PBSA buffer (8 g/liter NaCl, 0.2 g/liter KCl, 1.44 g/liter Na_2HPO_4, 0.24 g/liter KH_2PO_4, pH 7.4, and 1% BSA). The cells were first incubated with 100–250 nM biotinylated MMP-3cd and mouse anti-c-myc 9e10 (Sigma) for 1 h on ice. The cells were then washed and resuspended in 100 μl of cold PBSA buffer containing fluorescein-conjugated goat anti-mouse antibody (Thermo Fisher) and streptavidin-Alexa Fluor 647 (each at 1:100 dilution) and incubated on ice for 30 min. After harvesting and washing with cold PBSA buffer, the cells were centrifuged and resuspended in 750 μl of PBSA buffer. Flow cytometry data were then collected using an Attune NxT flow cytometer from at least 10,000 cell events per sample and analyzed using FlowJo software (FlowJo, LLC).

Generating the targeted library of TIMP-1 mutants

A library of human TIMP-1 gene variants, targeting for mutation 17 residues in five loops shown to interact with MMP catalytic domains in crystal structures (Fig. 2*C*), was purchased from Invitrogen GeneArt Gene Synthesis. The library of mutants was constructed by assembling gene blocks of synthetic oligonucleotides with 13% chance of NNS degenerate codon incorporation at each position targeted for mutation (where N = any nucleotide and S = G or C), to achieve on average three to four mutations per variant. The yeast display TIMP-1 mutant library was generated by PCR amplification of the TIMP-1 gene from the targeted TIMP-1 library using primers with 50-bp overhangs containing homology to sequence upstream and downstream of the TIMP-1 gene in the pCHA-TIMP-1 yeast display vector. PCR products of TIMP-1 gene variants were gel-purified and concentrated using Pellet Paint® Co-Precipitant (EMD Millipore) following the manufacturer's protocol. The pCHA-TIMP-1 vector was double-digested using BsrGI and BamHI restriction enzymes, and the pCHA digested vector (1 μg) and purified PCR product (5 μg) of the TIMP-1 mutant library were mixed and electrotransformed into yeast cells as described previously (51). Five separate electrotransformations were performed and combined. The yeast cells were then resuspended in cold YPD medium (20 g/liter glucose, 20 g/liter peptone, and 10 g/liter yeast extract) and grown at 30 °C with shaking for 1 h. The library size was estimated by plating yeast transformants in serial dilution and found to contain about 5×10^6 independent variants. The yeast cells containing the library of TIMP-1 mutants were pelleted and resuspended in 50 ml of SD-CAA medium, pH 4.5 (same as SD-CAA medium described above, but phosphate components were substituted with 13.7 g/liter sodium citrate dehydrate and 8.4 g/liter citric acid anhydrous) and grown for 16 h at 30 °C with shaking.

Screening the yeast-displayed TIMP-1 library using FACS

Prior to each round of sorting, yeast cells were grown and induced; counted (OD_{600} of 1 = 10^7 cells/ml); incubated with biotinylated MMP-3cd followed by anti-c-myc, streptavidin, and secondary antibody; washed; and suspended in PBSA buffer as described above under "Yeast surface display of TIMP-1." Samples were maintained on ice and covered from light until loading onto a flow cytometer for analysis (BD Accuri) or library sorting (BD Aria II). Sorted cells were recovered in SD-CAA, pH 4.5, containing 1% penicillin-streptavidin and incubated at 30 °C overnight. Yeast surface protein expression was then induced by culturing cells in SGR-CAA medium at 30 °C overnight. The initial library (~5×10^7 yeast) was subjected to two rounds of screening (staining, sorting, recovery, and regrowth) using a concentration of 100 nM biotinylated MMP-3cd. Screening was continued through four additional rounds, for a total of six rounds, under equilibrium sorting conditions employing incrementally decreasing MMP-3cd concentration from 50 to 5 nM.

DNA sequencing

Following rounds of sorting, recovered yeast were cultured on SD-CAA plates, and plasmid DNA was extracted from the isolated individual yeast clones using the Zymoprep™ yeast plasmid miniprep II kit (ZymoResearch). TIMP-1 mutant plasmids extracted from yeast were transformed into *Escherichia coli* cells and plated on LB-Amp (100 μg/ml ampicillin). The pCHA-TIMP-1 variant plasmid was then extracted and purified from the bacteria using the Qiagen Miniprep kit according to the manufacturer's protocol (Qiagen) and sequenced (Eurofins Scientific) with primers up- and downstream of the TIMP-1 gene. Sequences were analyzed using SnapGene software (SnapGene, GSL Biotech, LLC).

Soluble TIMP expression and purification

The pTT-TIMP-1 vector, a generous gift from Dr. B. Toussaint (Grenoble, France), was used for expression of full-length human TIMP-1 (52). TIMP-1 mutants were amplified from the

corresponding yeast display vector (pCHA-TIMP-1) using PCR and inserted between HindIII and BamHI restriction sites of the pTT-TIMP-1 vector. WT TIMP-1 and TIMP-1 variants were expressed in HEK293-FreeStyle cells (Thermo Fisher Scientific) in Gibco® FreeStyle™ 293 Expression Medium (Thermo Fisher Scientific) on a shaker incubator at 37 °C and 8% CO_2. The HEK293-FreeStyle cells were grown to a cell density of 1–1.5 × 10^6 in 300-ml culture, transfected with 300 μg of pTT-TIMP-1 plasmid using 0.9 ml of 1 mg/ml polyethylenimine (PEI) transfection reagent, and incubated on the shaker incubator for 72 h before harvesting the cells and collecting the supernatant media. For purification, the clarified medium was concentrated, dialyzed into buffer A (50 mM HEPES, pH 6.8, and 25 mM NaCl), and purified over an SP-Sepharose column using a linear gradient of buffer B (50 mM HEPES, pH 6.8, and 0.5 M NaCl). Fractions containing the WT or mutant TIMP-1 were assessed by silver-stained SDS-PAGE. To prepare homogenous purified proteins for crystallization, TIMP-1 variants were then enzymatically deglycosylated with peptide:*N*-glycosidase F (New England Biolabs). Deglycosylation of TIMP-1 protein was confirmed by SDS-PAGE followed by purification by size-exclusion chromatography using a Superdex-75 column (GE Healthcare) that was equilibrated and eluted with 50 mM HEPES, pH 6.8, containing 150 mM NaCl. The highly pure deglycosylated TIMP-1 fractions identified by silver-stained SDS-PAGE were combined and concentrated using Amicon Ultra-15 centrifugal filter units with a molecular weight cutoff of 10,000.

MMP expression, purification, and biotinylation

ProMMP-3cd was expressed from *E. coli* using a pET3a construct featuring human proMMP-3 lacking the C-terminal hemopexin domain, a generous gift of H. Nagase (53). ProMMP-3cd was refolded, purified, and activated as described previously (53). Briefly, recombinant protein was extracted from inclusion bodies in a solution containing 8 M urea, 20 mM Tris-HCl, pH 8.6, 20 mM DTT, and 50 μM $ZnCl_2$. The protein was purified on Q-Sepharose equilibrated with 8 M urea, 20 mM Tris-HCl, pH 8.6, and 50 μM $ZnCl_2$ and eluted using a linear gradient of NaCl to 0.5 M. Fractions containing proMMP-3cd were combined, diluted to an A_{280} of 0.3, and refolded by stepwise dialysis with 50 mM Tris-HCl, pH 7.5, 10 mM $CaCl_2$, and 150 mM NaCl. Subsequently, purified proMMP-3cd was activated overnight in the presence of the organomercurial compound 4-aminophenyl mercuric acetate (1 mM at 37 °C). Concentrations of active MMP-3cd were determined by titration against a TIMP-1 reference stock as described previously (54). MMP-3cd was biotinylated using the EZ-Link NHS-PEG4 biotinylation kit (Thermo Scientific) according to the manual with addition of biotin in a 1:10 molar ratio (protein:biotin) and incubated at room temperature for 30 min. The biotinylated MMP-3cd was purified using Zeba spin desalting columns (Thermo Scientific) and tested for degree of biotinylation using the 4′-hydroxyazobenzene-2-carboxylic acid assay as described in the kit protocol.

Active TIMP-1 concentration determination by titration

Concentrations of purified TIMP-1 variants were determined by titration against a reference stock of MMP-3cd previously titrated against WT TIMP-1, essentially as described previously (54). Briefly, MMP-3cd (200 nM) was preincubated for 1 h at 25 °C with a range of substoichiometric concentrations of the TIMP-1 variant. MMP/TIMP mixtures were then assayed for residual proteolytic activity using colorimetric thiopeptolide substrate Ac-Pro-Leu-Gly-[2-mercapto-4-methyl-pentanoyl]-Leu-Gly-OC_2H_5 (Enzo Life Sciences). MMP/TIMP mixtures were diluted 40-fold into a reaction cuvette containing the thiopeptolide substrate at a final concentration 100 μM in 50 mM HEPES, pH 6.0, 10 mM $CaCl_2$, 0.05% Brij-35, and 1 mM 5,5′-dithiobis(2-nitrobenzoic acid). Reactions were followed for 10 min at 37 °C on a Varian spectrophotometer (Thermo Scientific), and linear initial rates were measured as an increase in the absorbance at 410 nm (ϵ_{410} = 13,600 M^{-1} cm^{-1}). Data were fitted using linear regression analyses and extrapolated to the stoichiometric equivalence point in Prism 7 (GraphPad Software, San Diego, CA).

TIMP-1/MMP-3 inhibition studies

Equilibrium inhibition constants (K_i) of WT TIMP-1 and TIMP-1 variants toward MMP-3 were measured using a method appropriate for tight binding inhibition, similar to a method described previously (21). MMP-3cd (0.24 nM) was incubated with 0.04-2.5 nM WT TIMP-1 or TIMP-1 variant in TCNB buffer (50 mM Tris, pH 7.5, 100 mM NaCl, 10 mM $CaCl_2$, and 0.05% Brij) for 1 h at 37 °C. Thereafter, the fluorogenic substrate Mca-Pro-Leu-Gly-Leu-Dpa-Ala-Arg-NH_2 (where Mca is (7-methoxycoumarin-4-yl)acetyl and Dpa is *N*-3-(2,4-dinitrophenyl)-L-2,3-diaminopropionyl) (Anaspec, CA) was added to the reaction at a final concentration of 10 μM, and fluorescence was monitored with 340/30 excitation and 400/30 emission filters using a Synergy HT plate reader (BioTek, Winooski, VT) at 37 °C. Fluorescence readings were recorded every minute for 120 min, and enzymatic rates were determined from the slope of the linear portion of the fluorescence signal. To determine K_i, data were plotted as initial velocities *versus* TIMP-1 or variant concentration and fitted by multiple regression to Morrison's tight binding inhibition equation (55) (Equation 1) where V_t is enzyme velocity in the presence of inhibitor, V_0 is enzyme velocity in the absence of inhibitor, [*E*] is enzyme concentration, [*I*] is inhibitor concentration, [*S*] is substrate concentration, K_m is the Michaelis–Menten constant, and K_i^{app} is an apparent inhibition constant given by Equation 2. Data were fitted using Prism 7 (GraphPad Software) (Fig. 5). Reported inhibition constants are average values obtained from two independent experiments, each with duplicate samples. Calculations were performed using a K_m value of 11.23 μM for MMP-3cd as determined from three Michaelis–Menten kinetic experiments in our laboratory.

$$\frac{V_t}{V_0} = \frac{1 - ([E] + [I] + K_i^{app}) - \sqrt{([E] + [I] + K_i^{app})^2 - 4[E][I]}}{2[E]} \quad \text{(Eq. 1)}$$

$$K_i^{app} = K_i\left(1 + \frac{[S]}{K_m}\right) \quad \text{(Eq. 2)}$$

Crystallization and X-ray diffraction

TIMP-1 variants and MMP-3cd protein were mixed at a 1:1 molar ratio, and TIMP-1 variant/MMP-3cd protein complexes were concentrated to 2.8–4.8 mg/ml prior to crystallization screening. Crystallization was conducted using the hanging-drop method with the protein solution mixed 1:1 (v/v) with a reservoir solution. TIMP-1-L34G/MMP-3cd protein crystals were grown in condition 92 of the Anatrace Top96 crystallization kit (Anatrace) (0.1 M ammonium acetate, 0.1 M Bis-Tris HCl, pH 5.5, and 17% (w/v) PEG 10,000). TIMP-1-C1/MMP-3cd protein crystals were grown in condition 41 of the Anatrace Top96 crystallization kit (Anatrace) (0.2 M sodium acetate, 0.1 M sodium cacodylate HCl, pH 6.5, and 18% (w/v) PEG 8000). TIMP-1 variant/MMP-3cd protein crystals appeared over 48 h and were grown over a few weeks. Crystals were flash-cooled in liquid nitrogen using cryoprotectant buffer matched to the crystallization reservoir solution and additionally containing 30% dextrose. Single-wavelength (1.0 Å) native X-ray diffraction data were collected at 100 K at Advanced Light Source beamline 8.2.2, Lawrence Berkeley National Laboratory. TIMP-1 variant complex structures were each solved from single crystals that diffracted to 2.37 Å (for TIMP-1-L34G) and 2.67 Å resolution (for TIMP-1-C1). The X-ray data were processed with xia2 (56) using DIALS (57) for indexing, refinement, and integration with POINTLESS (58) and AIMLESS (59) for scaling and merging. R_{free} flags were assigned to a random 5% of reflections, and this test set was maintained throughout all subsequent stages of structure solution and refinement.

Structure determination and refinement

X-ray crystal structures of the protein complexes of MMP-3cd/TIMP-1 variants were solved using CCP4 software by molecular replacement using the program Molrep (60). The previously solved structure of human MMP-3cd/WT TIMP-1 (PDB code 1UEA) without the corresponding Zn and Ca ions was used as a search model. Following molecular replacement, Phenix.refine was used for sequential automated refinements (61) alternating with manual adjustments in Coot (62). Because of the flexibility of MMP-3cd and TIMP-1 protein segments and the possibility that they might demonstrate local trajectories of motion partially decoupled from the larger protein domains, we employed TLS refinement using the automatic TLS group finding tool in the Phenix software for refinement of both structures. Several residues in the TIMP-1 variant chains showed only weak and indistinct density and were left unmodeled in the final models, including residues Gly-52, Asp-53, Ala-54, and Ala-55 in both structures and additionally Leu-51 in the TIMP1-L34G/MMP-3cd structure. The final stage of restrained refinement included water molecules with peaks greater than 1σ and within acceptable H-bonding distances from neighboring protein atoms. The coordinates and structure factors for the TIMP-1-L34G/MMP-3cd and TIMP-1-C1/MMP-3cd structures have been submitted to the Worldwide Protein Data Bank under the accession codes 6MAV and 6N9D, respectively. Structure figures were generated using PyMOL (Schrödinger, LLC).

Author contributions—M. R.-S., G. P. D., D. C. R., and E. S. R. conceptualization; M. R.-S. and B. S. data curation; M. R.-S. and K. A. G. formal analysis; M. R.-S. and E. S. R. validation; M. R.-S., K. A. G., B. S., and E. S. R. investigation; M. R.-S. and E. S. R. visualization; M. R.-S. and B. S. methodology; M. R.-S. and E. S. R. writing-original draft; M. R.-S. and E. S. R. writing-review and editing; B. S. resources; G. P. D., D. C. R., and E. S. R. funding acquisition; E. S. R. supervision; E. S. R. project administration.

Acknowledgments—We thank Dr. Laura Lewis-Tuffin at the cell sorting facility at Mayo Clinic, Florida for help with FACS of TIMP-1 libraries; Rachel Henin and Alexandra Hockla for MMP-3 protein expression, purification, and biotinylation; and Matt Coban for advice with crystallographic data processing. We also thank Dr. Niv Papo for helpful discussions. Diffraction data were measured at beamline 8.2.2 of the Berkeley Center for Structural Biology, Advanced Light Source (ALS), Lawrence Berkeley National Laboratory. The Berkeley Center for Structural Biology is supported in part by the Howard Hughes Medical Institute. The Advanced Light Source is a Department of Energy Office of Science User Facility under Contract DE-AC02-05CH11231. The ALS-ENABLE beamlines are supported in part by the National Institutes of Health, National Institute of General Medical Sciences, Grant P30 GM124169.

References

1. Huang, J., Koide, A., Makabe, K., and Koide, S. (2008) Design of protein function leaps by directed domain interface evolution. *Proc. Natl. Acad. Sci. U.S.A.* **105,** 6578–6583 CrossRef Medline
2. Vogel, C., Bashton, M., Kerrison, N. D., Chothia, C., and Teichmann, S. A. (2004) Structure, function and evolution of multidomain proteins. *Curr. Opin. Struct. Biol.* **14,** 208–216 CrossRef Medline
3. Bagowski, C. P., Bruins, W., and Te Velthuis, A. J. (2010) The nature of protein domain evolution: shaping the interaction network. *Curr. Genomics* **11,** 368–376 CrossRef Medline
4. Brew, K., and Nagase, H. (2010) The tissue inhibitors of metalloproteinases (TIMPs): an ancient family with structural and functional diversity. *Biochim. Biophys. Acta* **1803,** 55–71 CrossRef Medline
5. Batra, J., and Radisky, E. S. (2014) Tissue inhibitors of metalloproteinases (TIMPs): inhibition of Zn-dependent metallopeptidases, in *Encyclopedia of Inorganic and Bioinorganic Chemistry* (Scott, R. A., ed) John Wiley and Sons, Chichester, UK
6. Gomis-Rüth, F. X., Maskos, K., Betz, M., Bergner, A., Huber, R., Suzuki, K., Yoshida, N., Nagase, H., Brew, K., Bourenkov, G. P., Bartunik, H., and Bode, W. (1997) Mechanism of inhibition of the human matrix metalloproteinase stromelysin-1 by TIMP-1. *Nature* **389,** 77–81 CrossRef Medline
7. Murphy, G., Houbrechts, A., Cockett, M. I., Williamson, R. A., O'Shea, M., and Docherty, A. J. (1991) The N-terminal domain of tissue inhibitor of metalloproteinases retains metalloproteinase inhibitory activity. *Biochemistry* **30,** 8097–8102 CrossRef Medline
8. Morgunova, E., Tuuttila, A., Bergmann, U., and Tryggvason, K. (2002) Structural insight into the complex formation of latent matrix metalloproteinase 2 with tissue inhibitor of metalloproteinase 2. *Proc. Natl. Acad. Sci. U.S.A.* **99,** 7414–7419 CrossRef Medline
9. Jung, K. K., Liu, X. W., Chirco, R., Fridman, R., and Kim, H. R. (2006) Identification of CD63 as a tissue inhibitor of metalloproteinase-1 interacting cell surface protein. *EMBO J.* **25,** 3934–3942 CrossRef Medline
10. Fernandez, C. A., Roy, R., Lee, S., Yang, J., Panigrahy, D., Van Vliet, K. J., and Moses, M. A. (2010) The anti-angiogenic peptide, loop 6, binds insu-

lin-like growth factor-1 receptor. *J. Biol. Chem.* **285,** 41886–41895 CrossRef Medline
11. Batra, J., Soares, A. S., Mehner, C., and Radisky, E. S. (2013) Matrix metalloproteinase-10/TIMP-2 structure and analyses define conserved core interactions and diverse exosite interactions in MMP/TIMP complexes. *PLoS One* **8,** e75836 CrossRef Medline
12. Huang, W., Suzuki, K., Nagase, H., Arumugam, S., Van Doren, S. R., and Brew, K. (1996) Folding and characterization of the amino-terminal domain of human tissue inhibitor of metalloproteinases-1 (TIMP-1) expressed at high yield in *E. coli*. *FEBS Lett.* **384,** 155–161 CrossRef Medline
13. Romero, P. A., and Arnold, F. H. (2009) Exploring protein fitness landscapes by directed evolution. *Nat. Rev. Mol. Cell Biol.* **10,** 866–876 CrossRef Medline
14. Bonsor, D. A., and Sundberg, E. J. (2011) Dissecting protein-protein interactions using directed evolution. *Biochemistry* **50,** 2394–2402 CrossRef Medline
15. Yuen, C. M., and Liu, D. R. (2007) Dissecting protein structure and function using directed evolution. *Nat. Methods* **4,** 995–997 CrossRef Medline
16. Boder, E. T., and Wittrup, K. D. (1997) Yeast surface display for screening combinatorial polypeptide libraries. *Nat. Biotechnol.* **15,** 553–557 CrossRef Medline
17. Boder, E. T., Raeeszadeh-Sarmazdeh, M., and Price, J. V. (2012) Engineering antibodies by yeast display. *Arch. Biochem. Biophys.* **526,** 99–106 CrossRef Medline
18. Mei, M., Zhou, Y., Peng, W., Yu, C., Ma, L., Zhang, G., and Yi, L. (2017) Application of modified yeast surface display technologies for non-antibody protein engineering. *Microbiol. Res.* **196,** 118–128 CrossRef Medline
19. Raeeszadeh-Sarmazdeh, M., Patel, N., Cruise, S., Owen, L., O'Neill, H., and Boder, E. T. (2019) Identifying stable fragments of *Arabidopsis thaliana* cellulose synthase subunit 3 by yeast display. *Biotechnol. J.* **14,** e1800353 CrossRef Medline
20. Arkadash, V., Radisky, E. S., and Papo, N. (2018) Combinatorial engineering of N-TIMP2 variants that selectively inhibit MMP9 and MMP14 function in the cell. *Oncotarget* **9,** 32036–32053 CrossRef Medline
21. Arkadash, V., Yosef, G., Shirian, J., Cohen, I., Horev, Y., Grossman, M., Sagi, I., Radisky, E. S., Shifman, J. M., and Papo, N. (2017) Development of high affinity and high specificity inhibitors of matrix metalloproteinase 14 through computational design and directed evolution. *J. Biol. Chem.* **292,** 3481–3495 CrossRef Medline
22. Shirian, J., Arkadash, V., Cohen, I., Sapir, T., Radisky, E. S., Papo, N., and Shifman, J. M. (2018) Converting a broad matrix metalloproteinase family inhibitor into a specific inhibitor of MMP-9 and MMP-14. *FEBS Lett.* **592,** 1122–1134 CrossRef Medline
23. Radisky, E. S., Raeeszadeh-Sarmazdeh, M., and Radisky, D. C. (2017) Therapeutic potential of matrix metalloproteinase inhibition in breast cancer. *J. Cell. Biochem.* **118,** 3531–3548 CrossRef Medline
24. Chakrabartty, A., Schellman, J. A., and Baldwin, R. L. (1991) Large differences in the helix propensities of alanine and glycine. *Nature* **351,** 586–588 CrossRef Medline
25. Blaber, M., Zhang, X.-J., and Matthews, B. W. (1993) Structural basis of amino acid α helix propensity. *Science* **260,** 1637–1640 CrossRef Medline
26. Pace, C. N., and Scholtz, J. M. (1998) A helix propensity scale based on experimental studies of peptides and proteins. *Biophys. J.* **75,** 422–427 CrossRef Medline
27. Butler, G. S., Hutton, M., Wattam, B. A., Williamson, R. A., Knäuper, V., Willenbrock, F., and Murphy, G. (1999) The specificity of TIMP-2 for matrix metalloproteinases can be modified by single amino acid mutations. *J. Biol. Chem.* **274,** 20391–20396 CrossRef Medline
28. Meng, Q., Malinovskii, V., Huang, W., Hu, Y., Chung, L., Nagase, H., Bode, W., Maskos, K., and Brew, K. (1999) Residue 2 of TIMP-1 is a major determinant of affinity and specificity for matrix metalloproteinases but effects of substitutions do not correlate with those of the corresponding P1′ residue of substrate. *J. Biol. Chem.* **274,** 10184–10189 CrossRef Medline
29. Williamson, R. A., Hutton, M., Vogt, G., Rapti, M., Knäuper, V., Carr, M. D., and Murphy, G. (2001) Tyrosine 36 plays a critical role in the interaction of the AB loop of tissue inhibitor of metalloproteinases-2 with matrix metalloproteinase-14. *J. Biol. Chem.* **276,** 32966–32970 CrossRef Medline
30. Nagase, H., and Brew, K. (2003) Designing TIMP (tissue inhibitor of metalloproteinases) variants that are selective metalloproteinase inhibitors. *Biochem. Soc. Symp.* **70,** 201–212 Medline
31. Wei, S., Chen, Y., Chung, L., Nagase, H., and Brew, K. (2003) Protein engineering of the tissue inhibitor of metalloproteinase 1 (TIMP-1) inhibitory domain. In search of selective matrix metalloproteinase inhibitors. *J. Biol. Chem.* **278,** 9831–9834 CrossRef Medline
32. Lee, M. H., Rapti, M., and Murphy, G. (2003) Unveiling the surface epitopes that render tissue inhibitor of metalloproteinase-1 inactive against membrane type 1-matrix metalloproteinase. *J. Biol. Chem.* **278,** 40224–40230 CrossRef Medline
33. Lee, M. H., Rapti, M., Knaüper, V., and Murphy, G. (2004) Threonine 98, the pivotal residue of tissue inhibitor of metalloproteinases (TIMP)-1 in metalloproteinase recognition. *J. Biol. Chem.* **279,** 17562–17569 CrossRef Medline
34. Lee, M. H., Rapti, M., and Murphy, G. (2005) Total conversion of tissue inhibitor of metalloproteinase (TIMP) for specific metalloproteinase targeting: fine-tuning TIMP-4 for optimal inhibition of tumor necrosis factor-α-converting enzyme. *J. Biol. Chem.* **280,** 15967–15975 CrossRef Medline
35. Hamze, A. B., Wei, S., Bahudhanapati, H., Kota, S., Acharya, K. R., and Brew, K. (2007) Constraining specificity in the N-domain of tissue inhibitor of metalloproteinases-1; gelatinase-selective inhibitors. *Protein Sci.* **16,** 1905–1913 CrossRef Medline
36. Bahudhanapati, H., Zhang, Y., Sidhu, S. S., and Brew, K. (2011) Phage display of tissue inhibitor of metalloproteinases-2 (TIMP-2): identification of selective inhibitors of collagenase-1 (metalloproteinase 1 (MMP-1)). *J. Biol. Chem.* **286,** 31761–31770 CrossRef Medline
37. Fersht, A. R. (1987) The hydrogen bond in molecular recognition. *Trends Biochem. Sci.* **12,** 301–304 CrossRef
38. Lo Conte, L., Chothia, C., and Janin, J. (1999) The atomic structure of protein-protein recognition sites. *J. Mol. Biol.* **285,** 2177–2198 CrossRef Medline
39. Jeffrey, G. A., and Jeffrey, G. A. (1997) *An Introduction to Hydrogen Bonding*, Oxford University Press, New York
40. Moreira, I. S., Fernandes, P. A., and Ramos, M. J. (2007) Hot spots—a review of the protein-protein interface determinant amino-acid residues. *Proteins* **68,** 803–812 CrossRef Medline
41. Binz, H. K., Amstutz, P., Kohl, A., Stumpp, M. T., Briand, C., Forrer, P., Grütter, M. G., and Plückthun, A. (2004) High-affinity binders selected from designed ankyrin repeat protein libraries. *Nat. Biotechnol.* **22,** 575–582 CrossRef Medline
42. Kessenbrock, K., Plaks, V., and Werb, Z. (2010) Matrix metalloproteinases: regulators of the tumor microenvironment. *Cell* **141,** 52–67 CrossRef Medline
43. Hu, J., Van den Steen, P. E., Sang, Q. X., and Opdenakker, G. (2007) Matrix metalloproteinase inhibitors as therapy for inflammatory and vascular diseases. *Nat. Rev. Drug Discov.* **6,** 480–498 CrossRef Medline
44. Coussens, L. M., Fingleton, B., and Matrisian, L. M. (2002) Matrix metalloproteinase inhibitors and cancer: trials and tribulations. *Science* **295,** 2387–2392 CrossRef Medline
45. Turk, B. (2006) Targeting proteases: successes, failures and future prospects. *Nat. Rev. Drug Discov.* **5,** 785–799 CrossRef Medline
46. Nagase, H., and Brew, K. (2002) Engineering of tissue inhibitor of metalloproteinases mutants as potential therapeutics. *Arthritis Res.* **4,** Suppl. 3, S51–S61 CrossRef Medline
47. Levin, M., Udi, Y., Solomonov, I., and Sagi, I. (2017) Next generation matrix metalloproteinase inhibitors—novel strategies bring new prospects. *Biochim. Biophys. Acta Mol. Cell Res.* **1864,** 1927–1939 CrossRef Medline
48. Bhaskara, R. M., and Srinivasan, N. (2011) Stability of domain structures in multi-domain proteins. *Sci. Rep.* **1,** 40 CrossRef Medline
49. Itoh, K., and Sasai, M. (2008) Cooperativity, connectivity, and folding pathways of multidomain proteins. *Proc. Natl. Acad. Sci. U.S.A.* **105,** 13865–13870 CrossRef Medline
50. Mata-Fink, J., Kriegsman, B., Yu, H. X., Zhu, H., Hanson, M. C., Irvine, D. J., and Wittrup, K. D. (2013) Rapid conformational epitope mapping of

anti-gp120 antibodies with a designed mutant panel displayed on yeast. *J. Mol. Biol.* **425,** 444–456 CrossRef Medline
51. Chao, G., Lau, W. L., Hackel, B. J., Sazinsky, S. L., Lippow, S. M., and Wittrup, K. D. (2006) Isolating and engineering human antibodies using yeast surface display. *Nat. Protoc.* **1,** 755–768 CrossRef Medline
52. Crombez, L., Marques, B., Lenormand, J. L., Mouz, N., Polack, B., Trocme, C., and Toussaint, B. (2005) High level production of secreted proteins: example of the human tissue inhibitor of metalloproteinases 1. *Biochem. Biophys. Res. Commun.* **337,** 908–915 CrossRef Medline
53. Suzuki, K., Kan, C. C., Hung, W., Gehring, M. R., Brew, K., and Nagase, H. (1998) Expression of human pro-matrix metalloproteinase 3 that lacks the N-terminal 34 residues in *Escherichia coli*: autoactivation and interaction with tissue inhibitor of metalloproteinase 1 (TIMP-1). *Biol. Chem.* **379,** 185–191 Medline
54. Batra, J., Robinson, J., Soares, A. S., Fields, A. P., Radisky, D. C., and Radisky, E. S. (2012) Matrix metalloproteinase-10 (MMP-10) interaction with tissue inhibitors of metalloproteinases TIMP-1 and TIMP-2: binding studies and crystal structure. *J. Biol. Chem.* **287,** 15935–15946 CrossRef Medline
55. Morrison, J. F. (1969) Kinetics of the reversible inhibition of enzyme-catalysed reactions by tight-binding inhibitors. *Biochim. Biophys. Acta* **185,** 269–286 CrossRef Medline
56. Winter, G. (2010) xia2: an expert system for macromolecular crystallography data reduction. *J. Appl. Crystallogr.* **43,** 186–190 CrossRef
57. Winter, G., Waterman, D. G., Parkhurst, J. M., Brewster, A. S., Gildea, R. J., Gerstel, M., Fuentes-Montero, L., Vollmar, M., Michels-Clark, T., Young, I. D., Sauter, N. K., and Evans, G. (2018) DIALS: implementation and evaluation of a new integration package. *Acta Crystallogr. D Struct. Biol.* **74,** 85–97 CrossRef Medline
58. Evans, P. (2006) Scaling and assessment of data quality. *Acta Crystallogr. D Biol. Crystallogr.* **62,** 72–82 CrossRef Medline
59. Evans, P. R., and Murshudov, G. N. (2013) How good are my data and what is the resolution? *Acta Crystallogr. D Biol. Crystallogr.* **69,** 1204–1214 CrossRef Medline
60. McCoy, A. J., Grosse-Kunstleve, R. W., Adams, P. D., Winn, M. D., Storoni, L. C., and Read, R. J. (2007) Phaser crystallographic software. *J. Appl. Crystallogr.* **40,** 658–674 CrossRef Medline
61. Afonine, P. V., Grosse-Kunstleve, R. W., and Adams, P. D. (2005) The Phenix refinement framework, in *CCP4 Newsletter*, Number 42, Summer 2005, Daresbury Laboratory, Daresbury, UK
62. Emsley, P., and Cowtan, K. (2004) Coot: model-building tools for molecular graphics. *Acta Crystallogr. D Biol. Crystallogr.* **60,** 2126–2132 CrossRef Medline

Directed evolution of the metalloproteinase inhibitor TIMP-1 reveals that its N- and C-terminal domains cooperate in matrix metalloproteinase recognition

Maryam Raeeszadeh-Sarmazdeh, Kerrie A. Greene, Banumathi Sankaran, Gregory P. Downey, Derek C. Radisky and Evette S. Radisky

J. Biol. Chem. 2019, 294:9476-9488.
doi: 10.1074/jbc.RA119.008321 originally published online April 30, 2019